

THESIS APPROVED BY

07-31-2019

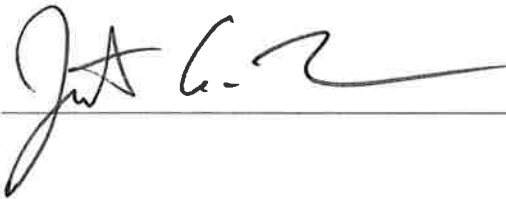
Date



Elton Jeffrey North, Ph.D., Chair



Naser Alsharif, Ph.D.



Justin Tolman, Ph.D.



Gail M. Jensen, Ph.D.

TITLE OF THESIS

DESIGN, SYNTHESIS, AND EVALUATION OF NOVEL ANTIMYCOBACTERIAL
AGENTS WITH ENHANCED PHARMACOKINETIC PROFILES

By

PANKAJ BHATTARAI

A THESIS

Submitted to the faculty of the Graduate School of the Creighton University in Partial
Fulfillment of the Requirements for the degree of Master of Science in the Department of
Pharmaceutical Sciences

Omaha, NE

(June 10, 2019)

© Pankaj Bhattarai, 2019

Abstract:

Tuberculosis (TB), caused by *Mycobacterium tuberculosis* (*M. tb*), is one of the leading causes of death worldwide. The present short-course therapy is six months long for drug-susceptible *M. tb* strains, and up to two years for multi-drug-resistant TB (MDR-TB) and extensively drug-resistant TB (XDR-TB) due to a lack of effective treatment. Non-tuberculous mycobacteria (NTM) such as the *M. avium* and *M. abscessus* complexes (MAC and MABSC, respectively) are opportunistic pathogens found ubiquitously in the environment. NTM infections have increasing prevalence in patients with structural lung diseases, including chronic obstructive pulmonary disease and cystic fibrosis. Current treatment recommendations for MAC and MABSC infections last for at least 12 months and include multidrug therapy with combinations of intravenous and oral antibiotics. The long-combined therapy is accompanied with many adverse effects and is routinely ineffective. Therefore, novel anti-TB and -NTM agents with greater efficacy and shorter treatment times are the need of the hour.

One of the common drug targets for antibiotic intervention is the inhibition of bacterial cell wall biosynthesis. Mycolic acids, which are α -alkylated β -hydroxylated fatty acids, are the primary lipid constituents of the mycobacterial cell wall and are synthesized intracellularly in the cytoplasm. Mycobacterial membrane protein large 3 (MmpL3) is an essential transporter protein that translocates mycolic acids as trehalose monomycolates (TMM), an ester comprising trehalose sugar and a mycolic acid, across the plasma membrane. The inhibition of this novel target obstructs the TMM transport, disrupting the cell wall assembly, leading to the inhibition of cell growth. Our group has previously developed urea- and indole-based compounds that are putative MmpL3 inhibitors with high activity at concentrations of sub- $\mu\text{g/mL}$ against a panel of mycobacteria. However, they have poor

aqueous solubility limiting their translational potential. Our efforts to improve the aqueous solubility of the indole-based compounds has yielded the acetamide series. The design is based on the hypothesis that ‘Medicinal chemistry ligand-based optimization of the indole series to generate the acetamide series maintains the pharmacophore while decreasing the percentage of lipophilic carbon atoms, thus retaining potent antimycobacterial activity and increasing aqueous solubility.’ Minimum inhibitory concentration values against a panel of mycobacteria, including *M. abscessus* and *M. tuberculosis* were assessed along with *in vitro* cytotoxicity profiles, pharmacokinetic and physicochemical parameters, including aqueous solubility, permeability, and human plasma protein binding. Based on the preliminary data, of the 39 compounds tested, compounds **192** and **200** were identified as the best leads, with potent activity against both *M. tb* and *M. abscessus* strains and 20- to 30-fold improvement in aqueous solubility compared to indoles, while maintaining optimal ADME-Tox.

*Dedicated to my parents, Basanti Devi Bhattarai, Nityanand Bhattarai, and Namita
Dhakal Bhattarai and my grandparents Bhanumaya Bhattarai and Krishna Prashad
Bhattarai*

Acknowledgements

I would like to extend my hearty thanks to my research advisor Dr. E. Jeffrey North for his continuous guidance and support throughout my master's degree. I would like to extend my gratitude to the committee members of my graduate thesis committee, Dr. Naser Alsharif and Dr. Justin Tolman, for their invaluable suggestions and inputs. I am thankful to Dr. Alekha K. Dash and Dr. Somnath Singh for their tremendous support during my studies in M.S. in Pharmaceutical Sciences program. I am grateful with the School of Pharmacy and Health Professions for funding me throughout my master's program.

I would like to express my vote of thanks to Dr. Mary Jackson and her team at Colorado State University for performing microbial testing. I am immensely thankful to Dr. Amit Pandya, Dr. Pavan Pratipathi, and Mr. Dan Munt for training me in various aspects of my research project. I express my hearty thanks to Mrs. Susie L Sullivan-Tuncan for teaching and guiding me in English writing. I would also like to thank Mrs. Dawn Trojanowski for her continuous support and assistance. I express my thankful note to Taunya Plater, LuAnn Schwery, administrative staff members at the School of Pharmacy and Health Professions, and Graduate School for their administrative guidance.

Kudos, reverence and hearty thanks to my parents for instilling in me a reflection of a nice human and pushing me forward in every aspects of my life. A hearty thanks to my brother, Chandan Bhattarai for his love and care. A hearty thanks to my girlfriend Sadikshya Aryal for her support at all points of my life. 'Omaha is a home away from home.', and my friends Aayushi, Aditya, Ashish, Chetan, Deepal, Gayathri, Kinnari, Leonce, Neetu, Melanie, Shambhavi, Saina, Segoo, and Shrestha had promoted me for that feeling. I would like to take a moment to thank them all for making Omaha a beautiful place to live.

Table of Contents

| | |
|---|-----------|
| Abstract | iii |
| Acknowledgements | vi |
| Table of contents | vii |
| List of Figures | x |
| List of Tables | xii |
| List of equations | xiv |
| List of abbreviations | xv |
| Chapter 1: Introduction | 1 |
| 1.1 Background | 2 |
| 1.2 TB: Therapy, resistance, and limitation | 3 |
| 1.3 NTM-infections: Therapy, resistance, and limitations | 5 |
| 1.4 Primary Antibiotic Targets | 6 |
| 1.5 Mycobacterial membrane protein large 3 (MmpL3): A novel antimycobacterial target essential for mycobacterial cell wall biosynthesis | 8 |
| 1.6 Urea- and indole-based MmpL3 inhibitors | 12 |
| 1.6.1 Pharmacophore of urea- and indole-based MmpL3 inhibitors | 12 |
| 1.6.2 SAR of urea-based MmpL3 inhibitors | 13 |
| 1.6.3 SAR of indole-based MmpL3 inhibitors compounds | 17 |
| 1.7 Summary | 22 |
| Chapter 2: Design, synthesis, and assessment of mycobacterial activity of novel antimycobacterial agents | 24 |
| 2.1 Introduction | 25 |
| 2.2 Ligand-based drug design approach identifying novel acetamides | 25 |
| 2.3 Novel acetamide SAR | 27 |
| 2.4 Synthesis of acetamide series | 28 |

| | | |
|--|---|-----------|
| 2.5 | Microbiological assessment | 28 |
| 2.6 | Structure activity relationship (SAR) of acetamide series | 30 |
| 2.7 | Summary | 40 |
| 2.8 | Experimental section | 41 |
| 2.8.1 | Materials, methods, and instrumentation | 41 |
| 2.8.2 | General procedure for the preparation of N-(cycloalkyl)-2-(N-phenylamino)acetamides | 41 |
| Chapter 3: Assessment of in vitro physicochemical, pharmacokinetic, and cytotoxicity profiles of active compounds | | 54 |
| 3.1 | Introduction | 55 |
| 3.2 | Importance of in vitro ADME-Tox assessment | 57 |
| 3.3 | Aqueous Solubility | 58 |
| 3.3.1 | Assessment of kinetic aqueous solubility | 60 |
| 3.4 | Permeability | 65 |
| 3.4.1 | Parallel artificial membrane permeability assay (PAMPA) | 67 |
| 3.5 | Plasma protein binding (PPB) | 76 |
| 3.5.1 | Determination of human plasma protein binding | 77 |
| 3.6 | Cytotoxic profiles | 79 |
| 3.6.1 | MTT assay | 83 |
| 3.7 | Summary | 88 |
| 3.8 | Experimental Section | 88 |
| 3.8.1 | Quantitative assessment using LC-MS-MS | 88 |
| 3.8.2 | Determination of kinetic aqueous solubility | 89 |
| 3.8.3 | Determination of PAMPA permeability | 89 |
| 3.8.4 | Determination of human plasma protein binding | 90 |
| 3.8.5 | Determination of cell viability | 91 |
| Chapter 4: Conclusion, Future Direction, and Global Perspective | | 92 |
| 4.1 | Conclusion | 93 |
| 4.2 | Future Directions | 96 |

| | | |
|-------|--|------------|
| 4.2.1 | Development of the current acetamide series | 96 |
| 4.2.2 | Extension and optimization of the current series | 97 |
| 4.2.3 | Modification of the acetamide core | 98 |
| 4.3 | Global Perspectives of the research project | 100 |
| | References and Bibliography | 101 |
| | Appendix: Characterization data of representative compounds 192 and 200 | 118 |

List of Figures

| | | |
|-----------|---|----|
| Figure 1 | First line antitubercular drugs | 4 |
| Figure 2 | Antitubercular fluoroquinolones | 4 |
| Figure 3 | Antitubercular injectable aminoglycosides | 5 |
| Figure 4 | Primary antibiotic targets | 7 |
| Figure 5 | Mycobacterial membrane protein large 3 (MmpL3): A novel antimycobacterial target essential for mycobacterial cell wall biosynthesis | 11 |
| Figure 6 | MmpL3 inhibitors discussed in the literature | 11 |
| Figure 7 | Pharmacophore requirements of urea- and indole-based compounds | 13 |
| Figure 8 | Pharmacophore of indole-based compounds | 25 |
| Figure 9 | Medicinal chemistry strategy to enhance aqueous solubility | 27 |
| Figure 10 | Moieties within the acetamides | 27 |
| Figure 11 | A reaction depicting REMA | 29 |
| Figure 12 | MIC determination by visual screening method | 30 |
| Figure 13 | The principles of ADME | 56 |
| Figure 14 | <i>In vitro</i> assays that relate to ADME-Tox | 58 |
| Figure 15 | Method to assess kinetic aqueous solubility | 61 |
| Figure 16 | Calibration curve of 192 for kinetic aqueous solubility | 62 |
| Figure 17 | Mechanisms of drug transport | 66 |
| Figure 18 | Structure of cell membrane | 68 |
| Figure 19 | PAMPA model to assess permeability | 69 |
| Figure 20 | Calibration curve of 192 for PAMPA | 70 |
| Figure 21 | Panel A – RED insert device in RED plate, Panel B – Principle of RED | 78 |
| Figure 22 | Calibration curve of 192 for HPPB assay | 79 |
| Figure 23 | Principle of MTT assay: conversion of MTT to Formazan | 84 |
| Figure 24 | Concentration vs % cell viability to determine IC ₅₀ | 86 |
| Figure 25 | Contemporary functional groups at R ₂ | 98 |

Figure 26 Classical and non-classical bioisosteric replacement of indole-based MmpL3 inhibitors

100

List of Tables

| | | |
|----------|---|----|
| Table 1 | MIC of <i>M. tb</i> in modified urea pharmacophore | 14 |
| Table 2 | MIC of different groups on R ₁ | 15 |
| Table 3 | Effects of substitutions on phenyl ring with adamantyl head group | 16 |
| Table 4 | Physicochemical and PK properties of 14 and 23 | 17 |
| Table 5 | <i>M. tb</i> MIC of various indole-based scaffolds | 19 |
| Table 6 | MIC of different substitution at indole ring with cyclooctyl head group | 21 |
| Table 7 | Physicochemical and PK profiles of 15 and 36 | 22 |
| Table 8 | Antimycobacterial activity of unsubstituted aniline with various cycloaliphatic groups | 31 |
| Table 9 | MIC of substituted aniline at para positions with (1R,2R,3R,5S)-(-)-isopinocampheyl head group against <i>M. abscessus</i> and <i>M. tb</i> | 33 |
| Table 10 | MIC of substituted aniline at para positions with 1-adamantyl head group against <i>M. abscessus</i> and <i>M. tb</i> | 35 |
| Table 11 | MIC of substituted aniline at para positions with 2-adamantyl group against <i>M. abscessus</i> and <i>M. tb</i> | 36 |
| Table 12 | MIC of substituted aniline at para positions with cyclooctyl head group against <i>M. abscessus</i> and <i>M. tb</i> | 37 |
| Table 13 | MIC of substituted aniline at para positions with transmethylcyclohexyl head group against <i>M. abscessus</i> and <i>M. tb</i> | 38 |
| Table 14 | MIC of substituted aniline at ortho and para positions of some active hits against <i>M. abscessus</i> and <i>M. tb</i> | 39 |
| Table 15 | Sample area, IS area, area ratio and standard concentration of 192 for kinetic aqueous solubility | 62 |
| Table 16 | Kinetic aqueous solubility data of all active compounds | 63 |
| Table 17 | Description of aqueous solubility by USP | 65 |

| | | |
|----------|--|----|
| Table 18 | Sample area, IS area, area ratio and standard concentration of 192 for PAMPA | 70 |
| Table 19 | PAMPA permeability of all active compounds | 73 |
| Table 20 | Sample area, IS area, area ratio and standard concentration of 192 for HPPB assay | 79 |
| Table 21 | HPPB of all the active compounds and ranitidine | 81 |
| Table 22 | Absorbance, concentration, and IC ₅₀ of compound 192 | 86 |
| Table 23 | IC ₅₀ and selectivity indices of all active compounds | 87 |
| Table 24 | Summary of acetamides MIC and ADME-Tox data | 95 |

List of Equations

| | | |
|------------|--------------------------------|----|
| Equation 1 | Apparent Permeability Equation | 71 |
| Equation 2 | % Free drug concentration | 80 |
| Equation 3 | % Cell viability | 85 |
| Equation 4 | Selectivity index (SI) | 86 |

List of abbreviations

ADME: Absorption, distribution, metabolism, and excretion

ATP: Adenosine triphosphate

AUC: Area under the curve

BCS: Biopharmaceutical classification system

BDDCS: Biopharmaceutics drug disposition classification system

CF: Cystic fibrosis

CDC: Centers for disease control and prevention

COPD: Chronic obstructive pulmonary disease

CFU: Colony forming units

cLogP: Calculated LogP

DCM: Dichloromethane

DDIs: Drug-drug interactions

DMSO: Dimethyl sulfoxide

DNA: Deoxyribonucleic acid

EPTB: Extra-pulmonary tuberculosis

ESI: Electrospray Ionization

FAS: Fatty acid synthase

FBS: Fetal bovine serum

FDA: Food and Drug Administration

GI: Gastrointestinal

HIV-AIDS: human immunodeficiency virus – acquired immune deficiency syndrome

HPLC: High pressure liquid chromatography

IC: Inhibitory concentration

IUPAC: International Union of Pure and Applied Chemistry

LC-MS: Liquid chromatography – mass spectroscopy

Ln: Natural log

MABSC: *M. abscessus complex*

MAP: Mycolic acid-arabinogalactan-peptidoglycan

M. avium complex (MAC)

MDR-TB: Multidrug-resistant TB

MEM: Minimum essential media

MIC: Minimum inhibitory concentration

MmpL: Mycobacterial membrane protein large

M. tb: Mycobacterium tuberculosis

MS: Mass spectrometry

MTT: (3-(4,5-dimethylthiazol-2-yl)-2,5-diphenyl tetrazolium bromide)

m/z: Mass to charge

NAD: Nicotinamide adenine dinucleotide

NADP: Nicotinamide adenine dinucleotide phosphate

NCE: New chemical entity

NMR: Nuclear magnetic resonance

NTM: Non-tuberculous mycobacteria

PAMPA: Parallel artificial membrane permeability assay

PBS: Phosphate buffer saline

PPB: Plasma protein binding

Pe: Apparent permeability

PK: Pharmacokinetics

Pks: Polyketide synthase

PD: Pharmacodynamics

PTB: Pulmonary tuberculosis

RED: Rapid equilibrium dialysis

RNA: Ribonucleic acid

RND: Resistance-nodulation division

REMA: Resazurin-based microtiter plate assays

SAR: Structure activity relationship

SDS: Sodium dodecylsulphate

SI: Selectivity index

TB: Tuberculosis

TEA: Triethylamine

THF: Tetrahydrofuran

TLC: Thin layer chromatography

TMM: Trehalose monomycolate

TDM: trehalose dimycolate

US-FDA: United States Food and Drug Administration

USP: United States Pharmacopoeia

WHO: World health organization

XDR-TB: Extensively drug-resistant TB

Chapter 1: Introduction

1.1 Background

Tuberculosis (TB) is a granulomatous infection caused by the bacterial pathogen *Mycobacterium tuberculosis* (*M. tb*) (Ahmad 2010). TB was the tenth leading cause of death globally in 2017, and the number one cause of death from a single infectious agent, even exceeding human immunodeficiency virus – acquired immune deficiency syndrome (HIV-AIDS) (WHO TB report, 2018). Populations that are immunocompromised, suffering from HIV-AIDS, or malnourished are predisposed to develop active TB infections. Statistics suggest that in 2017, death toll for TB has risen to 1.3 million, and 10 million new cases were identified (WHO TB report, 2018), clearly confirming that TB is a huge global burden. The emergence of resistant strains of *M. tb* and the HIV pandemics have made the management of TB more difficult. *M. tb* is a slow-growing aerobic bacteria with a doubling time of approximately 20 hours (Wang et al. 2014). It is transmitted from person to person via aerosolized droplets (Forrellad et al. 2013) causing pulmonary tuberculosis (PTB) (Sunnecioglu et al. 2015). *M. tb* can also cause extra-pulmonary tuberculosis (EPTB) by establishing infections in tissues and organs outside the lungs, including lymph nodes, bones, pleura, and cutaneous tissue (Sunnecioglu et al. 2015).

Non-tuberculous mycobacteria (NTM) are ubiquitous in nature and are mostly non-pathogenic (Faria et al. 2015; CDC, 2019). However, a few of the NTM species, including *M. abscessus complex* (MABSC), *M. avium complex* (MAC), *M. massiliense*, *M. bolletii*, and *M. fortuitum*, are opportunistic pathogens and infects patients with structural lung disorders, including chronic obstructive pulmonary disease, bronchiectasis, and cystic fibrosis (Faria et al. 2015; Van der Werf et al. 2014). It is not mandatory to report NTM infections in the US and other countries, therefore data for these infections are not precise (Bodle et al. 2008). A 2007 -2011 study performed in

US-affiliated Pacific Island in patients with a respiratory infection showed an increasing prevalence of NTM infections, with 0.5% of the patients with respiratory infections had NTM isolated in 2007 and the percentage went to as high as 11% in 2011 (Lin et al. 2018). Another study (1994 – 2014) carried out in Spain demonstrated an annual increase in MAC and MABSC related pulmonary infections by 13% and 24% respectively (Santin et al. 2018). These data suggested that the prevalence of these infections is growing every year.

1.2 TB: Therapy, resistance, and limitation

The short course therapy for drug-susceptible TB comprised of two phases: intensive phase and continuation phase (WHO TB report, 2018). In the intensive phase, comprising the first two months, four first-line therapy drugs, namely isoniazid, rifampicin, ethambutol, and pyrazinamide (Figure 1) are administered (WHO TB report, 2018). In the continuation phase, rifampicin and isoniazid are administered for the later four months (WHO TB report, 2018). Although this recommended therapy for the drug-susceptible strain is highly effective when the patients are compliant, with 85% success rate (Shin and Kwon 2015; CDC, 2019), the course of treatment is lengthy and the success of the therapeutic intervention is dependent upon patient adherence (Shin and Kwon 2015). Poor adherence to first-line therapy is one of the primary causes for the emergence of multidrug-resistant TB (MDR-TB), where *M. tb* develops resistance to at least both isoniazid and rifampicin, and 35% of the total TB patients have developed MDR-TB (WHO TB report, 2018).

Isolated in 2007, extensively drug-resistant TB (XDR-TB) is a strain of *M. tb* that has developed resistance to at least one of the fluoroquinolones (Figure 2) and a second-line injectable (amikacin, kanamycin or capreomycin; Figure 3), in addition to rifampicin and isoniazid (Chan and Iseman 2008). Approximately 8.5% of MDR-TB

cases had developed into XDR-TB in 2017 (WHO TB report, 2018). Treating TB in HIV-AIDS patients is more complicated due to increased pill burden, drug-drug interactions, and toxicities (Padmapriyadarsini et al. 2011). Considering the limitations in current anti-TB therapeutic regimens, novel agents with shorter durations of treatment and novel mechanisms of action with efficacy against MDR-TB and XDR-TB are in great demand (WHO TB report, 2018; CDC, 2018).

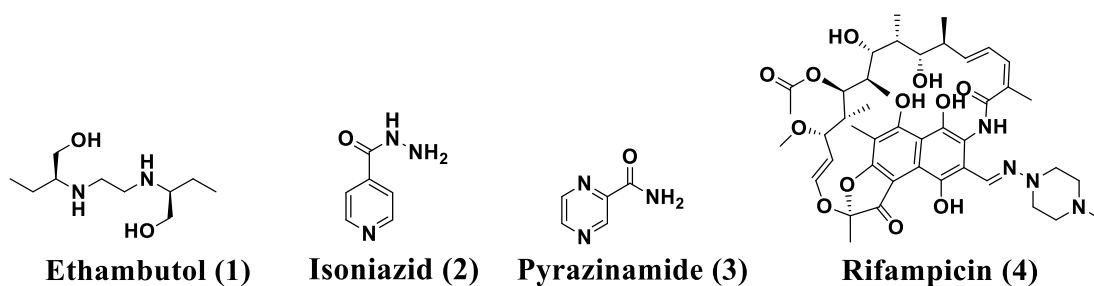


Figure 1. First line antitubercular drugs (Shakya et al. 2012).

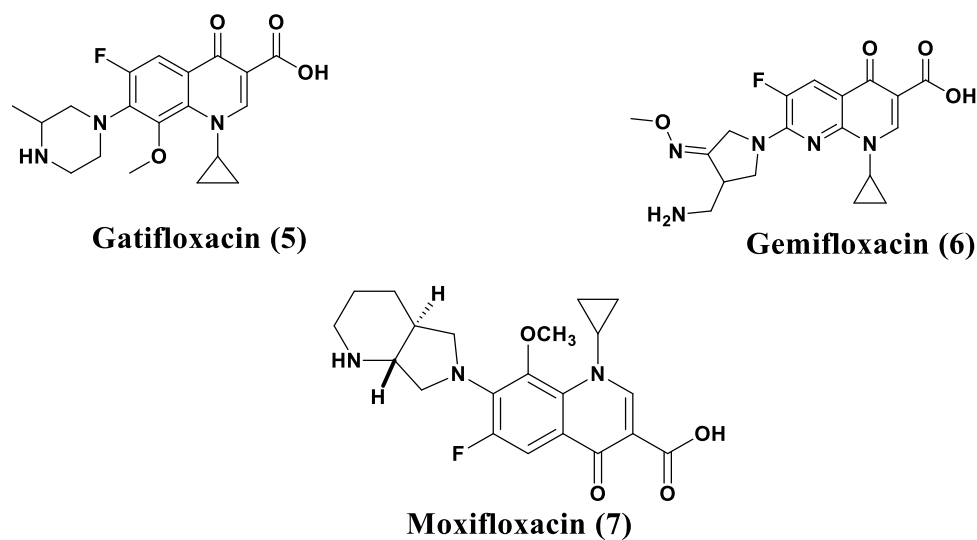
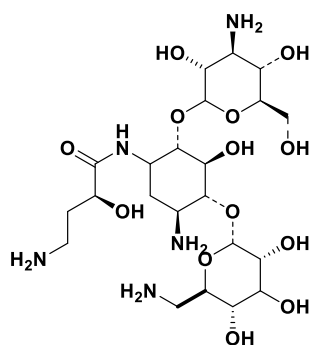
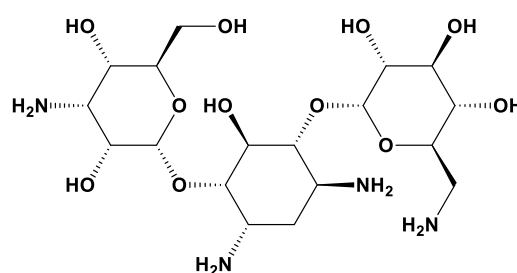


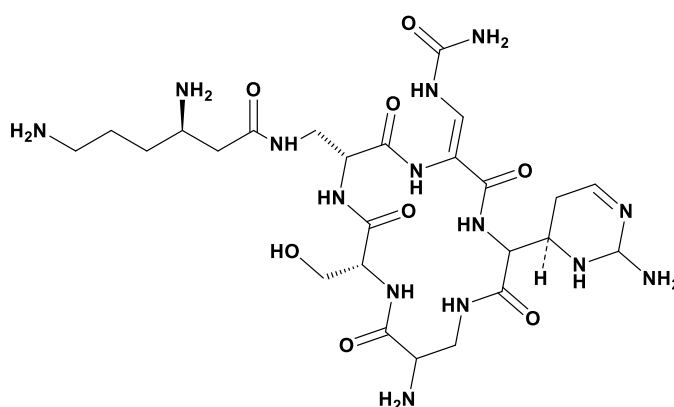
Figure 2. Antitubercular fluoroquinolones (Saravolatz and Leggett 2003).



Amikacin (8)



Kanamycin (9)



Capreomycin (10)

Figure 3. Antitubercular injectable aminoglycosides (Reeves et al. 2013).

1.3 NTM-infections: Therapy, resistance, and limitations

NTM are opportunistic pathogens found widespread in the environment and are increasingly infecting patients with structural lung diseases such as chronic obstructive pulmonary disease (COPD), cystic fibrosis (CF), and bronchiectasis (Park and Olivier 2015). The *Mycobacterium avium* complex (MAC; *M. avium*, *M. chimaera*, and *M. intercellularae*) and *Mycobacterium abscessus* complex (MABSC; *M. abscessus*, *M. massiliense*, and *M. bolletii*) comprise more than 95% of reported NTM infections (Lee et al. 2015; Park and Olivier 2015; Lande et al. 2019). Current therapy for MAC infections is combination oral therapy consisting of a macrolide (clarithromycin or azithromycin), ethambutol, and either rifampin or rifabutin for 18-24 months (Floto and

Haworth 2015; Park and Olivier 2015). Treatment for MABSC infections consists of parenteral therapy with amikacin and ceftazidime or imipenem for two to four months, followed by macrolide therapy with other oral (Floto and Haworth 2015). There is a growing concern that the prevalence of MABSC infections is becoming higher than that of MAC infections in CF patients worldwide (Floto and Haworth 2015; Park and Olivier 2015). MABSC infections in CF patients are particularly problematic as they result in accelerated inflammatory lung damage, are often difficult to treat (with 60-70% treatment failures despite years of combination therapy), and they preclude lung transplantation in many US and European centers (Floto and Haworth 2015). The current NTM therapy is long, expensive, and includes multidrug therapy with combinations of intravenous and oral antibiotics that are routinely ineffective (Franz et al. 2017).

The huge death toll, 1.3 million deaths in 2017 due to TB (WHO TB report, 2018) and increasing prevalence of NTM infections are great challenges that need to be addressed. The long duration of treatment (at least more than six months), development of resistance by *M. tb* against available antitubercular agents, and HIV-pandemics, increased pill burden, drug-drug interactions (DDIs), and toxic effects have made the management of TB extremely challenging. There is a lack of specific and effective drug regimen to combat NTM infections. Novel antimycobacterial agents to address these limitations in TB and NTM therapy are in great demand.

1.4 Primary Antibiotic Targets

The primary targets of most antibiotics are: a) cell wall biosynthesis, b) protein biosynthesis, c) DNA and RNA replication, and d) folate metabolism as shown in Figure 4 (Walsh 2003).

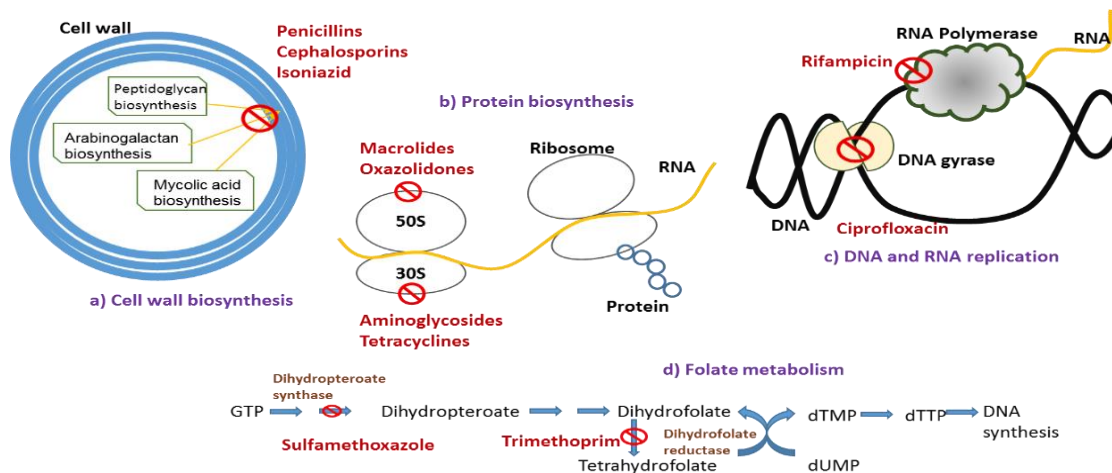


Figure 4. Primary antibiotic targets (modified from Walsh, 2003).

The cell wall is absent in mammalian cells, and is present in microorganisms, including bacteria and mycobacteria. The cell wall fortifies the cell membrane, and cytoplasmic organelles in microorganisms (Sarkar et al. 2017). Thus, inhibition of cell wall biosynthesis is one of the most successful strategies in treating bacterial infections. The most established classes of compounds that inhibit cell wall biosynthesis are penicillin and cephalosporin. Isoniazid, a potent first-line anti-TB drug also inhibits this target. Isoniazid inhibits an essential reductase (InhA) involved in the synthesis of mycolic acids (Timmins and Deretic 2006). Isoniazid is a pro-drug and needs the action of the mycobacterial catalase/oxidase KatG *in vivo* to convert into its active form, an isonicotinyl free radical (Timmins and Deretic 2006). This reactive free radical reacts with co-enzymes NAD^+ and NADP^+ generating isonicotinyl-NAD adducts that bind and inhibit InhA, resulting in the blocking of the mycolic acid biosynthetic pathway (Argyrou, Vetting, and Blanchard 2007) (Marrakchi et al. 2000). The mechanism involved in the resistance towards isoniazid by *M. tb* is the point mutation in the gene that encodes InhA encoded protein.

The inhibitors of protein biosynthesis in microorganisms act by inhibiting one of the important pathway in protein biosynthesis, including peptide chain elongation,

blocking ribosomes, or misreading the genetic code (Polikanov et al. 2018). The classes of antibiotics that inhibit protein biosynthesis are macrolides, aminoglycosides, and tetracyclines.

Nucleic acids (DNA and RNA) are the most important component of any living system. The process of cell division requires DNA replication first, and RNA is required for protein synthesis (Lindström 2009). The inhibition of nucleic acid synthesis inhibits the cell growth in no time. The classes of antibiotics that inhibit nucleic acids are quinolones and fluoroquinolones, metronidazole, and rifampin. Rifampicin disrupts the process of bacterial transcription by inhibiting RNA polymerase leading to the cell death (Wehrli 1983). *M. tb* had developed resistance against rifampicin by the modifications in beta subunits in RNA polymerase (Wehrli 1983).

Folic acid is also the most important requirement for cellular functioning primarily serving as a co-factor to methyl transferases for the biosynthesis of purine and thymidine (Kompis et al. 2005). The inhibition of folic acid leads to the inhibition of formation of the nucleic acid bases, ultimately leading to cell death. The class of antimicrobials that function by this mechanism are sulfonamides and trimethoprim.

The antimycobacterial drugs that act on different targets in mycobacteria is failing due to the development of resistance by mycobacterial pathogens against the available drugs. A novel compound that can block any of these primary target through novel mechanism is urgently needed.

1.5 Mycobacterial membrane protein large 3 (MmpL3): A novel antimycobacterial target essential for mycobacterial cell wall biosynthesis

The morphology, physiology, and normal functioning of *Mycobacteria* have been thoroughly studied. All bacteria, including *Mycobacteria*, possess a cell wall as a characteristic morphological requirement. The process of cell wall synthesis in

Mycobacteria has long been an attractive target for the discovery of antitubercular drugs, highlighted by isoniazid, one of the most effective and selective antitubercular agents.

The cell wall of *Mycobacteria* is comparatively thicker than the cell wall of other bacteria due to the presence of a thick mycolic acid layer in the form of mycolic acid-arabinogalactan-peptidoglycan (MAP) hetero-polymer complex (Jankute et al. 2015). Mycolic acids are large fatty acids called mycolic acids, which are long α -alkylated β -hydroxylated fatty acids (Figure 5), consisting of up to 90 carbon atoms (Al Dulayymi et al. 2006; Huang et al. 2001; Jackson 2014; Watanabe et al. 2002; Yuan and Barry 1996). The inhibition of mycolic acids biosynthesis or their transport to the cell wall from its site of synthesis in the cytoplasm disrupts the MAP assembly, which leads to weakened integrity of the cell wall and subsequent inhibition of cell growth (Jankute et al. 2015). Inhibition of the mycolic acids biosynthetic pathway is a viable anti-mycobacterial option.

The biosynthesis of mycolic acid (Figure 5) has been well studied and involves a series of biochemical reactions and enzymatic activity (Grzegorzewicz et al. 2012) (Marrakchi et al. 2014). Fatty acid synthase I (FAS-I) synthesizes C₂₂-C₂₆ chains, which are called as α -alkyl chains (Marrakchi et al. 2014). Fatty acid synthase II (FAS-II) catalyzes the addition of malonic acid in the C₂₂- C₂₆ chain to form meromycolyl chain (C₄₀-C₆₀) (Figure 5 Panel A) (Marrakchi et al. 2014; Li et al. 2014). The modification of the meromycolic chain is catalyzed by desaturases, methyl transferases, and dehydratases, which add essential functional groups (i.e. methyl, methoxy, cyclopropyl and ketone groups) (Figure 5, Panel A) in various positions of the meromycolyl chain (Li et al. 2014). The alpha chain is carboxylated by acyl CoA carboxylases (AccD4, AccD5) and the meromycolyl chain is adenylated by the acyl-AMP ligase FadD32.

These two activated chains are condensed together by the polyketide synthase (Pks13) followed by reduction by Corynebacterineae mycolate reductase A (CmrA), yielding mycolic acid (Grzegorzewicz et al. 2012). Mycolic acid as a trehalose ester (i.e. trehalose mono mycolate [TMM]), which is then shuttled to the periplasm by MmpL3 (Figure 5) (North et al. 2014). The antigen 85 complex (85A-C or Ag 85) transfers TMM to the arabinogalactan of the cell wall or converts it into trehalose dimycolate (TDM) (North et al. 2014). MmpL3 has a definite role in establishing the cell wall's virulence and integrity, however, little is known about the mechanism of the transporter protein. It is hypothesized that TMM transport is dependent upon the energy provided from the proton gradient across the membrane (Xu et al. 2017) (Li et al. 2019).

Structurally, MmpL3 is a protein belonging to the resistance-nodulation division (RND) superfamily, consisting of 12 transmembrane domains (Li et al. 2014). The inhibition of MmpL3 prevents the transport of mycolic acid in the form of TMM from the inner membrane to the outside of the cell wall (Grzegorzewicz et al. 2012), which results in the inhibition of cell growth. MmpL3 is a large protein transporter and a number of chemical scaffolds have been claimed in the literature that inhibit this transporter (Grzegorzewicz et al. 2012; Li et al. 2014; North et al 2014; Franz et al. 2017). Figure 6 depicts different MmpL3 inhibitors documented in the literature that possess various chemical scaffolds, suggesting MmpL3 is the target of multiple pharmacophores (Li et al. 2014). Inhibition of MmpL3 *in vivo* has resulted in significant protection against *M. tb*- and *M. abscessus*-infected mouse models supporting the high translational potential of this target (Pandya et al. 2019; Lun et al. 2013; Stec et al. 2016). Thus, MmpL3 is a novel drug target and an ideal pharmaceutical drug candidate that inhibits this target would potentially address the liabilities in the current anti-TB and anti-NTM therapies. Since, the MmpL3 is a novel target, where previous classes of

the marketed anti-TB agents have not been exposed to, it is believed that the novel inhibitors of this target would be active even against MDR- and XDR-TB.

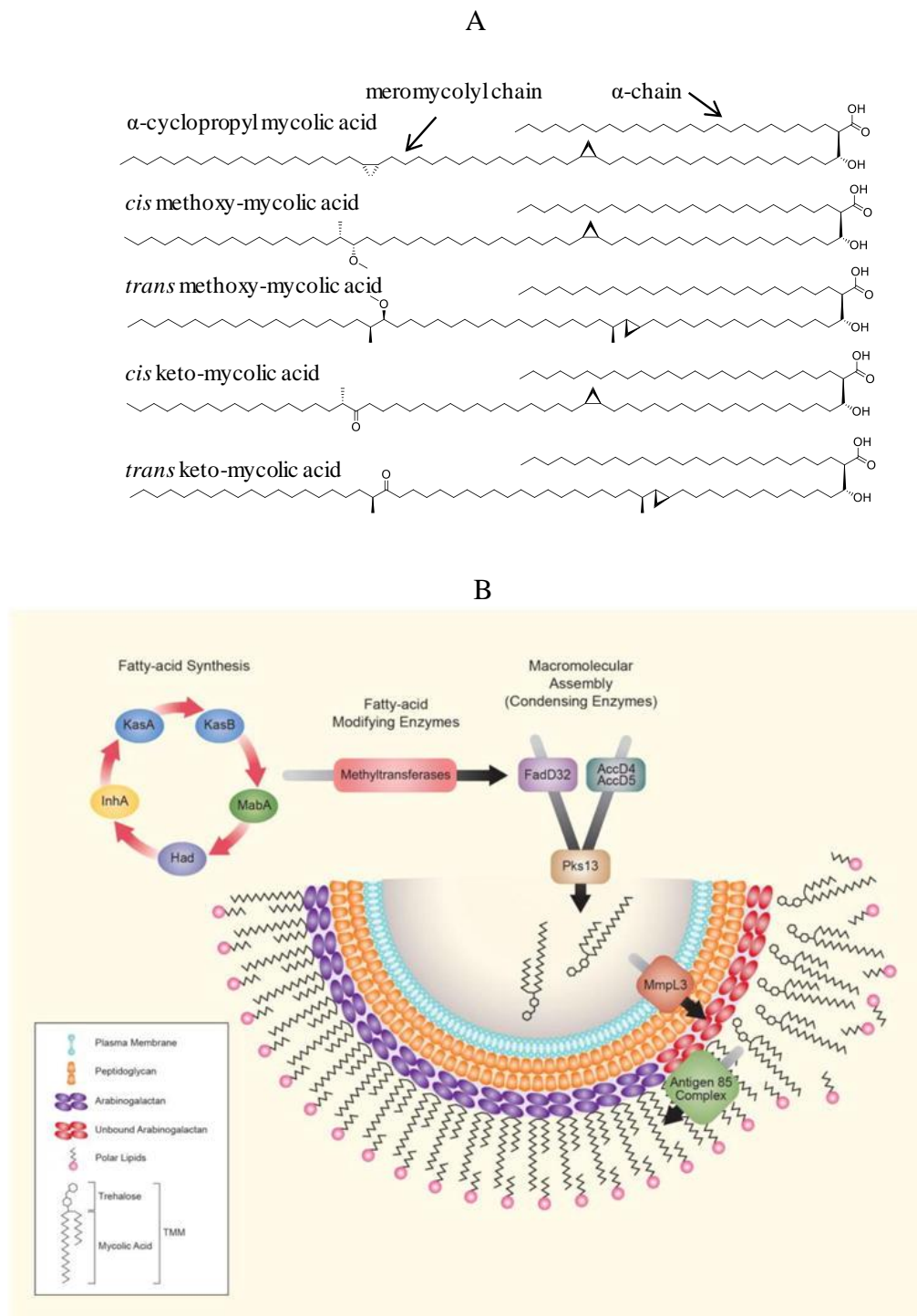


Figure 5. A) Structure of a mycolic acids depicting α -chain and meromycolyl chain;
 B) Process of mycolic acid biosynthesis and the role of MmpL3 (North et al. 2014).

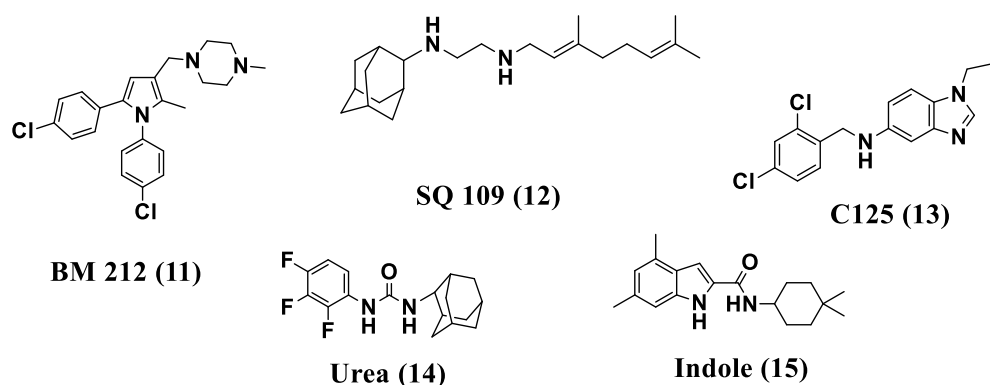


Figure 6. MmpL3 inhibitors discussed in the literature (North et al. 2014; Grzegorzewicz et al. 2012; Franz et al. 2017).

1.6 Urea- and indole-based MmpL3 inhibitors

1.6.1 Pharmacophore of urea- and indole-based MmpL3 inhibitors

Among the many chemical entities that seem to inhibit MmpL3, North lab identified and is currently developing urea- and indole-based inhibitors (Figure 6) (Li et al. 2014; North et al. 2013; Franz et al. 2017; Brown et al. 2011; Pandya et al. 2019). The urea- and indole-based inhibitors have demonstrated high potency against mycobacterial pathogens *in vitro* comparable or better than isoniazid MIC against *M. tb*, greater selectivity in their action as MmpL3 inhibitors compared to other gram positive and gram negative pathogens (Brown et al. 2011; Franz et al. 2017; North et al. 2013; Scherman et al. 2012) and have a good safety profile (Figure 7) (Brown et al. 2011; Scherman et al. 2012). For MmpL3 inhibition, the pharmacophore (3-D spatial arrangement of specific functional groups that elicit a desired biological action) for both the urea- and indole-based compounds is shown in Figure 7, consisting of: i) a bulky cycloaliphatic group (R_1), ii) an aromatic group **phenyl** (Figure 7, A) or **indole** (Figure 7, B), iii) two hydrogen bond (H-bond) donors (**NH**), and iv) one H-bond acceptor (**O**) (Li et al. 2014; Brown et al. 2011; North et al. 2013; Franz et al. 2017).

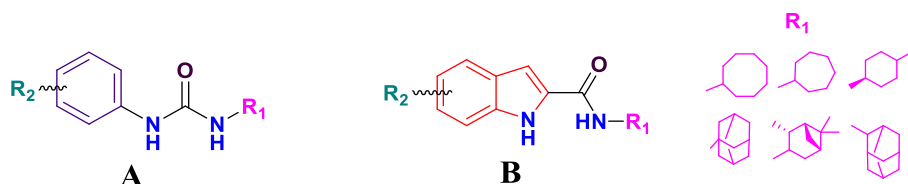
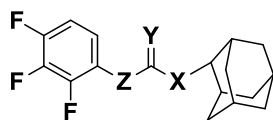


Figure 7. A) Pharmacophore requirements of urea- and B) indole-based compounds (Li et al. 2014; Brown et al. 2011; North et al. 2013; Franz et al. 2017)..

1.6.2 SAR of urea-based MmpL3 inhibitors

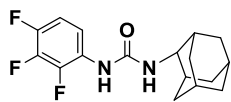
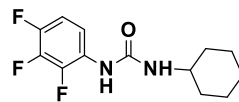
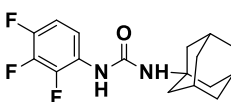
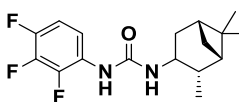
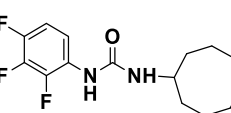
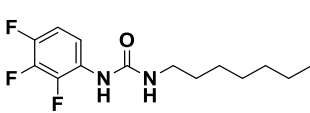
A high-throughput screening (HTS) is a routinely employed method utilized to identify hit candidates, and HTS was performed in 2011 by Brown et al. and identified a highly potent (*M. tb* MIC = 0.01 $\mu\text{g/mL}$; MIC, minimum inhibitory concentration is defined as the minimum concentration of the compounds to block the bacterial growth) and synthetically tractable urea-based compound (compound **14**) (Brown et al. 2011). An MIC value of 0.01 $\mu\text{g/mL}$ is excellent and comparable to INH, which has an MIC of approximately 0.02 $\mu\text{g/mL}$ (Rastogi et al. 1996). An operational definition of the potent compounds would be with an MIC \leq 0.4 $\mu\text{g/mL}$ and MIC \leq 2 $\mu\text{g/mL}$ would be considered as an optimal compound. In efforts to establish structure activity relationships (SAR), the importance of the urea moiety (pharmacophore points – two H-bond donors and one H-bond acceptor) was determined by modifying the urea core in compound **14** (Table 1). The replacement of the oxygen atom by a sulfur atom (S) in compound **16** (*M. tb* MIC = 0.8 $\mu\text{g/mL}$) resulted in a decrease in activity by 80-fold. This may be due to the fact that sulfur atom is a weaker H-bond acceptor than an oxygen atom because of lower electronegativity of S compared to O. The replacement of NH by O in compound **17** (*M. tb* MIC = 6 $\mu\text{g/mL}$) resulted in a greater drop in activity (600-fold). The methylation of one N atom in compound **21** (*M. tb* MIC = 6 $\mu\text{g/mL}$) or both N atoms in compound **19** (*M. tb* MIC = 12 $\mu\text{g/mL}$) resulted in depletion in the activity.

Table 1. MIC of *M. tb* in modified urea pharmacophore (Brown et al. 2011).

| No. | X | Y | Z | <i>M. tb</i> MIC ($\mu\text{g/mL}$) |
|-----------|-----|---|-----|---------------------------------------|
| 14 | NH | O | NH | 0.01 |
| 16 | NH | S | NH | 0.80 |
| 17 | O | O | NH | 6.00 |
| 18 | NH | O | NMe | 6.00 |
| 19 | NMe | O | NMe | 12.00 |

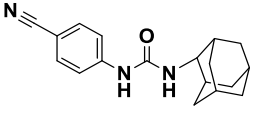
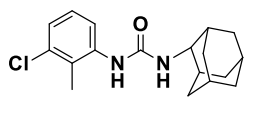
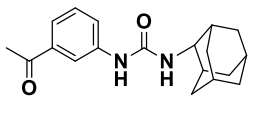
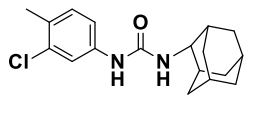
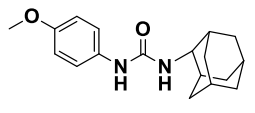
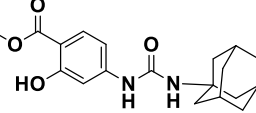
Compound **14** has a 2-adamantyl lipophilic head group which was replaced by various other lipophilic groups to determine head group SAR as shown in Table 2. The activity was maintained with the substitution by other bulky groups such as 1-adamantyl (compound **20**; *M. tb* MIC = 0.4 $\mu\text{g/mL}$), cyclooctyl (compound **21**; *M. tb* MIC = 0.8 $\mu\text{g/mL}$), and isopinocampheyl head group (compound **23**; *M. tb* MIC = 0.02 $\mu\text{g/mL}$). The 2-adamantyl substitution (compound **14**) was more potent than 1-adamantyl substitution (compound **20**) by 80-fold. The isopinocampheyl substitution (compound **23**) demonstrated an almost equivalent potency compared to lead compound **14**. Substitution with smaller cycloalkyl groups such as cyclohexyl in compound **22** (*M. tb* MIC = 12.5 $\mu\text{g/mL}$) and straight chain aliphatic groups such as n-heptyl (compound **24**; *M. tb* MIC = 6 $\mu\text{g/mL}$) resulted in greater loss of activity (600-fold and 1250-fold compared to the compound **14** respectively). These data suggested the necessity of the bulky aliphatic cycloalkyl head groups on the one side of the central urea moiety.

Table 2. MIC of different groups on R₁ (Brown et al. 2011).

| No. | Compounds | <i>M. tb</i> MIC ($\mu\text{g/mL}$) | No. | Compounds | <i>M. tb</i> MIC ($\mu\text{g/mL}$) |
|-----|---|---|-----|--|---|
| 14 |  | 0.01 | 22 |  | 12.50 |
| 20 |  | 0.40 | 23 |  | 0.02 |
| 21 |  | 0.80 | 24 |  | 6.00 |

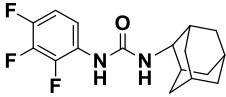
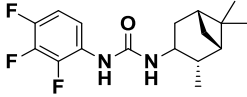
Finally, various substitutions on the phenyl ring, other than 2,3,4-trifluoro-substitutions at phenyl ring, were evaluated to determine the impact on activity (Table 3). Substitution at the para-position (compound **25**) or meta-position (compound **27**) of the phenyl ring resulted in potent compounds with MIC values of 0.4 $\mu\text{g/mL}$ and 0.1 $\mu\text{g/mL}$ respectively. The substitutions at the ortho-positions shown in compound **26** resulted in the largest decrease in activity. Compound **26** with an ortho-methyl (*M. tb* MIC = 1.6 $\mu\text{g/mL}$) substitution was 16-fold less potent than compound **28** with para-methyl substitution (*M. tb* MIC = 0.1 $\mu\text{g/mL}$). The incorporation of functional groups containing polar heteroatoms (seen in compounds **25**, **27**, **29**, and **30**) on the phenyl ring or substitutions with a lipophilic chloro group (compound **28**) did not greatly effect activity. Overall, various substitutions at either the meta- or ortho- positions were better tolerated than substitutions at the ortho-position.

Table 3. Effects of substitutions on phenyl ring with adamantyl head group (Brown et al. 2011).

| No | Compounds | <i>M. tb</i> MIC (µg/mL) | No | Compounds | <i>M. tb</i> MIC (µg/mL) |
|----|--|--------------------------|----|---|--------------------------|
| 25 |  | 0.4 | 26 |  | 1.6 |
| 27 |  | 0.1 | 28 |  | 0.1 |
| 29 |  | 0.4 | 30 |  | 0.4 |

The lead ureas have optimum potency comparable to isoniazid, however, the problems associated with them were poor aqueous solubility, leading to poor ADME. (Brown et al. 2011) (North et al. 2013). This is highlighted in Table 4 by two lead ureas. The human plasma protein binding of 98.2% of compound **14** and 99.2% of compound **23** is high, and may impact factors such as dosing regimen, drug-drug interactions (DDIs), and metabolism (North et al. 2013; Zeitlinger et al. 2011). Compounds **14** and **23** were potent at sub-µg/mL concentrations and were active against resistant strains of *M. tb*. However, high lipophilicity and low aqueous solubility (<0.1 µg/mL) prevented them from being ideal pharmaceutical leads.

Table 4. Physicochemical and PK properties of **14** and **23** (North et al. 2013).

| | Compound 14 | Compound 23 |
|-------------------|---|---|
| Properties |  |  |
| MIC | 0.01 µg/mL | 0.02 µg/mL |
| cLogP | 5.1 | 5.2 |
| Solubility | <0.1 µg/mL | <0.1 µg/mL |
| HPPB | 98.8% | 99.2% |
| Activity | Active against MDR-TB and XDR-TB | Active against MDR-TB and XDR-TB |

cLogP: calculated LogP, HPPB: Human Plasma Protein Binding

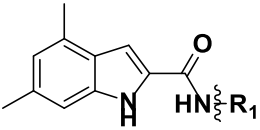
1.6.3 SAR of indole-based MmpL3 inhibitors compounds

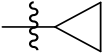
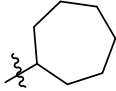
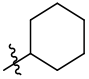
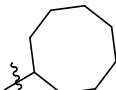
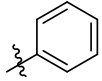
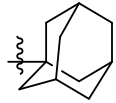
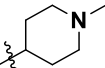

The indoles are bioisosteres of the urea-series, and indoles exhibited similar biological responses to that of urea-based inhibitors. The rationale to develop indoles from urea was to identify additional effective chemotypes and to improve the physicochemical and pharmacokinetic profiles of the urea analogs while maintaining the essential pharmacophore. The basic pharmacophore requirements are met by indole-based compounds, which are shown in Figure 7.

Initial SAR efforts were aimed at identifying an optimum head group (R_1) (Table 5) that conferred desired potency to the compounds. The substitutions by smaller groups such as cyclopropyl in compound **31** (*M. tb* MIC = 127 µg/mL) resulted in complete loss of activity while a cyclohexyl in compound **32** (*M. tb* MIC = 0.25 µg/mL) retained

high potency. However, the maximum potency was seen with 1-adamantyl in compound **37** (*M. tb* MIC = 0.0038 µg/mL), 2-adamantyl in compound **38** (*M. tb* MIC = 0.0038 µg/mL), and cyclooctyl in compound **36** (*M. tb* MIC = 0.0039 µg/mL). The cycloheptyl substitution **35** (*M. tb* MIC = 0.015 µg/mL) was also highly potent but slightly less than the adamantyl and cyclooctyl substitutions. Aromaticity in the head group, shown in the phenyl substitution (compound **33**) resulted in 200-fold loss in activity versus adamantyl substitutions. Heteroatom substitution in the alicyclic ring also resulted in a decrease in the activity. For instance, piperidine substitution (compound **34**) was approximately 500-fold less potent than cyclohexyl substitution (compound **32**). This showed that any heteroatom substitutions in the head group was detrimental to the antitubercular activity. Similar to the urea series, the bulky head groups such as cyclooctyl (cycloheptyl (compounds **35**), compound **36**), 1-adamantyl (compound **37**), and 2-adamantyl (compound **38**) were the ideal head groups based on their MIC values. On the other hand, the small head groups such as cyclopropyl (compound **31**), cyclopentyl (compound **32**), and phenyl (compound **33**) resulted in decreased potency.

Table 5. *M. tb* MIC of various indole-based scaffolds (Onajole et al. 2013).



| No. | R | <i>M. tb</i> MIC ($\mu\text{g/mL}$) | No. | R | <i>M. tb</i> MIC ($\mu\text{g/mL}$) |
|-----|---|--|-----|---|--|
| 31 |  | 127 | 35 |  | 0.015 |
| 32 |  | 0.25 | 36 |  | 0.0039 |
| 33 |  | 1 | 37 |  | 0.0038 |
| 34 |  | 127.6 | 38 |  | 0.0038 |

The difference in the potency due to various substitutions at the indole ring was also studied (Table 6). The mono-methyl substitution at 4-position (compound **39**; *M. tb* MIC=0.0312 $\mu\text{g/mL}$), 6-position (compound **40**; *M. tb* MIC = 0.0312 $\mu\text{g/mL}$), and 7-position (compound **41**; *M. tb* MIC = 0.994 $\mu\text{g/mL}$) were slightly less potent than 4,6-dimethylsubstituents (compound **36**; *M. tb* MIC = 0.0039 $\mu\text{g/mL}$). The dimethyl substituents imparted more lipophilicity, which may have accounted for higher potency. The mono-substitution at 7-position (compound **41**; *M. tb* MIC = 0.994 $\mu\text{g/mL}$) had a decreased activity by approximately 30-fold compared to mono-substitution at 4- or 6-positions (compound **39**; *M. tb* MIC = 0.031 $\mu\text{g/mL}$ and compound **40**; *M. tb* MIC

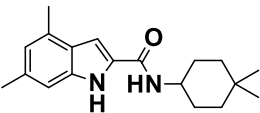
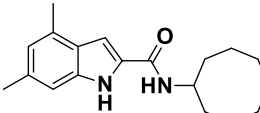
=0.031 $\mu\text{g/mL}$). The bromo-substitution at the 6-position in compound **42** (*M. tb* MIC= 0.03 $\mu\text{g/mL}$) imparted equivalent potencies compared to monomethyl substitution at the same position compound **40** (*M. tb* MIC= 0.031 $\mu\text{g/mL}$). The 4,6-ditrifluoromethane substitution in compound **43** (*M. tb* MIC = 0.016 $\mu\text{g/mL}$) was less potent than 4,6-dimethylsubstitutions in compound **36** (*M. tb* MIC = 0.0038 $\mu\text{g/mL}$). The most potent compound was with a 4,6-dichlorosubstitution shown in compound **45** (*M. tb* MIC = 0.0037 $\mu\text{g/mL}$). The bulky chlorine group imparts increased lipophilicity which might have resulted in increased mycobacterial membrane penetration leading to high activity. The introduction of 4,6-difluoro substitution in compound **44** (*M. tb* MIC =0.03061 $\mu\text{g/mL}$) did not improve activity over compound **45**.

Similar to the urea series, the indole series also possessed poor aqueous solubility, high lipophilicity, and poor absorption profiles (Kondreddi et al. 2013; Onajole et al. 2013; Stec et al. 2016; Pandya et. al 2019; Lun et al. 2013) as shown in Table 7. To highlight these properties, indoles representative compounds **15** and **36** are shown in Table 7. The indole lead compounds were active against resistant strains of *M. tb* and imparted desirable safety profiles, exemplified by compounds **15** and **36**. They achieved selectivity indices, a measure of safety profiles, of >1333 for compound **15** and >16000 for compound **36** (Onajole et al. 2013; Stec et al. 2016). However, they possessed aqueous solubility less than 1 $\mu\text{g/mL}$, and high lipophilicity (compound **15**; cLogP = 6.1, compound **36**; cLog P = 5.74) (Onajole et al. 2013; Stec et al. 2016), precluding both compounds from being considered ideal drug leads. Additionally, indoles exhibited *in vivo* efficacy against *M. tb* and *M. abscessus* in mouse models of acute infections (Pandya et al. 2019; Lun et al. 2013; Rao et al. 2013; Stec et al. 2016). These compounds also demonstrated excellent *in vivo* safety profiles. However, their poor aqueous solubility limited the further translational potential of indoles.

Table 6. MIC of different substitution at indole ring with cyclooctyl head group (Onajole et al. 2013; Stec et al. 2016; Franz et al. 2017).

| No. | Compounds | <i>M. tb</i> MIC ($\mu\text{g/mL}$) |
|-----|-----------|---------------------------------------|
| 36 | | 0.0038 |
| 39 | | 0.0312 |
| 40 | | 0.0312 |
| 41 | | 0.994 |
| 42 | | 0.03 |
| 43 | | 0.016 |
| 44 | | 0.0306 |
| 45 | | 0.0037 |

Table 7. Physicochemical and PK profiles of **15** and **36** (Onajole et al. 2013) (Stec et al. 2016).

| | 15 | 36 |
|-------------------|---|---|
| Properties |  |  |
| <i>M. tb</i> MIC | 0.015 µg/mL | 0.0038 µg/mL |
| cLogP | 6.1 | 5.74 |
| Solubility | <1 µg/mL | <1 µg/mL |
| Selectivity Index | >1333 | >16000 |
| Activity | Active against MDR-TB and XDR-TB | Active against MDR-TB and XDR-TB |

1.7 Summary

The lengthy course of treatment for drug-susceptible strains of *M. tb* and ineffective treatment against MDR-TB and XDR-TB have made TB a global challenge. The increasing prevalence of NTM-infections and lack of effective treatment regimen has rendered the treatment of NTM-infections problematic. Novel anti-TB and -NTM agents with shorter treatment durations and novel mechanisms that can treat all strains are urgently needed. The inhibition of cell wall biosynthesis is one of the most established drug targets in antimicrobial realm. MmpL3 is an important target, and its inhibition leads to the inhibition of cell growth. The lead ureas and indoles have been found to be potent MmpL3 inhibitors and have helped determine the role and essentiality of MmpL3 in mycobacterial cell wall biosynthesis. However, the ureas and indoles have poor physicochemical and pharmacokinetic profiles, mainly poor aqueous solubility. Therefore, they will likely have limited success through the drug

development process. New chemical entities that retain the essential pharmacophore requirements as MmpL3 inhibitors with enhanced pharmacokinetic profiles should lead to more ideal preclinical drug candidates.

This project is based on the hypothesis which is stated as, ‘Medicinal chemistry ligand-based optimization of the indole series to generate the acetamide series maintains the pharmacophore while decreasing the percentage of lipophilic carbon atoms, thus retaining potent antimycobacterial activity and increasing aqueous solubility.’ To test the hypothesis, following specific aims were proposed:

- Specific aim 1: Design, synthesis, and characterization of novel antimycobacterial agents (Chapter 2)
- Specific aim 2: Assessment of mycobacterial activity and study on SAR (Chapter 2)
- Specific aim 3: Assessment of physicochemical, pharmacokinetic, and safety profiles of the compounds (Chapter 3)

CHAPTER 2: Design, synthesis, and assessment of mycobacterial activity of novel antimycobacterial agents

2.1 Introduction

The previously published lead indole-based compounds achieved high potency with sub- $\mu\text{g/mL}$ MIC values with a safe pharmacological profile (Pandya et al. 2019; Franz et al. 2017). However, they had poor physicochemical properties, mainly aqueous solubility and pharmacokinetic profiles which will likely limit their translational potential. Therefore, the central hypothesis of this thesis is that medicinal chemistry optimization of the indole-based scaffolds to enhance the aqueous solubility will retain high antimycobacterial activity and lead to improved pharmacokinetic profiles.

2.2 Ligand-based drug design approach identifying novel acetamides

As mentioned in Chapter 1, the pharmacophore requirements of the indole-based compounds are: i) the bulky cycloaliphatic groups (R_1), ii) an aromatic group (phenyl or indole), iii) at least one H-bond donor (represented as NH), and iv) one H-bond acceptor (represented as O) (Li et al. 2014; Brown et al. 2011; North et al. 2013; Franz et al. 2017; Stec et al. 2016) as shown in Figure 8.

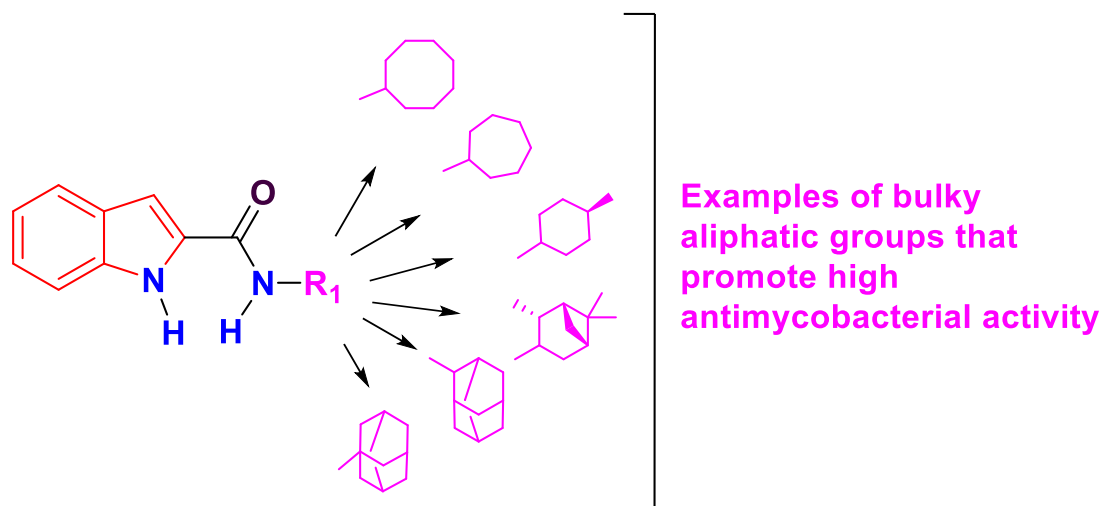


Figure 8. Pharmacophore of indole-based compounds.

Ligand-based drug design is an approach of designing new compounds by the bioisosteric replacement of specific functional groups while retaining the essential

pharmacophore points. The current research project utilized this approach to modify indoles to enhance the aqueous solubility of the compounds and maintain high antimycobacterial activity. A classic medicinal chemistry approach to improving the aqueous solubility of a compound is to increase its polarity. This can be done by a) increasing the number of polar heteroatoms, b) decreasing the number of lipophilic atoms or groups, c) introducing charge/ionizable groups or d) increasing 3-D sp³ characteristics (Lovering et al. 2009; Lovering 2013; Ishikawa and Hashimoto 2011; North et al. 2013). Our adopted approach was to “open” the indole ring by removal of the lipophilic 3-CH group as shown in Figure 9, yielding the acetamide series. The acetamides compared to the parent indole-based compounds have a) effectively increased the heteroatom percentage, b) reduced lipophilicity by removal of the lipophilic 3-CH group, and c) increased 3-D sp³ characteristics, thereby reducing planarity and decreasing the crystal lattice energy of the planar structure leading to enhanced aqueous solubility as solvation energy gets increased relatively (Lovering et al. 2009; Lovering 2013; Ishikawa and Hashimoto 2011). Thus, it was hypothesized that ‘Medicinal chemistry ligand-based optimization of the indole series to generate the acetamide series will maintain the pharmacophore while decreasing the percentage of lipophilic carbon atoms, thus retaining potent antimycobacterial activity and increasing aqueous solubility.’

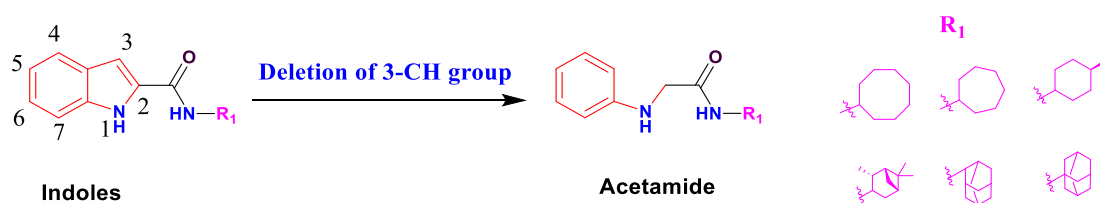


Figure 9. Medicinal chemistry strategy to enhance aqueous solubility.

2.3 Novel acetamide SAR

To facilitate understanding of the unique moieties in the scaffold and develop the SAR, the acetamides were divided into a cycloaliphatic bulky moiety, acetamide moiety, and phenyl moiety as shown in Figure 10.

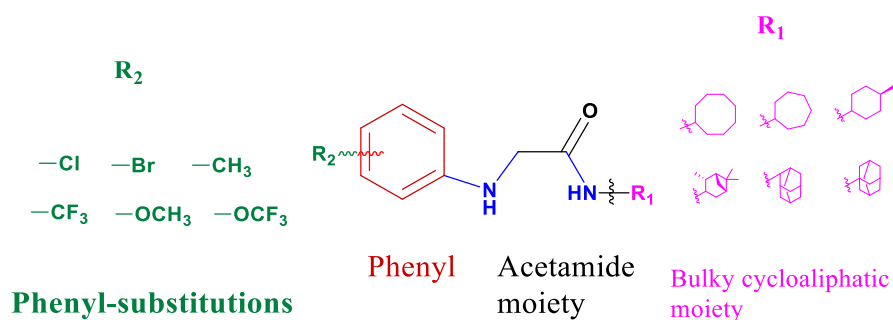
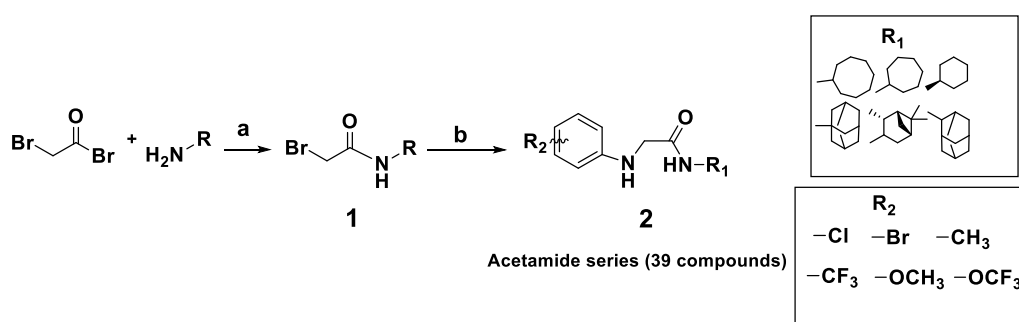


Figure 10. Moieties within the acetamides

The acetamides were designed to establish SAR, retain high antimycobacterial activity, and increase aqueous solubility over the indole-based inhibitors. The six cycloaliphatic groups as defined by R_1 (cyclooctyl, cycloheptyl, transmethylcyclohexyl, 1-adamantane, 2-adamantane, and (1R,2R,3R,5S)-(-)-isopinocamphe) in Figure 10, were the moieties that exhibited excellent MIC values with sub- $\mu\text{g/mL}$ concentrations in both the urea and indole series (Franz et al. 2017) (Brown et al. 2011). These groups (R_1) are the part of the essential pharmacophore requirement and typically promote optimal activity, and these groups must be present as they are a portion of pharmacophore points. The substitution in the aniline ring (R_2), as shown in Figure 10, was to modulate both activity and aqueous solubility, by introducing varying functional groups with various degrees of electronic, steric, and lipophilic/hydrophilic properties.

2.4 Synthesis of acetamide series

The synthetic scheme for the acetamide series is shown in Scheme 1. Briefly, acetamides were synthesized by reacting commercially available bulky cycloaliphatic amines with bromoacetyl bromide in the presence of triethylamine (TEA) at 0° Celsius (C) forming the acetamide intermediate **1**. The N-cycloalkyl-2-bromoacetamide intermediates (**1**) were then reacted with substituted aniline analogs in the presence of TEA under reflux conditions yielding acetamide final products (**2**). The overall percentage yields were 25% - 70%. The compounds were characterized by mass spectroscopy (molecular weight), ¹H and ¹³C NMR (structural connections), and HPLC (purity).



Scheme 1. Synthetic pathway for the production of acetamide series. Reagents and conditions: (a) Triethylamine (TEA), Dichloromethane (DCM), 0 °C, 4 h; (b) aniline analogs, TEA, THF, 60 °C, overnight.

2.5 Microbiological assessment

The *in vitro* phenotypic screening against whole-cell mycobacteria to determine MIC values is a routinely employed simple and rapid method to determine initial compound

antimicrobial efficacy (Li et al. 2019). MIC is defined as the minimum concentration of the compound required to prevent bacterial growth. To determine the MIC value, compounds are serially diluted into a 96-well plate to make inhibitor plates. Mycobacterial pathogens are then added to the inhibitor plates and incubated for seven days, where growth inhibition is determined. The most commonly used methods to determine MIC values are resazurin-based microtiter plate assays (REMA) and visual screening methods (Sharma et al. 2014; Li et al. 2019). Resazurin, which is a deep-blue color in physiological buffer, is reduced to resofurin, a pink fluorescent product, by the mitochondrial metabolic activity of the viable cells by the oxidation of reduced-nicotinamide adenine dinucleotide (NADH) to NAD^+ (Figure 11) (Riss et al. 2016). The amount of resofurin produced is proportional to the number of viable cells, which can be quantified via microplate fluorometer at an excitation wavelength of 560 nm and an emission wavelength of 590 nm (Riss et al. 2016).

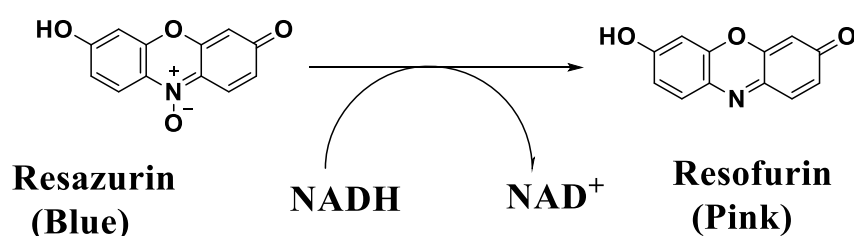


Figure 11. A reaction depicting REMA (Riss et al. 2016).

The other commonly used method is the visual screening method. In this method, the cell pellets are visually inspected to determine bacterial growth inhibition. An example of a visually screened microplate is shown in Figure 12. Generally, REMA accounts for the viable cells, which include both static cells and growing cells while visual screening accounts only for the growing cells. Visual screening method was used to determine MIC value of the novel compounds. For the initial assessment of the activity,

the acetamides were screened against *Mycobacterium tuberculosis* (*M. tb* H37Rv mc2 6206 strain) and *Mycobacterium abscessus* (ATCC 19977). The assessment of antimycobacterial activity was performed at Colorado State University by Dr. Mary Jackson's lab.

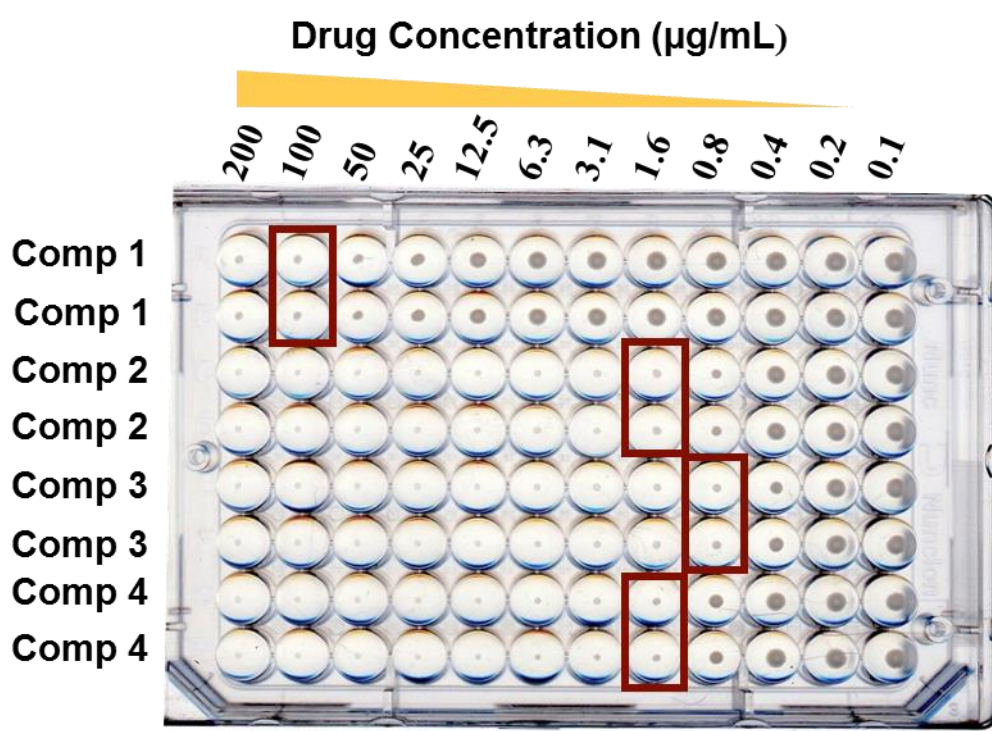


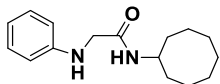
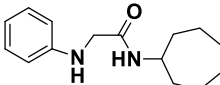
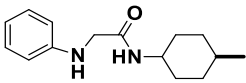
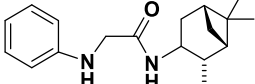
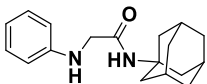
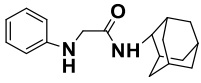
Figure 12. MIC determination by visual screening method

2.6 Structure activity relationship (SAR) of acetamide series

To facilitate the understanding of SAR, two points of structural diversity i) cycloaliphatic groups, R_1 and ii) substitutions on aniline, R_2 were studied. First, the influence of these various cycloaliphatic groups on their antimycobacterial activity (Table 8) was assessed. The cyclooctyl, cycloheptyl, and transmethylcyclohexyl head groups (**149**, **150**, and **151** respectively) were inactive with MIC values of 64 µg/mL or higher against both the *M. abscessus* and *M. tb* strains. The acetamide with

(1R,2R,3R,5S)-(-)-isopinocampheyl head group (**152**) exhibited the highest activity among all the unsubstituted anilines with an MIC value of 8 µg/mL against both *M. abscessus* and *M. tb*. The 1-adamantyl head group substituted acetamide (**153**) also exhibited some activity against *M. abscessus* (16 µg/mL) and *M. tb*. (32 µg/mL). However, the 2-adamantyl head group (**182**) was inactive against *M. abscessus* but moderately active against *M. tb*. (16 µg/mL). Also, the acetamide with the 2-adamantyl head group and unsubstituted aniline (**182**) was active against *M. tb* but was inactive against *M. abscessus*. The 1-adamantyl, 2-adamantyl, and (1R,2R,3R,5S)-(-)-isopinocampheyl head groups were more active compared to the cyclooctyl, cycloheptyl, and transmethylcyclohexyl head groups.

Table 8. Antimycobacterial activity of unsubstituted aniline with various cycloaliphatic groups.

| North No. | Structure | <i>M. abscessus</i> MIC (µg/mL) | <i>M. tb</i> MIC (µg/mL) |
|-----------|---|---------------------------------|--------------------------|
| 149 |  | >64 | 64 |
| 150 |  | >64 | 64 |
| 151 |  | >64 | 64 |
| 152 |  | 8 | 8 |
| 153 |  | 16 | 32 |
| 182 |  | >64 | 16 |

After determining the optimal head groups for antimycobacterial activity, various functional groups with varying steric, electronic and lipophilic/hydrophilic properties were substituted at the ortho, meta, and para positions on aniline were evaluated to further determine SAR for the acetamides. These functional groups were chloro, bromo, methyl, methoxy, trifluoromethyl, and trifluoromethoxy. Chloro and bromo groups are bulky lipophilic moieties and impart overall increase in lipophilicity, with the bromo group being bulkier than the chloro group. Chloro- and bromo-substitutions are also electron withdrawing groups through induction but donate electrons to the system through resonance. The methyl group is an electron donating group through induction, while trifluoromethyl is an electron withdrawing group. The methoxy and trifluoromethoxy groups are midrange bulky groups (i.e. larger than methyl and hydrogen but smaller than chloro and bromo) and are complimentary to each other. Methoxy is a strong electron donating group through resonance, however trifluoromethoxy is a long-range electron withdrawing group. These various substitutions helped us understand the influence of sterics and electronics on antimycobacterial activity.

Initial efforts to determine SAR on the aniline ring were with using the optimal head group (1R,2R,3R,5S)-(-)-isopinocamphe (Table 8, compound **152**) and aniline substituted at the para position (Table 9). The para-position was chosen to be evaluated first since CYP-mediated para-hydroxylation is a common metabolic reaction on phenyl rings. Compounds para-substituted with chloro or bromo groups had 2-fold enhanced activity against *M. abscessus* over the unsubstituted analog (compound **152**). They had no improvement against *M. tb*. The para-methyl substitution (**161**) did not

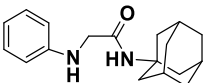
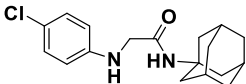
show any increased potency as compared to unsubstituted counterpart, however the para-methoxy decreased activity against both strains. The para-trifluoromethyl substitution, **189**, did not exhibit significant activity, whereas para-trifluoromethoxy aniline, **190**, achieved the highest activity in this series against *M. abscessus* and *M. tb* with MIC values of 1 µg/mL and 4 µg/mL respectively. Therefore, all the compounds with (1R,2R,3R,5S)-(-)-isopinocampheane head group exhibited antimycobacterial activity, with the para-trifluoromethoxy having optimal activity.

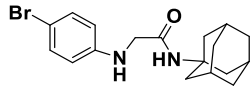
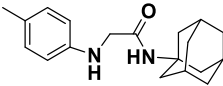
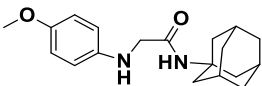
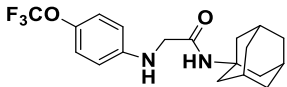
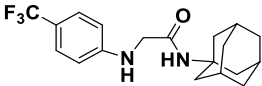
Table 9. MIC of substituted aniline at para positions with (1R,2R,3R,5S)-(-)-isopinocampheyl head group against *M. abscessus* and *M. tb*.

| North No. | Structure | <i>M. abscessus</i> MIC (µg/mL) | <i>M. tb</i> MIC (µg/mL) |
|-----------|-----------|---------------------------------------|-----------------------------|
| 152 | | 8 | 8 |
| 159 | | 4 | 16 |
| 160 | | 4 | 16 |
| 161 | | 8 | 16 |
| 162 | | 32 | 64 |
| 189 | | 32 | 16 |
| 190 | | 1 | 4 |

The six para-substituted aniline analogs were also evaluated with the 1-adamantyl head group and are shown in Table 10. The para-chloro substituted (**175**) was more potent than unsubstituted counterpart (**153**, *M. abscessus* MIC = 16 µg/mL, *M. tb* MIC = 32 µg/mL) by 2-fold against *M. abscessus* and 4-fold against *M. tb*. Similarly, bromo-substituted, **176**, was more potent than para-chloro substitutions by 2-fold for both *M. abscessus* and *M. tb*. This suggested that bulky, electron withdrawing and lipophilic p-substitutions also resulted in increased activity, even more so with the 1-adamantyl head group. The para-methyl and para-methoxy analogs (**177** and **178**) resulted in a decreased activity. The trifluoromethoxy substitution with 1-adamantyl head group (**179**) resulted in an augmented activity with 8-fold increment against *M. abscessus* and 2-fold increment against *M. tb*. The trifluoromethyl substitution with 1-adamantyl head group (**180**) also resulted in an increased activity compared to unsubstituted aniline. Similar to the (1R,2R,3R,5S)-(-)-isopinocamphe series, bulky, electron withdrawing and lipophilic groups at the para position were optimal for antimycobacterial activity.

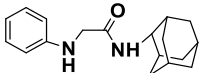
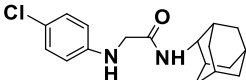
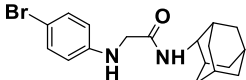
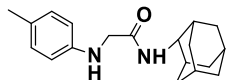
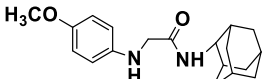
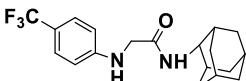
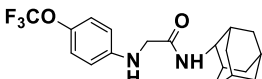
Table 10. MIC of substituted aniline at para positions with 1-adamantyl head group against *M. abscessus* and *M. tb*.

| North No. | Structure | <i>M. abscessus</i> MIC (µg/mL) | <i>M. tb</i> MIC (µg/mL) |
|------------|---|------------------------------------|-----------------------------|
| 153 |  | 16 | 32 |
| 175 |  | 4 | 16 |

| North No. | Structure | <i>M. abscessus</i> MIC | <i>M. tb.</i> MIC |
|-----------|--|-------------------------|----------------------|
| | | ($\mu\text{g/mL}$) | ($\mu\text{g/mL}$) |
| 176 |  | 2 | 8 |
| 177 |  | 32 | 32 |
| 178 |  | 32 | 32 |
| 179 |  | 2 | 16 |
| 180 |  | 8 | 8 |

The six para-substituted anilines were also evaluated with the 2-adamantyl head group, which was the third head group that achieved antimycobacterial activity in the unsubstituted series (Table 11). A similar SAR was seen in 2-adamantane substituted compounds. Despite the para-chloro substituted aniline (**183**) being inactive, the para-bromo substituted aniline (**184**) was 16-fold more potent against *M. abscessus* and 4-fold more potent against *M. tb* in comparison to unsubstituted aniline (**182**). The trifluoromethyl substituted aniline (**187**, *M. abscessus* MIC = 4 $\mu\text{g/mL}$, *M. tb* MIC = 2 $\mu\text{g/mL}$) and trifluoromethoxy substituted aniline (**188**, *M. abscessus* MIC = 2 $\mu\text{g/mL}$, *M. tb* MIC = 4 $\mu\text{g/mL}$) exhibited good potencies against both strains. Aside from the para-chloro analog being inactive, which is contrary to the established SAR from the (1R,2R,3R,5S)-(-)-isopinocampheyl and 1-adamantyl series, bulky, electron withdrawing and lipophilic substituents were optimal for activity.

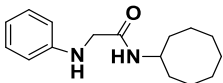
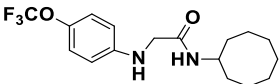
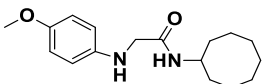
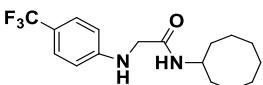
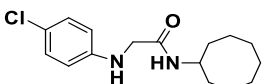
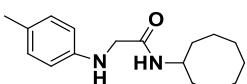
Table 11. MIC of substituted aniline at para positions with 2-adamantyl head group against *M. abscessus* and *M. tb.*

| No. | Structure | <i>M. abscessus</i> MIC ($\mu\text{g/mL}$) | <i>M. tb.</i> MIC ($\mu\text{g/mL}$) |
|-----|---|--|---|
| 182 |  | >64 | 16 |
| 183 |  | >64 | 64 |
| 184 |  | 4 | 4 |
| 185 |  | 16 | 4 |
| 186 |  | 32 | 32 |
| 187 |  | 4 | 2 |
| 188 |  | 2 | 4 |

In an effort to determine if para-substituted aniline groups could restore antimycobacterial activity of the cyclooctyl head group, which is arguably the most potent head group across a panel of mycobacterial pathogens in the indole series (Franz

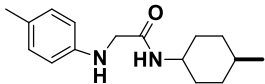
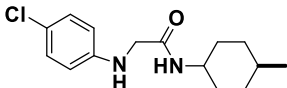
et al. 2017), six compounds with this head group was tested for their antimycobacterial activity. The cyclooctyl head group did not exhibit significant activity regardless of the identity of any para substitution on the aniline moiety (Table 12). As expected, the bulky, electron withdrawing, and lipophilic chloro substituent (**157**) achieved modest activity against *M. abscessus* (32 $\mu\text{g/mL}$) but not against *M. tb*. In addition, the trifluoromethoxy substitution seen in compound **154** showed the highest activity against *M. abscessus* (8 $\mu\text{g/mL}$) and *M. tb* (32 $\mu\text{g/mL}$). Despite the modest activity seen with the para-chloro and para-trifluoromethoxy groups, no para-substituted aniline was able to appreciably improve the activity with a cyclooctyl head group (Table 12).

Table 12. MIC of substituted aniline at para positions with cyclooctyl head group against *M. abscessus* and *M. tb*.

| North No. | Structure | <i>M. abscessus</i> MIC ($\mu\text{g/mL}$) | <i>M. tb</i> MIC ($\mu\text{g/mL}$) |
|-----------|---|--|---------------------------------------|
| 149 |  | >64 | 64 |
| 154 |  | 8 | 32 |
| 155 |  | >64 | 64 |
| 156 |  | 64 | 32 |
| 157 |  | 32 | 64 |
| 158 |  | >64 | 32 |

The para-substituted anilines were also unable to restore activity with trans-methylcyclohexyl head group as shown in Table 13. Compounds **163** and **164** possessed trans-methylcyclohexyl head groups with para-methyl substitution and para-chloro substitution respectively, and both were inactive. This pointed towards the importance of lipophilic and rigid bulky groups in imparting antimycobacterial activity.

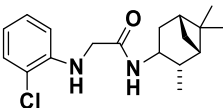
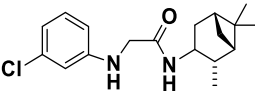
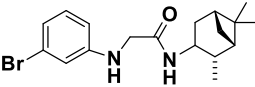
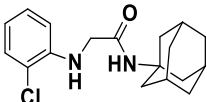
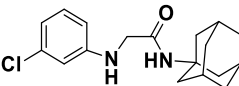
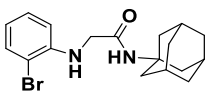
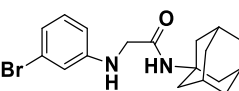
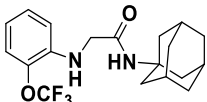
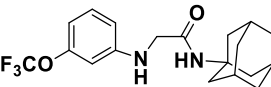
Table 13: MIC of substituted aniline at para positions with trans-methylcyclohexyl head group against *M. abscessus* and *M. tb*.

| North No. | Structure | <i>M. abscessus</i> MIC (µg/mL) | <i>M. tb</i> MIC (µg/mL) |
|------------|---|---------------------------------|--------------------------|
| 163 |  | >64 | 64 |
| 164 |  | >64 | 64 |

After determining the optimal identity of para-substitutions on the aniline ring, the role of ortho and meta substitutions were determined. The ortho and meta analogs using chloro, bromo, and trifluoromethoxy groups, which exhibited good potencies in either *M. abscessus* or *M. tb* (**159**, **160**, **175**, **176**, and **179**) were also screened for their antimycobacterial activity shown in Table 14. These were determined using the two most active head groups (1R,2R,3R,5S)-(-)- isopinocampheane and 1-adamantane. Compounds **191** (*M. abscessus* MIC = 1 µg/mL, *M. tb* MIC = 0.25 µg/mL) and **192** (*M. abscessus* MIC = 0.5 µg/mL, *M. tb* MIC = 0.25 µg/mL) were ortho-chloro and meta-chloro substituted aniline analogs respectively with (1R,2R,3R,5S)-(-)-isopinocampheyl head group and achieved optimum antimycobacterial activity. The increase in activity at the meta-substitutions (bromo and trifluoromethoxy) was seen

for all the compounds tested. However, except for compound **191**, all other ortho-substitutions (**195**, **197**, and **199**) resulted in either a decrease in activity or no change. Compound **194**, a meta-bromo substituted analog with (1R,2R,3R,5S)-(-)-isopinocamphe head group was found to have *M. abscessus* MIC = 1 µg/mL and *M. tb* MIC = 0.5 µg/mL and greater activity than the para substituted counterpart (**160**) by 4-fold against *M. abscessus* and 32-fold against *M. tb*. Compound **196** (*M. abscessus*

Table 14. MIC of substituted aniline at ortho and para positions of some active hits against *M. abscessus* and *M. tb*.

| North No. | Structure | <i>M. abscessus</i> MIC (µg/mL) | <i>M. tb.</i> MIC (µg/mL) |
|------------|---|---------------------------------|---------------------------|
| 191 |  | 1 | 0.25 |
| 192 |  | 0.5 | 0.25 |
| 194 |  | 1 | 0.5 |
| 195 |  | 16 | 8 |
| 196 |  | 1 | 1 |
| 197 |  | 8 | 8 |
| 198 |  | 1 | 1 |
| 199 |  | >64 | 32 |
| 200 |  | 0.5 | 0.25 |

MIC = 1 $\mu\text{g/mL}$, *M. tb* MIC = 1 $\mu\text{g/mL}$) and compound **198** (*M. abscessus* MIC = 1 $\mu\text{g/mL}$, *M. tb* MIC = 1 $\mu\text{g/mL}$) were meta-chloro and meta-bromo analogs with 1-adamantyl head groups. Compound **196** exhibited four-fold increase in potency against *M. abscessus* and 16-fold increase in potency against *M. tb* compared to its para-substituted counterpart, compound **175**. Similarly, compound **200** exhibited 4-fold increase in potency against *M. abscessus* and 64-fold increase in potency against *M. tb* compared to its para-substituted counterpart, compound **179**. These data suggested that the bulky, electron withdrawing, and lipophilic groups at the meta-position are optimal for antimycobacterial activity.

2.8 Summary

These results support that bioisosteric replacement from indoles antimycobacterial agents to lead acetamides maintained the required pharmacophore and achieved optimal antimycobacterial potency, validating the first part of the hypothesis. The targeted compounds were successfully synthesized and isolated in moderate to good yields of 25% - 70%. The microbiological assessment of the acetamides identified 11 compounds from the acetamides series that have achieved an MIC value of at least 2 $\mu\text{g/mL}$ against either *M. abscessus* or *M. tb*, with three compounds reaching MIC value of 0.25 $\mu\text{g/mL}$ against *M. tb*. SAR studies suggest that the 1-adamanatane, 2-adamantane, and (1R,2R,3R,5S)-(-)-isopinocamphe head groups were optimal. Bulky, electron withdrawing, and lipophilic groups in either the meta- or para-position promoted antimycobacterial activity with meta-substitution being optimal. Generally, ortho-substitutions were detrimental for activity.

2.8. Experimental section

2.8.1 Materials, methods, and instrumentation

All the reagents, glassware, solvents, and chemicals were purchased from commercially available sources. All the chemicals were reagent-grade and were used directly without further purification. The reactions were tracked and monitored by using fluorescent-silica gel coated thin layer chromatography (TLC) plates, and the spots were visualized using UV lamp or iodine condensation. The purification of the compounds was performed using flash chromatography on a Biotage® Isolera One with a Biotage® silica gel column. ¹H and ¹³C NMR were recorded on 400 MHz Bruker NMR system, and the chemical shifts were reported relative to the solvent peaks. Mass spectra was obtained on Agilent 1200 / AB Sciex® API 5500 QTrap LC/MS/MS using electrospray ionization and a single quadrupole analyzer (Q1). The analytical reverse phase – HPLC was performed on Shimadzu's HPLC system equipped with Kinetex® C18 column (50 X 3 mm; 5 μm), flow rate of 0.5 mL/min, and a gradient of solvent A (water with 0.1% formic acid) and solvent B (acetonitrile): 0 – 1 min 5% B, 1 – 8 min 5 – 95% B, 8 – 9 min 95% B, 9 – 10 min 95 – 5% B. The UV detection with the absorbance at 254 nm was used as the HPLC detector system. All compounds were found to have a purity of >95% with the described analytical methods.

2.8.2 General procedure for the preparation of N-(cycloalkyl)-2-(N-phenylamino)acetamides

To a solution of 1 eq. of aliphatic cycloalkylamine dissolved in anhydrous DCM was added TEA (1.2 eq.) and allowed to stir for 15 minutes at 0 °C under N₂ atmosphere. Bromoacetyl bromide (1.2 eq.) was added dropwise to the mixture and the reaction was carried for 4 hours. The completion of the reaction was monitored by the derivatization of the spot by spraying H₂SO₄/ethanol solution followed by charring or by iodine-

condensation method. The crude mixture was extracted twice with DCM. The DCM layer was collected, dried with anhydrous sodium sulphate (Na_2SO_4) and evaporated under a reduced pressure. Without purification, the crude product was dissolved in anhydrous THF, and TEA (1.2 eq.) and aniline analogues (1 eq.) were added. The reaction was carried at 60 °C overnight. The completion of the reaction was monitored by spotting the crude in a TLC plate and observed using UV lamp. The crude mixture was extracted by ethyl acetate twice, collected, dried with anhydrous Na_2SO_4 , concentrated under reduced pressure, and adsorbed in silica. The crude product was purified using Flash Chromatography with ethyl acetate – hexane solvent system, and the gradient was determined with the help of TLC, yielding the pure acetamides.

2.8.3 North 149 - N-(Cyclooctyl)-2-(N-phenylamino)acetamide: 718 mg (70.0%) of pale yellow powder; ^1H NMR (CDCl_3) δ = 1.29 – 1.79 (14H, m), 3.78 (2H, s), 4.07 (1H, s), 6.63 (2H, d, J = 8 Hz), 6.84 (1H, t, J = 8 Hz), 7.24 (2H, t, J = 8 Hz); ^{13}C NMR (CDCl_3) δ = 23.55, 25.29, 27.15, 32.17, 49.12, 113.38, 119.19, 129.42, 147.23, 168.92; ESI-MS $[\text{M}+\text{H}]^+$ calculated for $\text{C}_{16}\text{H}_{24}\text{N}_2\text{O}$: 261.2, found: 261.4.

2.8.4 North 150 - N-(Cycloheptyl)-2-(N-phenylamino)acetamide: 739 mg (68.0%) of pale yellow powder; ^1H NMR (CDCl_3) δ = 1.36 – 1.61 (11H, m), 1.85 – 1.92 (2H, m), 3.79 (2H, s), 6.67 (2H, d, J = 8Hz), 6.86 (1H, t, J = 8 Hz), 7.25 (2H, t, J = 8 Hz); ^{13}C NMR (CDCl_3) δ = 24.01, 27.87, 35.02, 49.39, 50.20, 113.73, 119.61, 129.46, 146.8, 168.75; ESI-MS $[\text{M}+\text{H}]^+$ calculated for $\text{C}_{15}\text{H}_{22}\text{N}_2\text{O}$: 247.2, found: 247.5.

2.8.5 North 151 - N-(Trans-methylcyclohexyl)-2-(N-phenylamino)acetamide: 426 mg (49%) of white powder; ^1H NMR (CDCl_3) δ = 0.89 (2H, d, J = 4 Hz), 1.03 – 1.13 (4H, m), 1.68 – 1.71 (2H, m), 1.91 – 1.93 (2H, m), 3.72 – 3.80 (1H, m), 3.83 (2H, s), 6.75 (2H, d, J = 8 Hz), 6.92 (1H, t, J = 8Hz), 7.26 (2H, t, J = 4 Hz); ^{13}C NMR (CDCl_3)

$\delta = 22.14, 31.85, 33.00, 33.76, 48.20, 49.21, 113.35, 119.19, 129.42, 148.0, 169.0$; ESI-MS $[M+H]^+$ calculated for $C_{15}H_{22}N_2O$: 247.2, found: 247.3.

2.8.6 North 152 - N-(1R,2R,3R,5S)-(-)-Isopinocampheyl-2-(N-phenylamino)acetamide: 364 mg (65%) of pale yellow powder; 1H NMR ($CDCl_3$) $\delta = 0.76 - 0.79$ (1H, m), 1.07 - 1.10 (6H, m), 1.12 (3H, s), 1.45 - 1.50 (1H, m), 1.68 - 1.72 (1H, m), 1.78 - 1.81 (1H, m), 1.91 - 1.95 (1H, m), 2.34 - 2.38 (1H, m), 2.56 - 2.63 (1H, m), 3.81 (2H, s), 4.30 - 4.38 (1H, m), 6.59 (1H, d, $J = 8$ Hz), 6.66 (2H, d, $J = 8$ Hz), 6.83 (1H, t, $J = 8$ Hz), 7.23 (2H, t, $J = 8$ Hz), ^{13}C NMR ($CDCl_3$) $\delta = 20.67, 23.37, 28.01, 35.24, 36.93, 38.40, 41.52, 46.08, 47.70, 49.19, 113.35, 119.14, 129.41, 147.30, 169.67$; ESI-MS $[M+H]^+$ calculated for $C_{18}H_{26}N_2O$: 287.2, found: 287.4.

2.8.7 North 153 - N-(1-Adamantyl)-2-(N-phenylamino)acetamide: 168 mg (60%) of pale yellow powder; 1H NMR ($CDCl_3$) $\delta = 1.59$ (6H, s), 1.90 (6H, s), 1.99 (3H, s), 3.60 (2H, s), 6.31 (1H, s), 6.57 (2H, d, $J = 8$ Hz), 6.76 (1H, t, $J = 8$ Hz), 7.15 (2H, t, $J = 8$ Hz), ^{13}C NMR ($CDCl_3$) $\delta = 29.39, 36.29, 41.49, 45.25, 49.78, 51.63, 113.41, 119.08, 129.38, 147.29, 169.26$; ESI-MS $[M+H]^+$ calculated for $C_{18}H_{24}N_2O$: 285.2, found: 285.3.

2.8.8 North 154 - N-(Cyclooctyl)-2-(N-4'-trifluoromethoxyphenylamino)acetamide: 595 mg (44%) of pale yellow powder; 1H NMR ($CDCl_3$) $\delta = 1.49 - 1.59$ (14H, m), 3.76 (2H, s), 4.04 - 4.07 (1H, m), 6.51 (1H, d, $J = 8$ Hz), 6.58 (2H, d, $J = 12$ Hz), 7.07 (2H, d, $J = 8$ Hz); ^{13}C NMR ($CDCl_3$) $\delta = 23.51, 25.28, 27.13, 32.14, 49.04, 49.21, 113.70, 122.53, 141.64, 146.02, 168.41$; ESI-MS $[M+H]^+$ calculated for $C_{17}H_{23}F_3N_2O_2$: 345.2, found: 345.5.

2.8.9 North 155 - N-(Cyclooctyl)-2-(N-4'-methoxyphenylamino)acetamide: 592 mg (52%) of yellow powder; 1H NMR ($CDCl_3$) $\delta = 1.49 - 1.59$ (14H, m), 3.72 (3H, s), 3.77 (2H, s), 4.04 - 4.06 (1H, m), 6.59 (2H, d, $J = 12$ Hz), 6.80 (2H, d, $J = 8$ Hz); ^{13}C NMR

(CDCl₃) δ = 23.54, 25.27, 27.17, 32.14, 49.04, 50.06, 55.72, 114.61, 114.91, 123.30, 141.20, 153.23, 169.17; ESI-MS [M+H]⁺ calculated for C₁₇H₂₆N₂O₂: 291.2, found: 290.4.

2.8.10 North 156 - N-(Cyclooctyl)-2-(N-4'-trifluoromethylphenylamino)acetamide: 590 mg (46 %) of amber oil; ¹H NMR (CDCl₃) δ = 1.47 – 1.57 (14H, m), 3.78 (2H, s), 4.56 – 4.59 (1H, m), 6.28 (1H, s), 6.62 (2H, d, *J* = 8 Hz), 7.44 (2H, d, *J* = 8 Hz); ¹³C NMR (CDCl₃) δ = 23.54, 25.30, 27.10, 32.17, 48.49, 49.43, 113.08, 126.82, 149.25, 167.70; ESI-MS [M+H]⁺ calculated for C₁₇H₂₃F₃N₂O: 329.2, found: 329.6.

2.8.11 North 157 - N-(Cyclooctyl)-2-(N-4'-chlorophenylamino)acetamide: 719 mg (68%) of pale yellow powder; ¹H NMR (CDCl₃) δ = 1.48 – 1.57 (14H, m), 3.72 (2H, s), 4.03 (1H, m), 6.52 (2H, d, *J* = 8 Hz), 7.14 (2H, d, *J* = 12 Hz); ¹³C NMR (CDCl₃) δ = 23.53, 25.28, 27.13, 32.17, 49.04, 49.18, 114.38, 123.80, 129.27, 145.81, 168.45; ESI-MS [M+H]⁺ calculated for C₁₆H₂₃ClN₂O: 295.1, found: 295.3.

2.8.12 North 158 - N-(Cyclooctyl)-2-(N-4'-methylphenylamino)acetamide: 527 mg (49%) of amber oil; ¹H NMR (CDCl₃) δ = 1.44 – 1.58 (14H, m), 2.24 (3H, s), 3.08 (2H, s), 3.71 (1H, s), 6.52 (2H, d, *J* = 8 Hz), 6.98 (2H, d, *J* = 8 Hz); ¹³C NMR (CDCl₃) δ = 23.53, 25.27, 27.25, 32.01, 49.15, 50.58, 55.43, 113.37, 128.37, 129.85, 145.05, 169.60; ESI-MS [M+H]⁺ calculated for C₁₇H₂₆N₂O: 275.2, found: 275.5.

2.8.13 North 159 - N-(1R,2R,3R,5S)-(-)-Isopinocampheyl-2-(N-4'-chlorophenylamino)acetamide: 638 mg (61%) of amber oil; ¹H NMR (CDCl₃) δ = 0.74 – 0.76 (1H, m), 1.05 – 1.08 (6H, m), 1.21 (3H, d, *J* = 4 Hz), 1.40 – 1.46 (1H, m), 1.65 – 1.69 (1H, m), 1.77 – 1.80 (1H, m), 1.91 – 1.93 (1H, m), 2.36 – 2.38 (1H, m), 2.55 – 2.61 (1H, m), 3.76 (2H, s), 4.25 – 4.33 (1H, s), 6.54 (2H, d, *J* = 8 Hz), 7.15 (2H, d, *J* = 8 Hz); ¹³C NMR (CDCl₃) δ = 20.67, 23.36, 27.98, 35.27, 36.93, 38.39, 41.48,

46.11, 47.65, 49.15, 62.16, 114.13, 114.69, 129.30, 169.08; ESI-MS $[M+H]^+$ calculated for $C_{18}H_{25}ClN_2O$: 321.2, found: 321.4.

2.8.14 North 160 - N-(1R,2R,3R,5S)-(-)-Isopinocampheyl-2-(N-4'-bromophenylamino)acetamide: 678 mg (57%) of amber oil; 1H NMR ($CDCl_3$) δ = 0.67 – 0.69 (1H, m), 0.98 – 1.01 (6H, m), 1.14 (3H, s), 1.33 – 1.39 (1H, m), 1.58 – 1.62 (1H, m), 1.70 – 1.73 (1H, m), 1.83 – 1.86 (1H, m) 2.28 – 2.31 (1H, m), 2.47 – 2.54 (1H, m), 3.69 (2H, s), 4.20 – 4.28 (1H, m), 6.43 (2H, d, J = 8 Hz), 7.22 (2H, d, J = 8 Hz); ^{13}C NMR ($CDCl_3$) δ = 20.69, 23.38, 28.00, 35.31, 37.01, 38.39, 41.48, 46.19, 47.65, 48.96, 110.99, 114.27, 114.89, 132.17, 132.35, 146.22, 169.00; ESI-MS $[M+H]^+$ calculated for $C_{18}H_{25}BrN_2O$: 365.1, found: 365.4.

2.8.15 North 161 - N-(1R,2R,3R,5S)-(-)-Isopinocampheyl-2-(N-4'-methylphenylamino) acetamide: 499 mg (51%) of amber oil; 1H NMR ($CDCl_3$) δ = 0.75 – 0.77 (1H, m), 1.05 – 1.08 (6H, m), 1.20 (3H, s), 1.42 – 1.48 (1H, m), 1.57 (3H, s) 1.66 – 1.70 (1H, m), 1.77 – 1.79 (1H, m), 1.90 – 1.94 (1H, m), 2.33 – 2.37 (1H, m), 2.55 – 2.61 (1H, m), 3.75 (2H, s), 4.30 – 4.36 (1H, m), 6.53 (2H, d, J = 8 Hz), 7.01 (2H, d, J = 8 Hz); ^{13}C NMR ($CDCl_3$) δ = 20.68, 23.38, 28.02, 35.26, 36.95, 38.41, 41.54, 46.11, 47.41, 47.72, 49.62, 113.44, 128.50, 129.9, 145.05, 169.82; ESI-MS $[M+H]^+$ calculated for $C_{19}H_{28}N_2O$: 301.2, found: 301.5.

2.8.16 North 162 - N-(1R,2R,3R,5S)-(-)-Isopinocampheyl-2-(N-4'-methoxyphenylamino) acetamide: 443 mg (43%) of dark amber oil; 1H NMR ($CDCl_3$) δ = 0.75 – 0.77 (1H, m), 1.05 – 1.08 (6H, m), 1.20 (3H, s), 1.42 – 1.48 (1H, m), 1.68 – 1.70 (1H, m), 1.76 – 1.79 (1H, m), 1.90 – 1.93 (1H, m), 2.34 – 2.37 (1H, m), 2.54 – 2.61 (1H, m), 3.73 (2H, s), 3.75 (3H, s), 4.29 – 4.34 (1H, m), 6.57 (2H, d, J = 8 Hz), 6.79 (2H, d, J = 8 Hz); ^{13}C NMR ($CDCl_3$) δ = 20.69, 23.38, 28.02, 35.26, 36.97,

38.40, 41.53, 46.14, 47.39, 47.71, 50.01, 55.74, 114.51, 114.94, 141.33, 153.20, 169.86;
ESI-MS $[M+H]^+$ calculated for $C_{19}H_{28}N_2O_2$: 317.2, found: 317.5.

2.8.17 North 163 - N-(Transmethylcyclohexyl)-2-(N-4'-methylphenylamino)acetamide: 527 mg (47%) dark amber oil; 1H NMR ($CDCl_3$) δ = 0.86 – 0.88 (2H, m), 1.02 – 1.09 (4H, m), 1.66 – 1.69 (2H, m), 1.80 – 1.84 (1H, m), 2.25 (3H, s), 3.72 (2H, s), 3.97 – 4.03 (1H, m), 6.51 (2H, d, J = 12 Hz), 7.01 (2H, d, J = 8 Hz); ^{13}C NMR ($CDCl_3$) δ = 20.46, 22.16, 31.84, 32.94, 33.77, 47.09, 48.29, 50.02, 60.89, 114.40, 129.96, 132.07, 169.05; ESI-MS $[M+H]^+$ calculated for $C_{16}H_{24}N_2O$: 261.2, found: 261.4.

2.8.18 North 164 - N-(Transmethylcyclohexyl)-2-(N-4'-chlorophenylamino)acetamide: 396 mg (32%) of amber oil; 1H NMR ($CDCl_3$) δ = 0.89 – 0.91 (4H, m), 1.06 – 1.13 (4H, m), 1.69 – 1.75 (1H, m), 1.83 – 1.92 (3H, m), 3.81 (2H, s), 6.73 (2H, d, J = 8 Hz), 7.20 (2H, d, J = 8 Hz); ^{13}C NMR ($CDCl_3$) δ = 22.15, 31.84, 32.99, 33.76, 48.25, 49.39, 113.69, 119.57, 129.45, 169.26 ESI-MS $[M+Na]^+$ calculated for $C_{16}H_{24}N_2O$: 303.1, found: 303.3.

2.8.19 North 175 - N-(1-Adamantyl)-2-(N-4'-chlorophenylamino)acetamide: 286 mg (30%) of white powder; 1H NMR ($CDCl_3$) δ = 1.69 (6H, s), 1.98 (6H, s), 2.09 (3H, s), 3.66 (2H, s), 6.23 (1H, s), 6.56 (2H, d, J = 8 Hz), 7.17 (2H, d, J = 8 Hz); ^{13}C NMR ($CDCl_3$) δ = 29.38, 36.26, 41.51, 49.54, 51.78, 114.43, 123.74, 129.25, 145.79, 168.69; ESI-MS $[M+H]^+$ calculated for $C_{18}H_{23}ClN_2O$: 319.1, found: 319.1.

2.8.20 North 176 - N-(1-Adamantyl)-2-(N-4'-bromophenylamino)acetamide: 283 mg (26%) of pale yellow powder; 1H NMR ($CDCl_3$) δ = 1.68 (6H, s), 1.98 (6H, s), 2.08 (3H, s), 3.64 (2H, s), 6.50 (2H, d, J = 8 Hz), 7.29 (2H, d, J = 8 Hz); ^{13}C NMR ($CDCl_3$) δ = 29.37, 36.25, 41.51, 49.43, 51.78, 110.80, 114.91, 132.11, 146.24, 168.67; ESI-MS $[M+H]^+$ calculated for $C_{18}H_{23}BrN_2O$: 363.1, found: 363.2.

2.8.21 North 177 - N-(1-Adamantyl)-2-(N-4'-methylphenylamino)acetamide: 259 mg (29%) of white powder; ^1H NMR (CDCl_3) δ = 1.68 (6H, s), 2.00 (6H, s), 2.08 (3H, s), 2.29 (3H, s), 3.67 (2H, s), 6.52 (1H, s) 6.60 (2H, d, J = 8 Hz), 7.04 (2H, d, J = 8 Hz); ^{13}C NMR (CDCl_3) δ = 29.39, 36.29, 41.47, 50.34, 51.61, 113.83, 128.78, 129.88, 144.63, 169.29; ESI-MS $[\text{M}+\text{H}]^+$ calculated for $\text{C}_{19}\text{H}_{26}\text{N}_2\text{O}$: 299.2, found: 299.4.

2.8.22 North 178 - N-(1-Adamantyl)-2-(N-4'-methoxyphenylamino)acetamide: 292 mg (31%) of dark amber oil; ^1H NMR (CDCl_3) δ = 1.68 (6H, s), 2.0 (6H, s), 2.08 (3H, s), 3.65 (2H, s), 3.78 (3H, s), 6.57 (1H, s), 6.63 (2H, d, J = 8 Hz), 6.81 (2H, d, J = 8 Hz); ^{13}C NMR (CDCl_3) δ = 29.39, 36.39, 41.48, 50.8, 51.63, 55.72, 114.91, 115.03, 140.72, 153.48, 169.30; ESI-MS $[\text{M}+\text{H}]^+$ calculated for $\text{C}_{19}\text{H}_{26}\text{N}_2\text{O}_2$: 315.2, found: 316.1.

2.8.23 North 179 - N-(1-Adamantyl)-2-(N-4'-trifluoromethoxyphenylamino)acetamide: 276 mg (25%) of dark amber oil; ^1H NMR (CDCl_3) δ = 1.69 (6H, s), 2.0 (6H, s), 2.09 (3H, s), 3.74 (2H, s), 6.33 (1H, s), 6.75 (2H, s, J = 8 Hz), 7.71 (2H, s, J = 8 Hz); ^{13}C NMR (CDCl_3) δ = 29.37, 36.23, 41.48, 50.30, 52.07, 115.40, 122.50, 142.8, 167.73; ESI-MS $[\text{M}+\text{H}]^+$ calculated for $\text{C}_{19}\text{H}_{23}\text{F}_3\text{N}_2\text{O}_2$: 369.2, found: 369.3.

2.8.24 North 180 - N-(1-Adamantyl)-2-(N-4'-trifluoromethylphenylamino)acetamide: 296 mg (28%) of white powder; ; ^1H NMR (CDCl_3) δ = 1.69 (6H, s), 2.0 (6H, s), 2.1 (6H, s), 3.75 (2H, s), 6.07 (1H, s), 6.70 (2H, d, J = 8 Hz), 7.47 (2H, d, J = 8 Hz), ^{13}C NMR (CDCl_3) δ = 29.37, 36.23, 41.52, 48.89, 52.06, 113.02, 126.76, 149.31, 167.91; ESI-MS $[\text{M}+\text{H}]^+$ calculated for $\text{C}_{19}\text{H}_{23}\text{F}_3\text{N}_2\text{O}$: 353.2, found: 353.1.

2.8.25 North 182 - N-(2-Adamantyl)-2-(N-phenylamino)acetamide: 675.73 mg (72%) of amber oil; ; ^1H NMR (CDCl_3) δ = 1.54 (4H, s), 1.62 – 1.67 (3H, m), 1.75 – 1.80 (8H, m), 3.83 (2H, s), 6.75 (2H, d, J = 8 Hz), 6.86 (1H, t, J = 8 Hz); 7.18 (2H, t, J = 8 Hz); ^{13}C NMR (CDCl_3) δ = 27.05, 31.76, 32.0, 37.07, 37.46, 49.42, 52.84, 113.55,

119.44, 129.45, 136.68, 153.72, 169.18; ESI-MS $[M+H]^+$ calculated for $C_{18}H_{24}N_2O$: 285.2, found: 285.2.

2.8.26 North 183 - N-(2-Adamantyl)-2-(N-4'-chlorophenylamino)acetamide: 673 mg (64%) of amber oil; 1H NMR ($CDCl_3$) δ = 1.63 (4H, s), 1.69 – 1.77 (3H, s), 1.79–1.86 (8H, m), 3.74 (2H, s), 6.57 (2H, d, J = 8 Hz), 7.10 (2H, d, J = 8 Hz); ^{13}C NMR ($CDCl_3$) δ = 27.07, 31.79, 37.05, 44.36, 50.88, 53.01, 55.36, 115.04, 116.69, 129.36, 144.41, 158.85, 169.69; ESI-MS $[M+Na]^+$ calculated for $C_{18}H_{23}BClN_2O$: 343.1, found: 343.5.

2.8.27 North 184 - N-(2-Adamantyl)-2-(N-4'-bromophenylamino)acetamide: 300 mg (31%) of amber oil; 1H NMR ($CDCl_3$) δ = 1.56 (4H, s), 1.71 – 1.76 (3H, m), 1.84 – 1.87 (8H, m), 3.79 (2H, s), 6.53 (2H, d, J = 12 Hz), 7.30 (2H, d, J = 8 Hz); ^{13}C NMR ($CDCl_3$) δ = 27.05, 31.74, 31.93, 37.04, 37.40, 53.48, 132.49, 144.76, 173.50; ESI-MS $[M+H]^+$ calculated for $C_{18}H_{23}BrN_2O$: 363.1, found: 363.3.

2.8.28 North 185 - N-(2-Adamantyl)-2-(N-4'-methylphenylamino)acetamide: 232 mg (26%) of amber oil; 1H NMR ($CDCl_3$) δ = 1.57 (4H, s), 1.71 – 1.75 (m, 3H), 1.85 – 1.89 (m, 8H), 2.27 (3H, s), 3.79 (2H, s), 6.58 (2H, d, J = 12 Hz), 7.03 (2H, d, J = 8 Hz); ^{13}C NMR ($CDCl_3$) δ = 20.43, 27.08, 30.95, 31.76, 37.06, 37.45, 49.83, 50.85, 52.84, 113.70, 119.67, 129.90, 144.74, 169.57; ESI-MS $[M+H]^+$ calculated for $C_{19}H_{26}N_2O$: 299.2, found: 299.7.

2.8.29 North 186 - N-(2-Adamantyl)-2-(N-4'-methoxyphenylamino)acetamide: 292 mg (31%) of amber oil; 1H NMR ($CDCl_3$) δ = 1.57 (4H, s), 1.71 – 1.75 (3H, m), 1.85 – 1.89 (8H, m), 3.78 (3H, s), 3.79 (2H, s), 6.64 (2H, d, J = 8 Hz), 6.80 (2H, d, J = 12 Hz); ^{13}C NMR ($CDCl_3$) δ = 27.09, 31.78, 32.02, 37.04, 37.46, 50.23, 52.87, 55.72, 114.79, 114.90, 123.42, 140.99, 153.36, 169.47; ESI-MS $[M+H]^+$ calculated for $C_{19}H_{26}N_2O$: 315.2, found: 314.6.

2.8.30 North 187 - N-(2-Adamantyl)-2-(N-4'-trifluoromethylphenylamino)acetamide: 338 mg (32%) of amber oil; ¹H NMR (CDCl₃) δ = 1.57 (4H, s), 1.72 – 1.77 (3H, m), 1.85 – 1.89 (8H, m), 3.88 (2H, s), 6.71 (2H, d, *J* = 8 Hz), 6.82 (1H, s), 7.47 (2H, d, *J* = 8 Hz); ¹³C NMR (CDCl₃) δ = 27.03, 31.78, 31.95, 37.02, 37.38, 48.52, 53.08, 112.89, 126.81, 136.53, 168.18; ESI-MS [M+H]⁺ calculated for C₁₉H₂₃F₃N₂O: 353.2, found: 353.4.

2.8.31 North 188 - N-(2-Adamantyl)-2-(N-4'-trifluoromethoxyphenylamino)acetamide: 530 mg (43.6%) of amber oil; ¹H NMR (CDCl₃) δ = 1.56 (4H, s), 1.72 – 1.75 (3H, m), 1.84 – 1.88 (8H, m), 3.83 (2H, s), 6.66 (2H, d, *J* = 8 Hz), 7.0 (1H, s), 7.09 (2H, d, *J* = 8 Hz); ¹³C NMR (CDCl₃) δ = 27.06, 31.74, 31.95, 37.04, 37.40, 49.83, 53.23, 63.85, 113.54, 115.39, 121.84, 122.56, 140.22, 144.20, 167.93; ; ESI-MS [M+H]⁺ calculated for C₁₉H₂₃F₃N₂O₂: 369.2, found: 369.0.

2.8.32 North 189 - N-(1R,2R,3R,5S)-(-)-Isopinocampheyl-2-(N-4'-trifluoromethylphenylamino)acetamide: 471 mg (41%) of amber oil; ¹H NMR (CDCl₃) δ = 0.67 (1H, d, *J* = 8 Hz), 0.97 – 1.01 (6H, m), 1.14 (3H, s), 1.35 – 1.40 (1H, m), 1.59 – 1.63 (1H, m), 1.70 – 1.73 (1H, m), 1.84 – 1.88 (1H, m), 2.27 – 2.33 (1H, m), 2.48 – 2.55 (1H, m), 3.75 (2H, s), 4.23 – 4.28 (1H, m), 6.22 (1H, s), 6.57 (2H, d, *J* = 8 Hz), 7.36 (2H, d, *J* = 8 Hz); ; ¹³C NMR (CDCl₃) δ = 20.67, 23.35, 27.96, 35.27, 36.99, 38.38, 41.46, 46.19, 47.63, 47.75, 48.27, 112.58, 126.70, 126.77, 149.80, 168.69; ESI-MS [M+Na]⁺ calculated for C₁₉H₂₅F₃N₂O: 377.2, found: 377.2.

2.8.33 North 190 - N-(1R,2R,3R,5S)-(-)-Isopinocampheyl-2-(N-4'-trifluoromethoxyphenylamino)acetamide: 384 mg (32%) of amber oil; ; ¹H NMR (CDCl₃) δ = 0.76 (1H, d, *J* = 12 Hz), 1.04 – 1.08 (6H, m), 1.21 – 1.27 (3H, m), 1.46 – 1.49 (1H, m), 1.68 – 1.71 (1H, m), 1.91 -1.94 (1H, m), 2.36 – 2.39 (1H, m), 3.78 (2H, s), 4.30 – 4.34 (1H, m), 6.51 (1H, s), 6.59 (2H, d, *J* = 8 Hz), 7.06 (2H, d, *J* = 8 Hz); ¹³C

NMR (CDCl₃) δ = 20.65, 23.34, 27.96, 35.23, 36.96, 38.38, 41.48, 46.09, 47.65, 49.03, 113.70, 112.52, 141.60, 146.09, 169.19; C₁₉H₂₅F₃N₂O₂ ESI-MS [M+H]⁺ calculated for C₁₉H₂₅F₃N₂O₂: 370.2, found: 370.7.

2.8.34 North 191 - N-(1R,2R,3R,5S)-(-)-Isopinocampheyl-2-(N-2'-chlorophenylamino)acetamide: 303 mg (29%) of amber oil; ¹H NMR (CDCl₃) δ = 0.77 (1H, d, *J* = 12 Hz); 1.07 (6H, s), 1.22 (3H, s), 1.67 – 1.69 (1H, m), 1.78 – 1.81 (1H, m), 1.91 – 1.95 (1H, m), 2.34 – 2.39 (1H, m), 2.56 – 2.62 (1H, m), 3.86 (2H, s), 4.30 – 4.37 (1H, m), 6.43 (1H, s), 6.58 (1H, d, *J* = 8 Hz), 6.77 (1H, t, *J* = 8 Hz), 7.17 (1H, t, *J* = 8 Hz), 7.31 (1H, d, *J* = 8 Hz); ¹³C NMR (CDCl₃) δ = 20.67, 23.39, 28.01, 35.26, 36.91, 38.41, 41.49, 46.02, 47.66, 48.83, 112.03, 119.28, 119.81, 128.06, 129.32, 143.26, 169.0; ESI-MS [M+H]⁺ calculated for C₁₈H₂₅ClN₂O: 321.2, found: 321.0.

2.8.35 North 192 - N-(1R,2R,3R,5S)-(-)-Isopinocampheyl-2-(N-3'-chlorophenylamino)acetamide: 260 mg (25%) of amber oil; ¹H NMR (CDCl₃) δ = 0.76 (1H, d, *J* = 8 Hz), 1.0 (3H, s), 1.04 – 1.06 (3H, m), 1.18 (3H, s), 1.44 – 1.49 (1H, m), 1.66 – 1.69 (1H, m), 1.74 – 1.77 (1H, m), 1.89 – 1.90 (1H, m), 2.31 – 2.36 (1H, m), 2.50 – 2.56 (1H, m), 3.74 – 3.78 (1H, m), 4.26 – 4.34 (1H, m), 4.94 – 4.96 (1H, m), 6.46 (1H, d, *J* = 8 Hz), 6.59 (1H, s), 6.71 (1H, d, *J* = 8 Hz), 7.06 (1H, t, *J* = 8 Hz); ¹³C NMR (CDCl₃) δ = 20.7, 23.33, 27.97, 35.18, 36.81, 38.36, 41.45, 45.88, 47.61, 48.48, 113.36, 113.31, 118.55, 130.35, 135.02, 148.64, 169.37; ESI-MS [M+H]⁺ calculated for C₁₈H₂₅ClN₂O: 321.2, found: 323.3.

2.8.36 North 194 - N-(1R,2R,3R,5S)-(-)-Isopinocampheyl-2-(N-3'-bromophenylamino)acetamide: 369 mg (31%) of amber oil; ¹H NMR (CDCl₃) δ = 0.77 (1H, d, *J* = 12 Hz), 1.06 – 1.10 (6H, m), 1.22 (3H, s), 1.45 – 1.50 (1H, m), 1.69 – 1.70 (1H, m), 1.93 – 1.96 (1H, m), 2.35 – 2.40 (1H, m), 2.57 – 2.63 (1H, m), 3.79 (2H, s), 4.31 – 4.38 (1H, m), 4.46 (1H, s), 6.39 (1H, s), 6.54 (1H, d, *J* = 8 Hz), 6.79 (1H, d,

$J = 4$ Hz), 6.92 (1H, d, $J = 8$ Hz), 7.07 (1H, t, $J = 8$ Hz); ^{13}C NMR (CDCl_3) $\delta = 20.67$, 23.38, 28.0, 35.30, 36.96, 38.40, 41.49, 46.16, 47.64, 48.64, 111.87, 116.15, 121.89, 123.33, 130.70, 148.5, 168.91; ESI-MS $[\text{M}+\text{H}]^+$ calculated for $\text{C}_{18}\text{H}_{25}\text{BrN}_2\text{O}$: 365.1, found: 365.2.

2.8.37 North 195 - N-(1-Adamantyl)-2-(N-2'-chlorophenylamino)acetamide: 357 mg (34%) of amber oil; ^1H NMR (CDCl_3) $\delta = 1.70$ (6H, s), 2.00 (6H, s), 2.09 (3H, s), 3.76 (2H, s), 6.61 (1H, d, $J = 8$ Hz), 6.77 (1H, t, $J = 8$ Hz), 7.19 (1H, t, $J = 8$ Hz), 7.31 (1H, d, $J = 8$ Hz); ^{13}C NMR (CDCl_3) $\delta = 29.38$, 36.26, 41.51, 49.13, 51.84, 111.46, 113.26, 118.87, 130.39, 135.13, 148.37, 168.45; ESI-MS $[\text{M}+\text{H}]^+$ calculated for $\text{C}_{18}\text{H}_{23}\text{ClN}_2\text{O}$: 319.2, found: 319.3.

2.8.38 North 196 - N-(1-Adamantyl)-2-(N-3'-chlorophenylamino)acetamide: 305 mg (29%) of amber oil; ^1H NMR (CDCl_3) $\delta = 1.68$ (6H, s), 1.99 (6H, s), 2.06 (3H, s), 3.66 (2H, s), 6.21 (1H, s), 6.48 (1H, d, $J = 8$ Hz), 6.61 (1H, s), 6.76 (1H, d, $J = 8$ Hz), 7.12 (1H, t, $J = 8$ Hz); ^{13}C NMR (CDCl_3) $\delta = 29.37$, 36.25, 41.49, 49.11, 51.82, 111.42, 113.42, 118.76, 130.39, 135.09, 148.46, 168.60; ESI-MS $[\text{M}+\text{H}]^+$ calculated for $\text{C}_{18}\text{H}_{23}\text{ClN}_2\text{O}$: 319.2, found: 319.1.

2.8.39 North 197 - N-(1-Adamantyl)-2-(N-2'-bromophenylamino)acetamide: 372 mg (31%) of amber oil; ^1H NMR (CDCl_3) $\delta = 1.68$ (6H, s), 2.0 (6H, s), 2.08 (3H, s), 3.74 (2H, s), 6.20 (1H, s), 6.57 (1H, d, $J = 8$ Hz), 6.71 (1H, t, $J = 8$ Hz), 7.23 (1H, t, $J = 8$ Hz), 7.47 (1H, d, $J = 8$ Hz); ^{13}C NMR (CDCl_3) $\delta = 29.37$, 36.25, 41.51, 49.45, 51.79, 110.86, 114.94, 132.13, 146.20, 168.62; ESI-MS $[\text{M}+\text{H}]^+$ calculated for $\text{C}_{18}\text{H}_{23}\text{BrN}_2\text{O}$: 364.3, found: 363.1.

2.8.40 North 198 - N-(1-Adamantyl)-2-(N-3'-bromophenylamino)acetamide: 383 mg (32%) of amber oil; ^1H NMR (CDCl_3) $\delta = 1.68$ (6H, s), 1.99 (6H, s), 2.06 (3H, s), 3.65 (2H, s), 6.20 (1H, s), 6.52 (1H, d, $J = 8$ Hz), 6.77 (1H, t, $J = 4$ Hz), 6.90 (1H, d, J

= 8 Hz), 7.06 (1H, t, $J = 8$ Hz); ^{13}C NMR (CDCl_3) $\delta = 29.37, 36.25, 41.49, 49.07, 51.84, 111.84, 116.15, 121.66, 123.26, 130.67, 148.59, 168.56$; ESI-MS $[\text{M}+\text{H}]^+$ calculated for $\text{C}_{18}\text{H}_{23}\text{BrN}_2\text{O}$: 364.3, found: 364.9.

2.8.41 North 199 - N-(1-Adamantyl)-2-(N-2'-trifluoromethoxyphenylamino)acetamide: 352 mg (29%) of amber oil; ^1H NMR (CDCl_3) $\delta = 1.68$ (6H, s), 1.97 (6H, s), 2.07 (3H, s), 3.74 (2H, s), 6.24 (1H, s), 6.65 (1H, d, $J = 8$ Hz), 6.81 (1H, t, $J = 8$ Hz), 7.18 – 7.22 (2H, m); ^{13}C NMR (CDCl_3) $\delta = 29.36, 36.23, 41.39, 48.67, 51.66, 112.53, 118.42, 128.01, 136.42, 139.61, 168.45$; ESI-MS $[\text{M}+\text{H}]^+$ calculated for $\text{C}_{19}\text{H}_{23}\text{F}_3\text{N}_2\text{O}_2$: 369.2, found: 369.2.

2.8.42 North 200 - N-(1-Adamantyl)-(3-trifluoromethoxyphenylamino)acetamide: 29 mg (37.6%) of amber oil; ^1H NMR (CDCl_3) $\delta = 1.68$ (6H, s), 1.99 (6H, s), 2.06 (3H, s), 3.68 (2H, s), 4.57 (1H, s), 6.45 (1H, s), 6.53 (1H, d, $J = 8$ Hz), 6.64 (1H, d, $J = 8$ Hz), 7.20 (1H, t, $J = 8$ Hz); ^{13}C NMR (CDCl_3) $\delta = 29.37, 36.23, 41.48, 49.10, 51.86, 105.69, 110.74, 111.57, 130.39, 148.75, 150.37, 168.44$; ESI-MS $[\text{M}+\text{H}]^+$ calculated for $\text{C}_{19}\text{H}_{23}\text{F}_3\text{N}_2\text{O}_2$: 369.2, found: 369.0.

2.8.43. MIC Testing:

MIC value was determined by microbroth dilution method following protocol of clinical and laboratory standards institute (CLSI) and Jackson lab at Colorado State University. *M. tb* H37Rv mc2 6206 was grown in Middlebrook 7H9 media and *M. abscessus* ATCC 19977 was grown in Mueller Hinton II (BD) media by incubating at 37 °C till optical density (OD) was measured 0.08 – 0.1. The compound was dissolved in DMSO at a concentration of 10 mg/ml and stored at -80 °C until required. 100 μL of the compound, two-fold serially diluted in Middlebrook 7H9 starting from 64 $\mu\text{g}/\text{mL}$, was added to the 96-well microtiter plates. 100 μL of the culture of these mycobacteria

were added to the drug plates and incubated at 37 °C for seven days. The plates were then visually inspected to determine the MIC value.

Chapter 3: Assessment of *in vitro* physicochemical, pharmacokinetic, and cytotoxicity profiles of active compounds

3.1 Introduction:

All drugs are chemicals, but all chemicals are not drugs. Any new chemical entity (NCE) that has the potential to be developed as a drug is termed as drug-like candidate. It should be noted that the most potent compounds with the least MIC value is not always the best drug-like candidate but may still need structural modifications to optimize physicochemical, pharmacokinetic (PK), pharmacodynamic (PD), and safety profiles.

Physicochemical properties generally include physical properties (viscosity, density, melting point, boiling point), solvation properties (aqueous solubility, partition coefficient), and molecular attributes relating the chemical properties and reactions (Council 2013). The pharmacokinetic profile of a drug describes how the drug is absorbed, distributed, distributed, metabolized, or excreted in a living system.

Figure 13 depicts the general understanding of ADME principles (Ahmad & Ahmad, 2019). Absorption is defined as the rate and extent to which the drug reaches the systemic circulation from the site of administration. The long-term goal of our project is to administer an effective drug orally, therefore the focus for absorption will be through an oral route. Distribution is the rate and extent by which the drug is distributed in the body fluids and tissues from the site of absorption (Chung, Terry, and Smith 2015). Only the drug that is not bound to plasma proteins is available to elicit its pharmacological action. Therefore, we are interested in assessing *in vitro* plasma protein binding which also has implications on duration of action, drug-drug interactions (DDIs), and dosing regimen. Metabolism is defined as the process by which a drug undergoes enzymatic action or biotransformation to be converted to an active or inactive form or to facilitate its elimination (Chung, Terry, and Smith 2015). The final

fate of the drug is excretion, in which the drug is eliminated via various routes after attaining a peak plasma concentration.

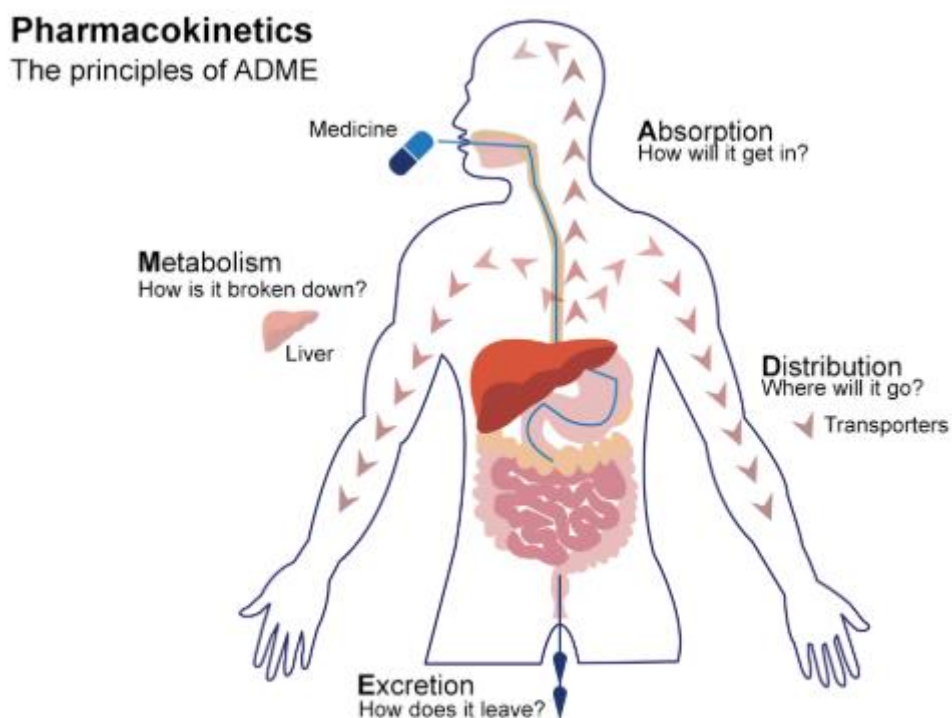


Figure 13. The principles of ADME (Ahmad & Ahmad, 2019)

The drug-like candidate should exhibit a safe pharmacological profile with a high selectivity index (SI), generally greater than 10 (North et al. 2013). SI is the ratio of IC_{50} (the minimum concentration of compound to inhibit 50 % of the normal cells) to MIC. A compound that is effective and possesses excellent SI is considered a promising candidate for early stage drug development.

3.2 Importance of *in vitro* ADME-Tox assessment

The drug discovery and development process is expensive, and on average costs greater than 800 million USD and typically takes 10 – 15 years of research from discovery to clinic (Lin and Lu 1997, Dickson and Gagnon 2004, Woodcock and Woosley 2008). The cost and time rise significantly with increasing number of attritions in the drug development process. One of the most prominent reasons for the NCE to undergo attrition is lack of appropriate ADME and safety profiles. Therefore, it is indispensable to identify the best leads early in the drug development process.

Performing *in vitro* ADME-Tox assessment in the early stages of drug discovery and development provides a rapid and economical way to identify successful candidates for further drug development. ADME-Tox assessment provides initial screening of compounds pharmacokinetics/pharmacodynamics profiles (PK/PD). Generally, aqueous solubility, LogP, permeability, human plasma protein binding, metabolic stability, and cytotoxicity assays are performed to assess PK/PD and safety profiles of the compounds (Hughes, Rees, Kalindjian & Philpott 2011). Figure 14 illustrates a link between various *in vitro* assays with ADME-Tox assessment (Ishida 2018). Briefly, aqueous solubility helps to determine the absorption profiles and bioavailability of the compounds. The permeability assays help to determine the absorption and distribution profiles of the compounds, and *in vitro* cell viability assay provides a general idea on the possible safety profile of drug candidates. These assays help to prioritize the lead compounds for additional preclinical drug development.

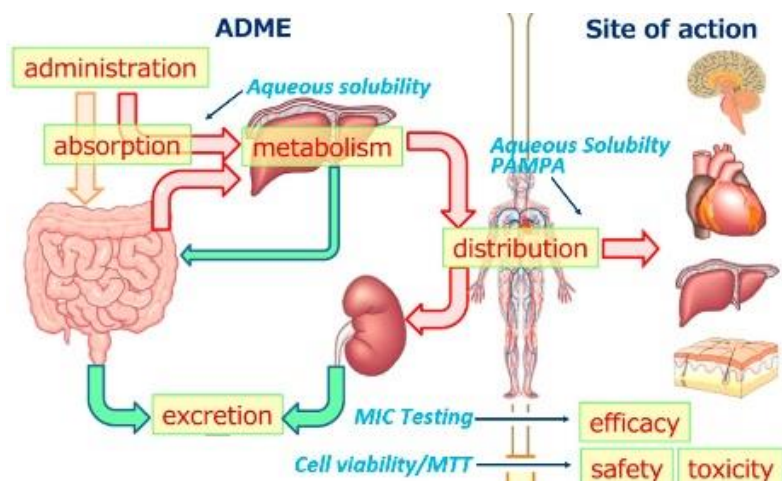


Figure 14. *In vitro* assays that relate to ADME-Tox (Ishida 2018).

For our research project, we performed assays to determine *in vitro* aqueous solubility, permeability, human plasma protein binding, and cell viability to prioritize a lead compounds discussed in Chapter 2 for further drug development. The rationale for performing each assay and how they influence ADME-Tox profiles are explained below. The assays were performed for all the drugs that reached an MIC value of 2 $\mu\text{g/mL}$ or better against either *M. abscessus* or *M. tb*, and 11 compounds reached this threshold.

3.3 Aqueous Solubility

According to International Union of Pure and Applied Chemistry (IUPAC), solubility is defined as ‘the analytical composition of a saturated solution, expressed in terms of the proportion of a designated solute in a designated solvent (IUPAC gold book). In other terms, solubility can be defined as the maximum proportion of the solute component in the solvent to form a solution. It is called aqueous solubility when the solvent is water.

Poorly water-soluble compounds possess many pharmacokinetic limitations. The urea- and indoles-based inhibitors have poor water solubility, which would likely reduce absorption and the rate and extent the drug reaches the systemic circulation. Due to this, high doses must be administered, which may cause further toxicity and increased drug-drug interactions (DDIs). The other problem is off target binding, leading to side effects and gastrointestinal mucosal toxicity (Savjani, Gajjar, and Savjani 2012). Therefore, NCEs must have an appropriate aqueous solubility (10 $\mu\text{g/mL}$ in drug discovery phase) to advance further in drug development.

The oral route is the most common route of drug administration owing to its high patient compliance, economic value, and ease in drug design. For a candidate to be considered for the oral route it should have adequate aqueous solubility. Acceptable aqueous solubility allows the drug to be absorbed into the systemic circulation. Greater than 40% of the NCEs are insoluble in water and commonly face attrition in the drug development process (Savjani, Gajjar, and Savjani 2012).

Kinetic and thermodynamic aqueous solubility are two ways to measure the aqueous solubility. Kinetic aqueous solubility is a measure of the extent to which compounds precipitate when dissolved in a buffered aqueous solution from an organic stock. This approach allows the pre-dissolved compound in organic solvent as the starting material (Saal and Petereit 2012). Thermodynamic aqueous solubility is the extent to which compounds dissolve directly in the buffered aqueous system when equilibrium is achieved (Saal and Petereit 2012). The values obtained from the thermodynamic aqueous solubility are more accurate, reliable, and conservative than values obtained from kinetic aqueous solubility assays (Brittain 2014). However, in early stage drug discovery platforms, kinetic aqueous solubility is widely used as it allows for rapid

high-throughput screening of a large number of compounds. Kinetic aqueous solubility is also correlative of thermodynamic aqueous solubility, however the value obtained in kinetic aqueous solubility is typically higher than thermodynamic aqueous solubility (Saal and Petereit 2012; Brittain 2014). Obtaining thermodynamic aqueous solubility is labor intensive and requires a large amount of sample and is preferred in the late preclinical stage of drug development. For this research project, we performed kinetic aqueous solubility for two reasons. First, it provides the solubility of a compound in a short period of time and second, our MIC values are measured starting with a 10 mg/mL DMSO stock and diluted 156 times to start with 64 µg/mL of compounds, with 0.64% DMSO in the final concentration. Maintaining same stock solution to measure kinetic aqueous solubility provides a direct correlation with MIC value and solubility value.

3.3.1 Assessment of kinetic aqueous solubility

Figure 15 shows the general procedure for the determination of kinetic aqueous solubility. A stock solution of each active compound in DMSO (10 mg/mL) was prepared and diluted into physiological buffer (pH = 7.4) at a concentration of 100 µg/mL and left for six hours at room temperature. After six hours, the sample was centrifuged, and the supernatant was diluted with methanol-water solution containing internal standard (IS) (Figure 15) and quantified using LC-MS-MS. The addition of the IS offers several advantages and provides the most accurate results. Since both the IS and samples are quantified simultaneously, and their ratio is calculated, where the signal to noise variability and the effects of external factors influencing ionization are minimized. Warfarin has a unique retention time, high ionization potential, and is stable in both organic and aqueous solutions and was selected as the IS for the quantification of the solubility of acetamides.

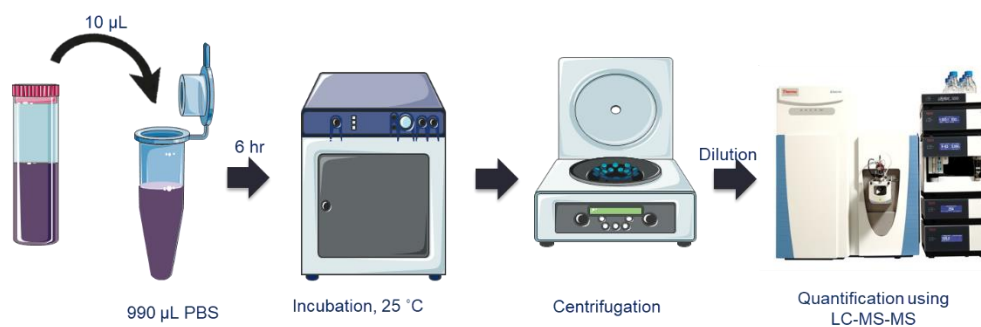


Figure 15. Method to assess kinetic aqueous solubility.

In order to correlate MS signal to drug concentration, a calibration curve was used. The calibration curve was established with seven-point standards prepared by a serial dilution in the range the sample signal would likely fall and exactly simulating the sample preparation and experimentation conditions including IS concentration. A plot of sample peak area/IS peak area ratio versus concentration of standards generated calibration curve with linear regression was produced. The unknown concentration (in triplicate) from the sample was determined using the calibration curve, and the solubility values were reported as mean \pm S.D.

The solubility determination of a representative compound **192** is explained below. The calibration curve shown in Figure 16 is generated using Microsoft Excel, plotting concentration on the x-axis and area ratio at y-axis. The sample area, IS area, area ratio, sample retention time, IS retention time, and concentration of the known standards are shown in Table 15.

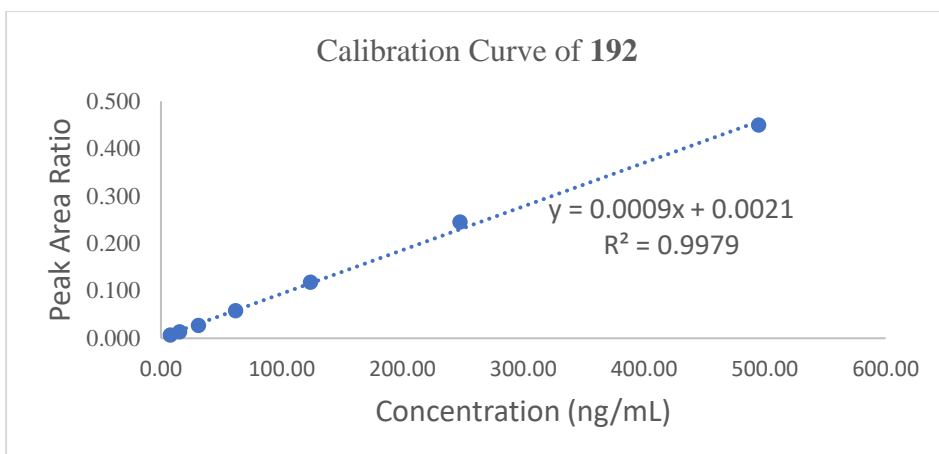


Figure 16. Calibration curve of **192** for kinetic aqueous solubility

Table 15. Sample area, IS area, area ratio and standard concentration of **192** for kinetic aqueous solubility.

| Sample Name | Area | IS Area | Area Ratio | Actual Concentration (ng/mL) | Sample RT | IS RT |
|------------------------|----------|----------|------------|------------------------------|-----------|-------|
| N192 Standard 1 | 171943 | 25342412 | 0.007 | 7.72 | 1.39 | 0.74 |
| N192 Standard 2 | 342886 | 25479272 | 0.013 | 15.44 | 1.38 | 0.74 |
| N192 Standard 3 | 691123 | 25651417 | 0.027 | 30.99 | 1.37 | 0.73 |
| N192 Standard 4 | 1453398 | 25078923 | 0.058 | 61.88 | 1.37 | 0.73 |
| N192 Standard 5 | 3017703 | 25534856 | 0.118 | 123.75 | 1.36 | 0.73 |
| N192 Standard 6 | 6104192 | 24898413 | 0.245 | 247.5 | 1.36 | 0.73 |
| N192 Standard 7 | 11379418 | 25304050 | 0.450 | 495 | 1.36 | 0.73 |
| Sample 1 | 3794250 | 25404191 | 0.149 | | 1.35 | 0.73 |
| Sample 2 | 3852686 | 26473602 | 0.146 | | 1.36 | 0.72 |
| Sample 3 | 3773216 | 24550160 | 0.154 | | 1.35 | 0.72 |

The solubility of each sample is calculated by using the linear equation ($y = 0.0009x + 0.0021$; $R^2 = 0.9979$) generated from the above calibration curve.

From above equation, we have,

$$x = \frac{y - 0.0021}{0.0009}$$

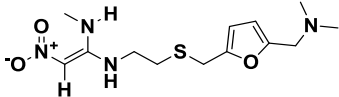
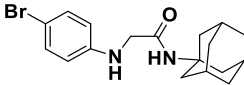
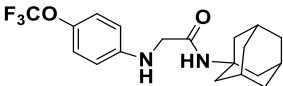
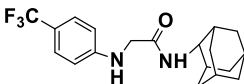
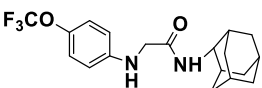
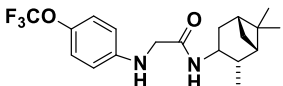
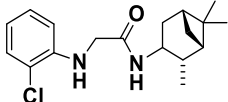
For sample 1,

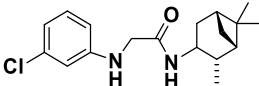
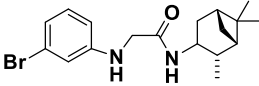
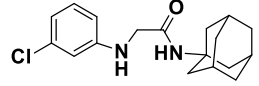
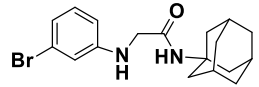
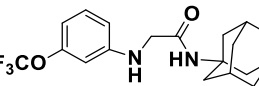
$$x = \frac{0.149 - 0.0021}{0.0009} = 163.22$$

The dilution factor in preparing the final sample was 100, therefore the solubility of sample 1 was $163.22 * 100 = 16322 \text{ ng/mL} = 16.32 \text{ }\mu\text{g/mL}$. Similarly, the solubility of the other two samples (Sample 2 and Sample 3) were also calculated and the mean value of these samples with standard deviation was reported as $16.3 \pm 0.30 \text{ }\mu\text{g/mL}$.

The solubility experiment was performed for all the active compounds and a known positive control, ranitidine (Table 16).

Table 16: Kinetic aqueous solubility data of all active compounds.

| North No. | Structure | <i>M. abscessus</i> MIC ($\mu\text{g/mL}$) | <i>M. tb.</i> MIC ($\mu\text{g/mL}$) | Aqueous Solubility ($\mu\text{g/mL}$) |
|------------|---|---|---|---|
| Ranitidine |  | | | 77.5 ± 1.8 |
| 176 |  | 2 | 8 | 1.3 ± 0.01 |
| 179 |  | 2 | 16 | 6.79 ± 0.5 |
| 187 |  | 4 | 2 | 23.9 ± 0.9 |
| 188 |  | 2 | 4 | 20.3 ± 0.4 |
| 190 |  | 1 | 4 | 4.5 ± 0.2 |
| 191 |  | 1 | 0.25 | 14.3 ± 0.4 |

| North No. | Structure | <i>M. abscessus</i> MIC (µg/mL) | <i>M. tb.</i> MIC (µg/mL) | Aqueous Solubility (µg/mL) |
|-----------|--|------------------------------------|---------------------------------|----------------------------------|
| 192 |  | 0.5 | 0.25 | 16.3 ± 0.3 |
| 194 |  | 1 | 0.5 | 18.6 ± 0.3 |
| 196 |  | 1 | 1 | 30.3 ± 1.0 |
| 198 |  | 1 | 1 | 22.2 ± 1.5 |
| 200 |  | 0.5 | 0.25 | 20.4 ± 2.4 |

Ranitidine was used as a positive control to verify with the published value. The reported value of kinetic aqueous solubility of ranitidine is 79.5 µg/mL (Drug bank, 2019) and the observed value is 77.5 ± 1.85 µg/mL indicating that the method we have adopted produced reproducible and accurate results.

There was upwards of a 30-fold increment in the aqueous solubility of the acetamides from indoles. The solubility ranged from 2 µg/mL to 30 µg/mL. The compounds **176**, **179**, and **190** were the least aqueous soluble compounds with aqueous solubility value of less than 10 µg/mL. Compounds **191**, **192**, and **194** exhibited solubility at a range of 10 – 20 µg/mL. The other active compounds **187**, **188**, **196**, **198**, and **200** demonstrated the highest aqueous solubilities in the range of 20-30 µg/mL.

The United States Pharmacopeia (USP) has classified solubility in various defined categories (Table 17). The aqueous solubility of the previous generation indoles was typically less than 1 µg/mL which falls in a category of practically insoluble as defined by USP. There is a definite boost in aqueous solubility profiles by around 30-fold in the acetamide class, however, acetamides also fall in practically insoluble or insoluble category

Table 17. Description of aqueous solubility by USP (USP-NF, 2015).

| Descriptive Term | Parts of solvents required per parts of solute |
|------------------------------------|---|
| Very soluble | Less than 1 |
| Freely soluble | From 1 to 10 |
| Soluble | From 10 to 30 |
| Sparingly soluble | From 30 to 100 |
| Slightly soluble | From 100 to 1,000 |
| Very slightly soluble | From 1,000 to 10,000 |
| Practically insoluble or insoluble | Greater than equal to 10,000 |

3.4 Permeability

Permeability is defined as the process by which compounds are absorbed from the gastrointestinal (GI) tract to enter systemic circulation (Kerns et al. 2004). A drug permeates from the GI tract to the systemic circulation across biological membranes via three different mechanisms: i) passive transport, ii) active transport, and iii) facilitated transport (Figure 17) (Yang and Hinner 2015). In passive transport, the compounds diffuse through biological membranes based on their concentration gradient. Generally, lipophilic compounds permeate the membrane by passive

transport, and around 80% - 95% of the available marketed drugs permeate by this process (Mandagere, Thompson, and Hwang 2002). Active transport requires energy in the form of ATP to facilitate transport against the concentration gradient. An example of active transport is the sodium-potassium pump ($\text{Na}^+ - \text{K}^+$ pump). Facilitated transport is passive transport of molecules via specific transporter proteins down their concentration gradients. It is also important to note that some membranes have secretory mechanisms such as efflux pumps for certain compounds and reduces the permeability.

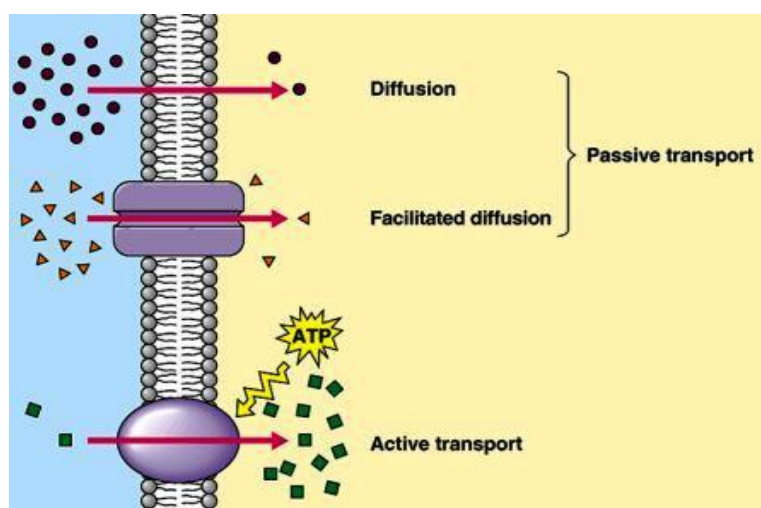


Figure 17. Mechanisms of drug transport (Yang and Hinner 2015).

Curatolo *et. al*, pointed that an efficacious candidate that is not absorbed is no better than an inactive candidate (Curatolo 1998). Permeability of a drug is directly related to the absorption and distribution profiles of the compounds, all of which provide information on bioavailability (Fortuna, Alves, and Falcão 2007). Therefore, determining the permeability profiles of lead compounds in the early stages of drug discovery is a common practice.

Preclinical permeability assays are performed in two primary ways: synthetic-based and cell-based permeability assays (Kerns et al. 2004). In synthetic-based permeability

assays, such as parallel artificial membrane permeability assay (PAMPA), an artificial membrane that simulates a biological membrane is used. In cell-based permeability assays, MDCK or Caco-2 cells are widely used (Fortuna, Alves, and Falcão 2007). Each assay has its own pros and cons. PAMPA offers high throughput screening of the permeability of NCEs in rapid, simple, easier, and cost-effective manner. PAMPA only accounts for permeability via passive diffusion. Conversely, the *in vitro* cell-based permeability assays provide information about the net permeability as they account for both permeability through facilitated diffusion and restricted permeability due to cell-mediated efflux mechanisms (Abbaci et al. 2008). However, each of these assays complement each other and help to identify a better lead in the drug development process. PAMPA is adopted in the early stages of drug screening while cell-based assays are preferred in later stages (Szymański, Markowicz, and Mikiciuk-Olasik 2012). Since our defined research project goal was to understand the general permeability patterns of the acetamide series, PAMPA was selected as the preferred permeability assay.

3.4.1 Parallel artificial membrane permeability assay (PAMPA)

PAMPA offers high throughput screening of permeability profiles of compounds. Kansy *et. al*, pioneered the concept of using artificial membranes to simulate biological membranes (Kansy, Senner, and Gubernator 1998). PAMPA has a strong correlation coefficient of 0.87% to the actual permeability values (Fortuna, Alves, and Falcão 2007). Cell membranes, which account for more than 90% of biological membranes, consist of glycolipids, cholesterol, and phospholipid bilayers comprised principally of phosphatidylcholine, phosphatidylethanolamine, phosphatidylserine, and sphingomyelin (Figure 18) (Cooper GM, 2000).

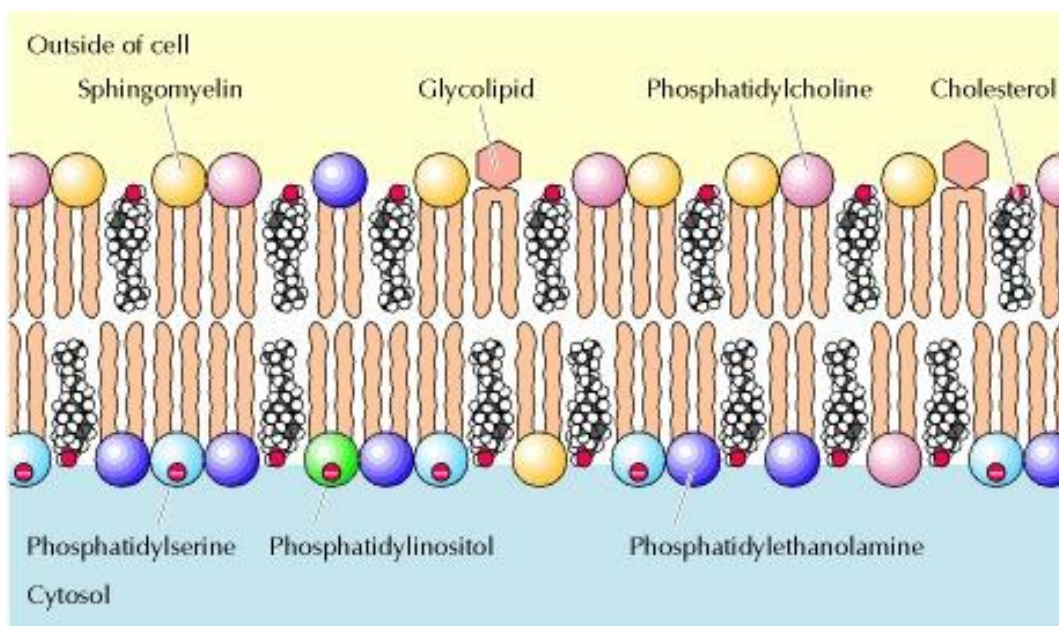


Figure 18. Structure of cell membrane (Cooper GM, 2000).

PAMPA helps determine the permeability of compounds being tested by measuring the quantity of compound that passes from a donor compartment to an acceptor compartment through the synthetic biological membrane (Figure 19). A 96-well membrane filter-based microtiter plate system with donor and acceptor compartment separated by the membrane was used. The protocol that was followed for this assay was developed by the North lab ((Brown et al. 2011) and is modified from the method published by Millipore Corporation. (Synthetic biological membranes utilized in PAMPA are generated by dissolving lecithin in an inert organic solvent and placed onto a hydrophobic PVDF filter (Faller 2008). The compounds were dissolved in 5% DMSO in phosphate-buffer saline (PBS) solution with Lucifer yellow, a dye used to assess membrane integrity. The solution was placed in the donor well, and PBS was added to the acceptor well. The plates were then allowed to incubate for 16 hours. After that, compound quantification from the donor and acceptor wells was assessed using high pressure liquid chromatography (HPLC). The Lucifer yellow was visually inspected for

presence in the acceptor plate after the incubation time, and absence of any color confirmed the integrity of the PAMPA membrane.

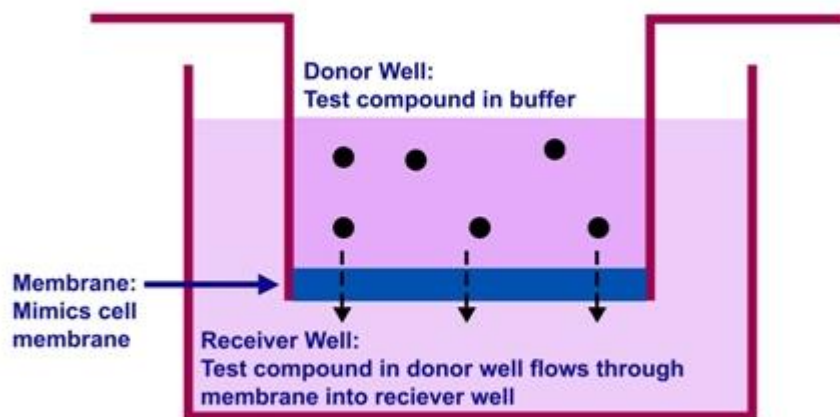


Figure 19. PAMPA model to assess permeability (Bioassay systems, 2019).

An HPLC method was developed for the simultaneous quantification of the acetamides and the IS (warfarin). For each compound, a concentration versus area ratio calibration curve with seven points was plotted, and the concentration of the compounds in the donor and acceptor compartments was quantified using the calibration curve. All experiments were performed in triplicate.

The PAMPA determination of a representative compound **192** is explained below. The calibration curve shown in Figure 20 was generated using Microsoft Excel by plotting concentration at x-axes and area ratio at y-axes. The area under the curve from sample, IS area, area ratio, sample retention time, IS retention time, and concentration of the known standards were obtained from HPLC (Table 18). The concentrations of the sample, donor and acceptor wells, were calculated using the calibration curve in

triplicate. The theoretical equilibrium, a resulting concentration made by mixing donor and acceptor compartment, was also determined.

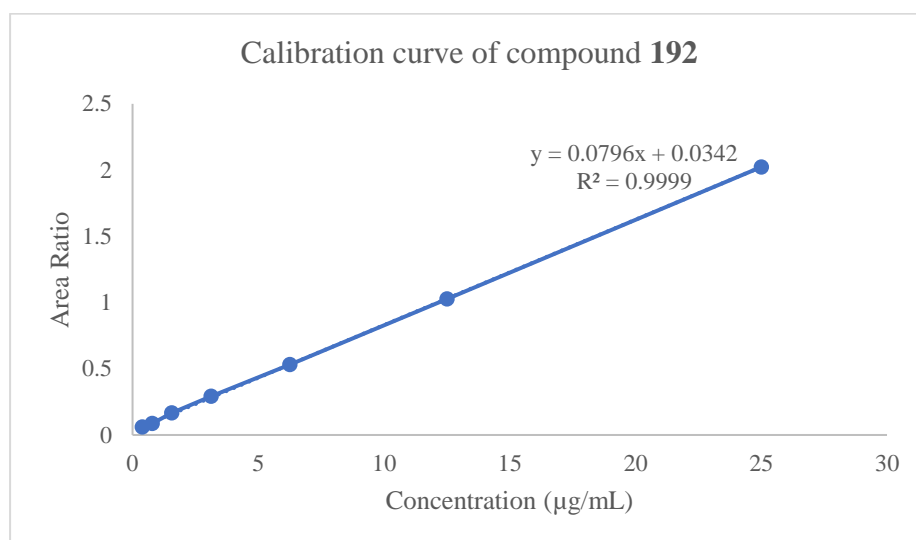


Figure 20. Calibration curve of **192** for PAMPA.

Table 18. Sample area, IS area, area ratio and standard concentration of **192** for PAMPA.

| Sample | Sample area | IS area | Area ratio | Sample RT (min) | IS RT (min) | Concentration (µg/mL) |
|--------------------|-------------|---------|------------|-----------------|-------------|-----------------------|
| Standard 1 | 16366 | 270723 | 0.06 | 1.41 | 0.89 | 0.39 |
| Standard 2 | 23492 | 272415 | 0.08 | 1.41 | 0.89 | 0.78 |
| Standard 3 | 45718 | 274238 | 0.16 | 1.42 | 0.89 | 1.56 |
| Standard 4 | 79228 | 272007 | 0.29 | 1.41 | 0.89 | 3.12 |
| Standard 5 | 143029 | 268952 | 0.53 | 1.41 | 0.89 | 6.25 |
| Standard 6 | 271233 | 264025 | 1.02 | 1.42 | 0.89 | 12.50 |
| Standard 7 | 535042 | 264481 | 2.02 | 1.41 | 0.88 | 25 |
| Donor 1 | 32883 | 280573 | 0.11 | 1.43 | 0.89 | 1.04 |
| Acceptor 1 | 20005 | 275296 | 0.07 | 1.42 | 0.89 | 0.48 |
| Donor 2 | 33976 | 278707 | 0.12 | 1.41 | 0.89 | 1.10 |
| Acceptor 2 | 19921 | 276222 | 0.07 | 1.42 | 0.89 | 0.47 |
| Donor 3 | 33134 | 280134 | 0.11 | 1.42 | 0.89 | 1.05 |
| Acceptor 3 | 20189 | 276375 | 0.07 | 1.42 | 0.89 | 0.48 |
| Equilibrium | 52004 | 235953 | 0.22 | 1.42 | 0.89 | 2.33 |

From the calibration curve, the equation of the linear regression ($R^2 = 0.999$) is:

$$y = 0.0796x + 0.0342$$

The concentration of the compound at *donor compartment* was:

$$x = \frac{0.11 - 0.0342}{0.079} = 0.96 \text{ } \mu\text{g/mL}$$

Since the dilution factor was 2, the actual concentration of the *donor compartment* after incubation was $0.96 * 2 = 1.92 \text{ } \mu\text{g/mL}$

Similarly, the concentration of the compound at *acceptor compartment* was $0.97 \text{ } \mu\text{g/mL}$.

Finally, the equilibrium concentration was determined to be $4.67 \text{ } \mu\text{g/mL}$

Equation 1. Apparent Permeability (P_e)

$$P_e = \left[\frac{V_D \times V_A}{(V_D + V_A) \times Area \times Time} \right] \times \left\{ -\ln \left[1 - \frac{C_A(t)}{C_{eq}} \right] \right\}$$

The equation 1 is the formula for the determination of permeability through the biological membrane. Permeability by diffusion in the microenvironment such as biological tissue are the function of thickness of the membrane, surface area of the membrane, concentration gradient, and time (Dudko, Berezhkovskii, and Weiss 2004).

The above equation considers all the factors responsible for the permeability via biological membrane. In the above equation, V_D , V_A , $Area$, $Time$, $C_A(t)$, and C_{eq} represents donor compartment volume (0.15 mL), acceptor compartment volume (0.3 mL), area of the membrane (0.3 cm^2), time of incubation (57,600 s), concentration of solution in the acceptor chamber after 16 hours, and the equilibrium concentration, respectively. On substituting all the values,

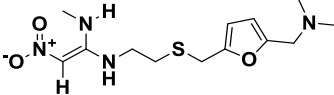
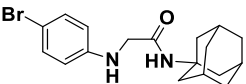
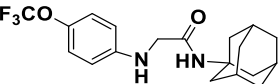
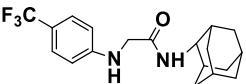
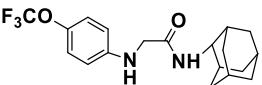
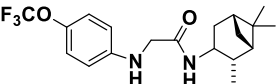
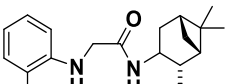
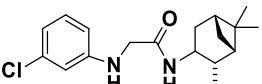
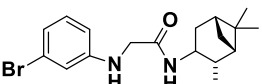
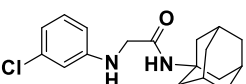
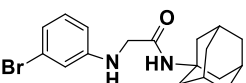
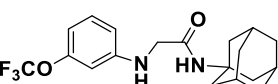
$$P_e = \left[\frac{0.15 \times 0.30}{(0.15 + 0.30) \times 0.3 \times 57600} \right] \times \left\{ -\ln \left[1 - \frac{0.97}{4.67} \right] \right\}$$

$$P_e = 1.34 * 10^{-6} \text{ cm/s}$$

Similarly, the P_e for other two wells were also calculated to obtain: $P_e = (1.34 \pm 0.01) * 10^{-6}$ cm/s. Compounds with a permeability $\geq 10 * 10^{-6}$ cm/s are considered highly permeable compounds, and permeability $< 0.5 * 10^{-6}$ cm/s are considered poorly permeable compounds (Alvarez-Figueroa et al. 2011). The compounds in the permeability range of 0.5 - $10 * 10^{-6}$ cm/s are considered moderately permeable compounds (Alvarez-Figueroa et al. 2011) (Cyprotex PAMPA assay, 2019).

Table 19 depicts the PAMPA permeability of all the active compounds. To validate the PAMPA permeability method, ranitidine was selected as a positive control for the experiments. The reported value for PAMPA permeability of ranitidine was $1.4 * 10^{-6}$ cm/s (Yu et al. 2015) and we determined the PAMPA permeability as $3.47 * 10^{-6}$ cm/s, confirming the accuracy of our methods and experiments (Table 19). Generally, most of the compounds were found to be moderately permeable, with a small number of compounds found to have low permeability. Compound **200** showed the highest permeability of $3.61 * 10^{-6}$ cm/s whereas compound **176** showed the lowest permeability of $0.28 * 10^{-6}$ cm/s. Compounds **176, 179, 187, and 191** were considered as poorly permeable compounds while compounds **188, 190, 192, 194, 196, 198, and 200** were considered moderately permeable compounds based on the above definitions.

Table 19. PAMPA permeability of all active compounds.

| North No. | Structure | <i>M. abs.</i> MIC ($\mu\text{g/mL}$) | <i>M. tb.</i> MIC ($\mu\text{g/mL}$) | PAMPA (* 10^{-6} cm/s) |
|------------|---|---|--|-----------------------------|
| Ranitidine |  | | | 3.47 ± 0.50 |
| 176 |  | 2 | 8 | 0.28 ± 0.04 |
| 179 |  | 2 | 16 | 0.47 ± 0.05 |
| 187 |  | 4 | 2 | 0.34 ± 0.19 |
| 188 |  | 2 | 4 | 3.12 ± 0.03 |
| 190 |  | 1 | 4 | 3.19 ± 0.03 |
| 191 |  | 1 | 0.25 | 0.38 ± 0.03 |
| 192 |  | 0.5 | 0.25 | 1.33 ± 0.01 |
| 194 |  | 1 | 0.5 | 1.01 ± 0.01 |
| 196 |  | 1 | 1 | 0.32 ± 0.005 |
| 198 |  | 1 | 1 | 1.02 ± 0.02 |
| 200 |  | 0.5 | 0.25 | 3.61 ± 0.04 |

Permeability above $0.5 * 10^{-6}$ cm/s is considered optimal for early stage drug development (Alvarez-Figueroa et al. 2011). Seven of the eleven active compounds surpassed this threshold, indicating that acetamides could be further developed from a permeability stance.

Biopharmaceutical classification system (BCS) also classifies drug substances based on their solubility and permeability. The primary intention of BCS is to assess the *in vivo* bioequivalence from the *in vitro* measurement of the solubility and permeability to identify if the drug products qualify for a biowaiver for bioequivalence testing. BCS system classifies drug products into the following four classes (US-FDA):

- Class 1: High Permeability, high solubility
- Class 2: High Permeability, Low solubility
- Class 3: Low Permeability, High Solubility
- Class 4: Low Permeability, Low Solubility

BCS solubility is defined as, ‘A drug substance is considered highly soluble when the highest marketed strength is soluble in 250 mL or less of aqueous media within the pH range of 1 - 6.8 at $37 \pm 1^{\circ}\text{C}$.’ The volume estimate of 250 mL is derived from typical bioequivalence study protocols that prescribe administration of a drug product to fasting human volunteers with an 8-fluid ounce glass of water. The BCS solubility definition applies to drug candidates in late-stage drug development, when the dose for the *in vivo* efficacy in human is identified or for FDA-approved drugs. The biopharmaceutics drug disposition classification system (BDDCS) is a tool to predict drug dispositions and drug-drug interactions (DDIs). BDDCS had also some criteria in the early stage drug discovery to relate where the NCE would land in the future. Generally, an NCE with an aqueous solubility profile of at least 200 $\mu\text{g/ml}$ would be

later developed and classified as a high solubility drug, and an NCE with a solubility profile of <200 µg/ml would typically later be classified as low solubility (Benet 2013; Varma et al. 2012). The acetamide leads possessed the aqueous solubility profiles of 20 – 30 µg/ml, which means further optimization of the scaffold to boost the solubility profile by 7 – 10-fold is required.

In the early stage of drug discovery, an aqueous solubility of 10 µg/mL or higher is a promising starting point for further drug development (Guha et al. 2011). Improved aqueous solubility profiles tend to have better absorption profiles *in vivo* and helps the drug to reach into systemic circulation. Of the 11 active compounds of acetamides series, 8 compounds achieved solubility profiles of 10 µg/mL or better. The aqueous solubility profiles of the acetamides increased by 20- to 30-fold compared to indoles, validating the second point of the hypothesis.

BCS defines permeability as the permeability class boundary is based indirectly on the extent of absorption (fraction of dose absorbed, not systemic bioavailability) of a drug substance in humans and directly on measurements of the rate of mass transfer across human intestinal membrane. Alternatively, other systems capable of predicting the extent of drug absorption in humans can be used (e.g. *in situ* animal, *in vitro* epithelial cell culture methods). A drug substance is considered to be highly permeable when the systemic bioavailability or the extent of absorption in humans is determined to be $\geq 85\%$ of an administered dose based on a mass balance determination (along with evidence showing stability of the drug in the GI tract) or in comparison to an intravenous reference dose. BCS permeability also applies to either the marketed drug formulation or a drug candidate whose *in vivo* pharmacokinetic has already been performed. However, based on the preliminary *in vitro* studies data, it could be predicted which

permeability profile would the NCE possess. The NCE with a PAMPA permeability profile higher than $3 * 10^{-6}$ cm/s would typically be classified as highly permeable according to BCS, while the NCE with a PAMPA permeability profile lower than $2.5 * 10^{-6}$ cm/s would typically be classified as a low permeability compound (Benet 2013, Varma et al. 2012). Only one compound, **200**, has a PAMPA permeability of $3.5 * 10^{-6}$. The other two compounds are between the range of $2 - 3.5 * 10^{-6}$ cm/s, which may be developed further to enhance permeability.

3.5 Plasma protein binding (PPB)

When a drug reaches the systemic circulation from the site of administration, it binds to proteins present in the plasma in a process called plasma protein binding (PPB). Generally, acidic drugs bind to albumin and basic drugs bind to α 1-acid glycoproteins (Routledge 1986). Plasma protein bound drug is not available to elicit its pharmacological response, so efficacy is only due to the unbound (free) fraction of the drug.

PPB influences the pharmacokinetics/pharmacodynamics (PK/PD) profiles of the compounds (Schmidt, Gonzalez, and Derendorf 2010). Only free drug is available to reach the tissue, and thus, metabolism, excretion and the pharmacological activity are dependent on the amount of the free drug (Rizk et al. 2017). DDIs may occur if another compound that competes for binding to the same protein displaces the drug, resulting in an increased concentration of free drug and potential adverse/toxic effects (Rizk et al. 2017). In such cases, it may be necessary to adjust the dose or change the regimen to avoid DDIs. Bound drugs can also inhibit metabolizing enzymes and transporters, which may cause adverse reactions (Rizk et al. 2017). Thus, understanding PPB of drug candidates in the early stages of drug development provides information on

pharmacological effects, ADME-Tox profiles, DDIs, safety regimens, and drug tolerability.

PPB profiles should not be considered a parameter to prioritize drug candidates in the drug discovery and development process (Smith, Di, and Kerns 2010), but may be used to augment understanding of various pharmacokinetic factors stemming from high/low PPB (Smith, Di, and Kerns 2010). A brief analysis of PPB profiles of 189 drugs approved by US FDA (United States Food and Drug Administration) elucidates that more than 45% of the drugs approved from 2003 to 2013 had a PPB of >95% and more than 24% of the drugs approved in the same time span have a PPB of >99% (Liu, Wright, and Hop 2014). This data reinforced that high PPB is not a setback and should not be a basis for attrition in the drug development.

3.5.1 Determination of human plasma protein binding

The information PPB provides are essential during drug development. Hence, there are various methods, both low to high throughput, developed for the assessment of PPB in drug discovery, including equilibrium dialysis, ultrafiltration, and ultracentrifugation (Kariv, Cao, and Oldenburg 2001; Wan and Rehngrén 2006; Ye, Zetterberg, and Gao 2017).

Equilibrium dialysis is a commonly employed method to determine PPB, where a selectively permeable dialysis membrane is used to separate the plasma and buffer chamber until an equilibrium is attained (Ye, Zetterberg, and Gao 2017). The dialysis membrane works on the principle of molecular weight-cutoff. The molecular weight-cutoff of the membrane allows unbound compound to freely diffuse across the membrane but prevents the higher molecular weight compound (ligand) and protein complex. This classical approach of determination of PPB by equilibrium has many

limitations in that it is highly labor-intensive and time consuming in terms of sample preparation and equilibration (Wan and Rehgren 2006; Waters et al. 2008). To overcome these limitations, rapid equilibrium dialysis (RED) was developed.

Rapid equilibrium dialysis (RED) provides high throughput screening of compounds to establish PPB profiles. The RED device contains a teflon-based plate with disposable dialysis cells (Figure 21 Panel A) (Sarathy et al. 2017). The increase in surface area to volume ratio in RED compared to classical equilibrium dialysis allows for decreased equilibrium time and a higher throughput assay (Waters et al. 2008). The compounds are added to human plasma and placed in plasma chambers. The dialysis membrane will permit unbound drug to diffuse into the buffer chamber on the principle of molecular cutoffs, while bound drug is trapped in the initial chamber (Figure 21 Panel B) (Sarathy et al. 2017).

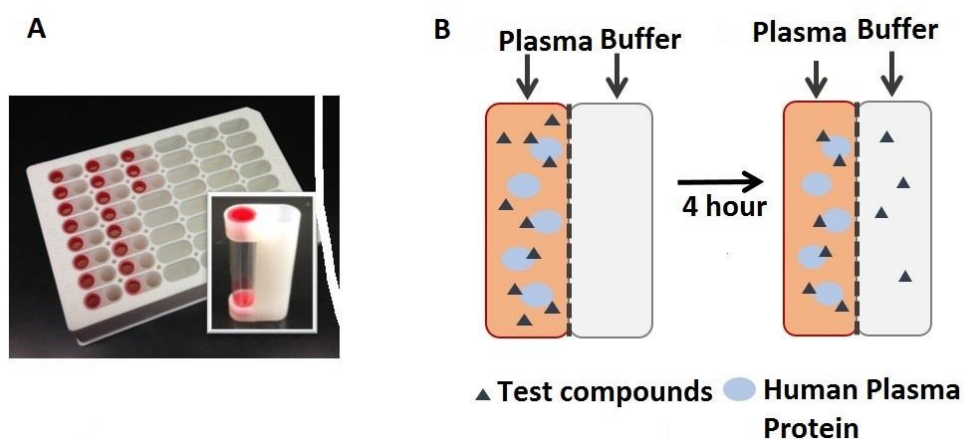


Figure 21. Panel A – RED insert device in RED plate; Panel B – Principle of RED (Sarathy et al. 2017).

The compounds were spiked with human plasma at 10 $\mu\text{g}/\text{mL}$ concentrations and placed in plasma chambers of the RED device. PBS was placed in the buffer chambers and the RED device was sealed and allowed to shake in an orbital shaker for four hours

at 37°C to achieve equilibrium. Equal volumes of plasma were added to the aliquots of the buffer chambers and vice versa to create identical matrices. The compounds were then precipitated using methanol (four times the aqueous phase) and centrifuged, then the compound concentration in the supernatant was quantified using LC-MS-MS.

The human plasma protein binding (HPPB) of a representative compound, **192** is explained here. The calibration curve shown in Figure 22 was generated using Microsoft Excel by plotting concentration vs area ratio. The sample area IS area, area ratio, sample retention time, IS retention time, and concentration of the known standards were obtained from LC-MS-MS (Table 20). The HPPB was obtained by calculating the concentration of the plasma chamber and buffer chamber.

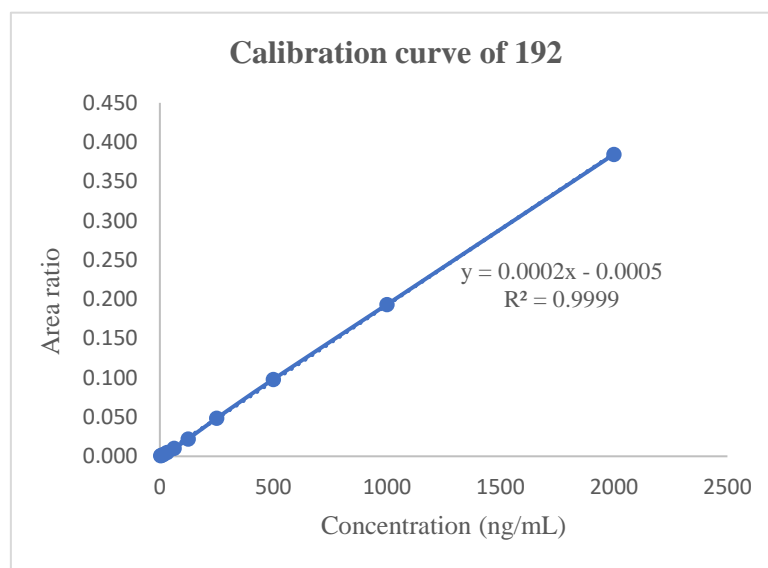


Figure 22. Calibration curve of **192** for HPPB assay.

Table 20. Sample area, IS area, area ratio and standard concentration of **192** for HPPB assay

| Sample Name | Area | IS Area | Area Ratio | Sample RT (min) | IS RT (min) | Actual Concentration (ng/mL) |
|-------------|-------|----------|------------|-----------------|-------------|------------------------------|
| Standard 1 | 16659 | 20432341 | 0.001 | 1.35 | 0.69 | 3.9 |
| Standard 1 | 26537 | 20163618 | 0.001 | 1.23 | 0.68 | 7.81 |

| Sample Name | Area | IS Area | Area Ratio | Sample RT (min) | IS RT (min) | Actual Concentration (ng/mL) |
|------------------|----------|----------|------------|-----------------|-------------|------------------------------|
| Standard 1 | 50242 | 20640229 | 0.002 | 1.23 | 0.68 | 15.63 |
| Standard 1 | 104981 | 20705808 | 0.005 | 1.23 | 0.68 | 31.25 |
| Standard 1 | 214104 | 20905786 | 0.010 | 1.23 | 0.68 | 62.5 |
| Standard 1 | 443379 | 20088965 | 0.022 | 1.23 | 0.66 | 125 |
| Standard 1 | 981064 | 20253964 | 0.048 | 1.22 | 0.67 | 250 |
| Standard 1 | 1975052 | 20131690 | 0.098 | 1.22 | 0.67 | 500 |
| Standard 1 | 3954054 | 20464611 | 0.193 | 1.23 | 0.68 | 1000 |
| Standard 1 | 8024363 | 20871064 | 0.384 | 1.23 | 0.68 | 2000 |
| Plasma Chamber 1 | 18122379 | 20950671 | 0.865 | 1.23 | 0.67 | |
| Buffer Chamber 1 | 1110937 | 21815839 | 0.051 | 1.23 | 0.69 | |
| Plasma Chamber 2 | 17968194 | 20772673 | 0.865 | 1.23 | 0.67 | |
| Buffer Chamber 2 | 1102434 | 21419841 | 0.051 | 1.23 | 0.69 | |
| Plasma Chamber 3 | 18472208 | 21231656 | 0.870 | 1.24 | 0.68 | |
| Buffer Chamber 3 | 1128150 | 21894861 | 0.052 | 1.23 | 0.68 | |

From the calibration curve, the equation of the straight line ($R^2 = 0.9999$) was:

$$y = 0.0002x - 0.0005$$

From above equation,

$$x = \frac{y - 0.0005}{0.0002}$$

The concentration of the compound at plasma chamber 1 was:

$$x = \frac{0.865 - 0.0005}{0.0002} = 4322.5 \text{ ng/ml}$$

With a dilution factor 2, the actual concentration at plasma chamber 1 was

$$A = 4322.5 * 2 = 8645 \text{ ng/ml}$$

Similarly, the actual concentration at buffer chamber 1 was 504 ng/ml.

Equation 2. % Free drug concentration

$$\% \text{ Free} = \frac{[\text{Buffer Chamber Compound Concentration}]}{[\text{Plasma Chamber Compound Concentration}]} \times 100$$

$$\% \text{ Free} = \frac{504}{8645} \times 100 = 5.82$$

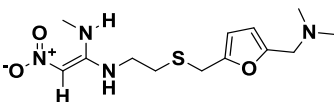
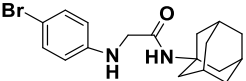
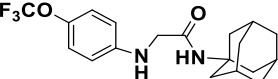
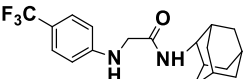
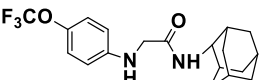
Equation 3: % Bound drug concentration

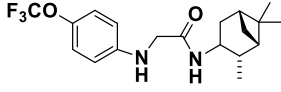
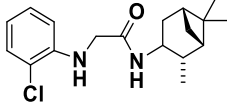
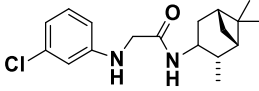
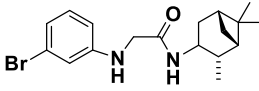
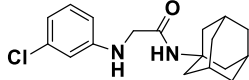
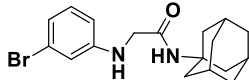
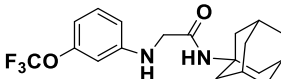
$$\% \text{ Bound} = 100 - \% \text{ Free}$$

$$\% \text{ Bound} = 100 - 5.82 = 94.18\%$$

The experiment was conducted in triplicate, and the % bound of **192** was found to be 94.134 ± 0.026 %. HPPB assays for all 11 active compounds and a positive control, ranitidine, were performed in the same manner. The HPPB for ranitidine reported in the literature was 15% (Drug Bank, 2019), and the value obtained from our assay was 20.7 ± 2.9 , validating the accuracy of our methods. Table 21 depicts the HPPB of all the active compounds and ranitidine.

Table 21. HPPB of all the active compounds and ranitidine

| North No. | Structure | <i>M. abs.</i> MIC ($\mu\text{g/mL}$) | <i>M. tb.</i> MIC ($\mu\text{g/mL}$) | % Bound |
|-------------------|---|---|--|-----------------------------------|
| Ranitidine |  | | | 20.7 ± 2.9 |
| 176 |  | 2 | 8 | 99.6 ± 0.14 |
| 179 |  | 2 | 16 | 99.8 ± 0.01 |
| 187 |  | 4 | 2 | 94.3 ± 0.5 |
| 188 |  | 2 | 4 | 96.7 ± 0.01 |

| North No. | Structure | <i>M. abs.</i> MIC ($\mu\text{g/mL}$) | <i>M. tb.</i> MIC ($\mu\text{g/mL}$) | % Bound |
|-----------|---|---|--|-----------------|
| 190 |  | 1 | 4 | 95.2 \pm 0.05 |
| 191 |  | 1 | 0.25 | 95.5 \pm 0.1 |
| 192 |  | 0.5 | 0.25 | 94.1 \pm 0.02 |
| 194 |  | 1 | 0.5 | 95.5 \pm 0.1 |
| 196 |  | 1 | 1 | 99.8 \pm 0.01 |
| 198 |  | 1 | 1 | 93.2 \pm 0.1 |
| 200 |  | 0.5 | 0.25 | 94.9 \pm 0.3 |

Generally speaking, compounds with plasma protein binding greater than 85% are considered highly protein bound and the consequent pharmacokinetic implications should be considered (Sarathy et al. 2017). Results from the RED PPB assays indicate that all the active compounds of the acetamides series were highly PPB (Table 21). Compounds **196**, **179**, and **176** were found to have the highest HPPB values with % bound values of 99.8%, 99.8% and 99.6%, respectively. Excepting these three, all the other compounds fall within the percentage bound range of 93.2% to 96.7%.

In summary, the acetamides in the series had high PPB profiles (94% to 99%), encouraging awareness of the possible consequences on PK/PD profiles, DDIs, and certain disease states throughout drug development. High PPB also offers some advantages such as prolonged half-life and reduced dosing frequency. Most of our compounds were highly protein bound, and they remain promising potential drug candidates with the considerations mentioned above.

3.6 Cytotoxic profiles

The two most important criteria an NCE should meet to be developed as a potential drug candidate are efficacy and safety profiles. Regardless of the efficacy of the compounds, a compound that fails to achieve enough safety profile undergoes an immediate attrition in drug development. However, it could be repurposed as a potential antineoplastic agent. Hence, assessment of cytotoxicity is routinely performed in the early stages of drug development.

The safety profile is generally established based on selectivity index (SI), the ratio of IC_{50} to MIC. IC_{50} is defined as the minimum concentration of the drug that inhibit the growth of 50% of the cells. Higher selectivity indices values, which means low MIC and high IC_{50} values, are preferred in drug development. In drug development, SI values ≥ 10 are considered ideal in the antimicrobial realm (North et al. 2013). The cell viability for the acetamides was determined by MTT (3-(4,5-dimethylthiazol-2-yl)-2,5-diphenyltetrazolium) assay, a routinely used assay for the determination of cell viability.

3.6.1 MTT assay

MTT assay works on the principle that mitochondrial activity of the viable cells can convert MTT into formazan (Figure 23), and the uniform purple colored formazan

solution can be quantified using a plate reader (Riss et al. 2016). The mitochondrial activity, which is a conversion of NADH to NAD⁺, promotes reduction of MTT to formazan, and the concentration of formazan crystal formation is directly proportional to the concentration of the mitochondrial activity (Kumar, Nagarajan, and Uchil 2018).

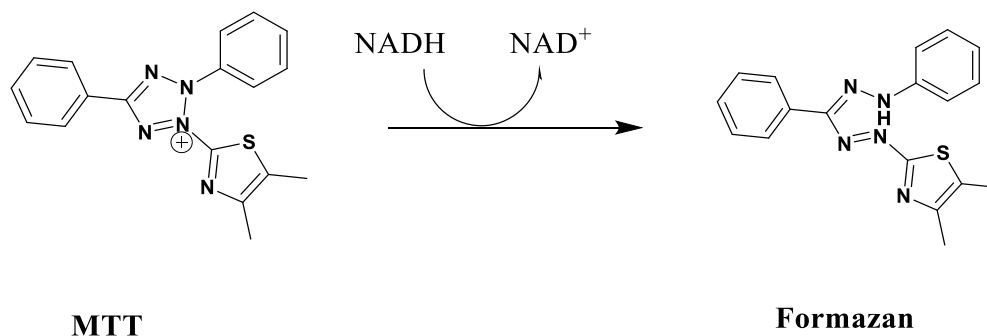


Figure 23. Principle of MTT assay: conversion of MTT to Formazan (Riss et al. 2016).

3.6.2 Determination of cell viability of acetamides using MTT assay. The IC₅₀ of the acetamides were determined in WI-26 VA4 cell lines, which are derivatives of human embryonic lung cell lines (ATCC, 2019). Since the site of action of antimycobacterial agents are human lungs, the human lung cell lines were taken. WI-26 VA4 cell lines were cultured and grown per ATCC protocol (ATCC, 2019).

The MTT assay was performed following Vybrant MTT assay protocol (Vybrant cell proliferation protocol, 2002). Briefly, the trypsinized cells were seeded in each well of a 96 well plate in a 37 °C incubator with 5% CO₂. Active compounds were prepared by serial dilution from 20 µg/mL to 0.00002 µg/mL with 10-fold dilutions using MEM/FBS with 0.2% DMSO. After 24 hours, when the cell reached approximately 10-15% confluency, the media was replaced by 100 µl of freshly prepared dilutions of acetamides, and it was performed in triplicate. The cells were allowed to grow for 72 hours. After 72 hours, the media was replaced by MEM/FBS and 10 µL of 5 mg/mL MTT in sterile PBS was added to each well. The plates were incubated at 37 °C for four

hours. After four hours, the treatment, media, and MTT reagent were replaced by sodium dodecylsulphate (SDS) in 0.01 M HCl solution to aid in dissolution of formazan crystals. The dissolved formazan was incubated at 37 °C for 30 min. and shaken in an orbital shaker for another 30 min. to ensure the dissolution of formazan crystals. The absorbance of dissolved formazan was measured using plate reader at 570 nm. One set of wells were untreated controlled wells, where cells in MEM/10% FBS with 0.2% DMSO without the compounds were placed. The percentage cell viability was calculated using the following equation:

Equation 3. % Cell Viability

$$\% \text{ Cell Viability} = \frac{\text{Absorbance of sample}}{\text{Absorbance of untreated control}} * 100\%$$

The IC₅₀ of the compound was determined using concentration vs % cell viability plot. The determination of cell viability, expressed in terms of IC₅₀ for a representative compound **192**, is explained below.

Table 22 shows the absorbance and % cell viability at different concentration of compound **192**. Figure 24 shows the concentration versus % cell viability plot to determine the IC₅₀. The average absorbance at 20 µg/mL was 0.29 ± 0.1, and the average absorbance of the control was 0.33 ± 0.07 (Table 22). The percentage cell viability at 20 µg/mL was:

$$\% \text{ Cell Viability} = \frac{0.29}{0.33} * 100\% = 87.87\%$$

The percentage viability of compound **192** at 20 µg/mL was found to be 87.87%. Percentage viability was determined similarly for all other concentrations, and, at all concentrations, percentage viability was greater than 50%. This confirmed that the

minimum concentration of compound **192** required to kill more than 50% of cells is more than 20 µg/mL, and hence the IC₅₀ of compound **192** was reported to be >20 µg/mL.

The SI is also a measure of the selectivity of an NCE for the microorganism of interest over human cells and given by:

Equation 4. Selectivity Index (SI)

$$SI = \frac{IC_{50}}{MIC}$$

Table 22. Absorbance, concentration, and IC₅₀ of compound **192**.

| Concentration (µg/mL) | Abs Sample 1 | Abs Sample 2 | Abs Sample 3 | Average | % Viability | IC ₅₀ |
|-----------------------|--------------|--------------|--------------|---------|-------------|------------------|
| Control | | | | 0.334 | 100.00 | |
| 0.00002 | 0.371 | 0.266 | 0.265 | 0.300 | 89.82 | |
| 0.0002 | 0.441 | 0.215 | 0.233 | 0.296 | 88.52 | |
| 0.0002 | 0.261 | 0.248 | 0.213 | 0.240 | 71.89 | >50% |
| 0.002 | 0.243 | 0.216 | 0.209 | 0.222 | 66.52 | |
| 0.02 | 0.214 | 0.202 | 0.197 | 0.204 | 61.04 | |
| 0.2 | 0.29 | 0.273 | 0.236 | 0.266 | 79.56 | |
| 20 | 0.314 | 0.283 | 0.274 | 0.290 | 86.73 | |

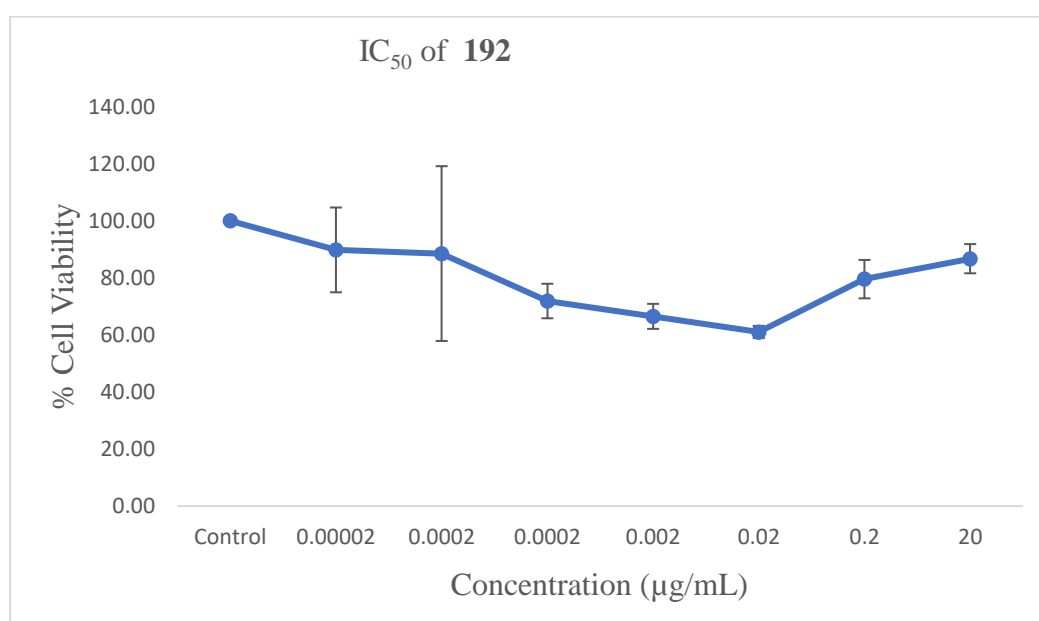


Figure 24. Concentration vs % cell viability to determine IC₅₀.

The SI of compound **192** against *M. abscessus* is given by:

$$SI = \frac{> 20}{0.5} = > 40$$

Similarly, the SI of compound **192** against *M. tb* is given by:

$$SI = \frac{> 20}{0.25} = > 80$$

The IC₅₀ and SI of all 11 active compounds were calculated in the same manner (Table 23). All the active compounds tested possessed an IC₅₀ value of >20 µg/mL which means no compounds could kill 50% of the cells even at the highest concentration of 20 µg/mL, suggesting that they are pharmacologically safe compounds.

Table 23. IC₅₀ and selectivity indices of all active compounds.

| North No. | <i>M. absc.</i> MIC (µg/mL) | <i>M. tb.</i> MIC (µg/mL) | IC ₅₀ (µg/mL) | SI (<i>M. absc.</i>) | SI (<i>M. tb</i>) |
|-----------|-----------------------------|---------------------------|--------------------------|------------------------|---------------------|
| 176 | 2 | 8 | >20 | >10 | >2.5 |
| 179 | 2 | 16 | >20 | >10 | >1.25 |
| 187 | 4 | 2 | >20 | >5 | >10 |
| 188 | 2 | 4 | >20 | >10 | >5 |
| 190 | 1 | 4 | >20 | >20 | >5 |
| 191 | 1 | 0.25 | >20 | >20 | >80 |
| 192 | 0.5 | 0.25 | >20 | >40 | >80 |
| 194 | 1 | 0.5 | >20 | >20 | >40 |
| 196 | 1 | 1 | >20 | >20 | >20 |
| 198 | 1 | 1 | >20 | >20 | >20 |

| 200 | 0.5 | 0.25 | >20 | >40 | >80 |
|-----|-----|------|-----|-----|-----|
|-----|-----|------|-----|-----|-----|

The acetamide series not only possessed optimal efficacy, physicochemical, and pharmacokinetic profiles, but also exhibited a high safety profile and high selectivity indices.

3.7. Summary:

The set of preliminary data had thrown more light on the general understanding of the acetamide series and had helped in prioritizing a lead candidate. From drug discovery perspective, an optimal aqueous solubility was achieved, however there needed to be further boost to hit a 200 µg/mL limit through further optimization. From BCS stand point, these NCEs as of now would develop as low aqueous solubility and low-high permeability compounds. Plasma protein binding was generally high, and the acetamides showed a high safety profile against the embryonic lung cell lines.

3.8 Experimental Section

3.8.1 Quantitative assessment using LC-MS-MS

The instrument was first tuned for each compounds for the determination of mass spectrometer compound parameters, including multiple reaction monitoring (MRM) transitions, declustering potentials (DP), entrance potentials (EP), cell exit potentials (CXP), and collision energies (CE) and mass spectrometer source parameters, including source temperature, ion spray voltage, and gas pressure were also set. These parameters were determined using 500 ng/mL solution in 50% methanol-water solution with 0.1% formic acid. The liquid chromatographic separation was carried out using a reverse phase C-18 column with a mobile phase composition of 70% acetonitrile and 30% water with 0.1% formic acid.

3.8.2 Determination of kinetic aqueous solubility

Kinetic aqueous solubility was performed by protocol developed by North lab. The compounds were first dissolved in DMSO at a concentration of 10 mg/ml. In 10 μ L of the DMSO stock solution was added 990 μ L of PBS solution and allowed it to stand for six hours at room temperature (25 °C). The sample was then centrifuged and the known volume of the aliquots of the supernatant was diluted 100 times with 50-50 methanol-water with warfarin as an internal standard. The experiment was performed in triplicates, and the concentration and was determined using LC-MS-MS to determine the kinetic aqueous solubility.

3.8.3 Determination of PAMPA permeability

PAMPA permeability was performed by protocol of North lab, which is slightly modified from Millipore Corporation's protocol. 5 μ L of 1% lecithin solution in dodecane served as PAMPA membrane. The compound stock solution was prepared by dissolving the compound in DMSO at a concentration of 10 mg/mL. 50 μ g/ml solution of compound were prepared from the stock by diluting with 5% DMSO in PBS containing 25 μ g/mL of Lucifer yellow in it. To each well of donor plate, 150 μ L of compound solution was added in triplicate. To each well of acceptor well, 300 μ L of 5% DMSO in PBS was added. The drug-filled donor plate was placed into the acceptor plate ensuring the underside of the membrane was in contact with the solution in the acceptor plate. Sealing tape was placed on the top of the donor plate and incubated for 16 hours at 37 °C. After incubation, 100 μ L of aliquots from donor compartment was diluted with 50-50 methanol and water with warfarin as an internal standard. To determine the drug equilibrium concentration, 150 μ L of the donor plate solution and 300 μ L of the acceptor plate solution were mixed and diluted with equal volume of

methanol containing internal standard. The donor, acceptor, and equilibrium concentration were determined by using HPLC, and PAMPA permeability was determined using following equation. The Lucifer yellow solution was visually inspected to ensure the membrane integrity.

$$P_e = \left[\frac{V_D \times V_A}{(V_D + V_A) \times Area \times Time} \right] \times \left\{ -\ln \left[1 - \frac{C_A(t)}{C_{eq}} \right] \right\}$$

3.8.4 Determination of human plasma protein binding

Human plasma was purchased from Innovative Research, Inc, Michigan. HPPB was determined using protocol developed by North lab. Human plasma was thawed and centrifuged at 1000 rpm for two minutes to remove any particulates. Each compound was prepared at 10 µg/mL by spiking compound from 10 mg/mL DMSO stock solution in human plasma. 300 µl of 10 µg/mL compound spiked in human plasma was placed in the sample chamber (red ring) of the RED insert and 500 µL of PBS was placed into the adjacent buffer chamber and the experiment was performed in triplicates. The plate was sealed and incubated at 37 °C on an orbital shaker at 250 rpm for 4 hours. After incubation, to 100 µL of aliquots from plasma chamber was added 100 µL of PBS, and to 100 µL of aliquots from buffer chamber was added 100 µL of plasma to create an identical sample matrix. To each mixture, 800 µL of methanol containing the internal standard (warfarin) was added, and protein was precipitated which was then centrifuged at 13,000 rpm for 10 minutes. The concentration of the aliquot in the supernatant were analyzed by LC-MS-MS. The % free and % bound fraction were calculated using following formulae:

$$\% Free = \frac{[Buffer Chamber Compound Concentration]}{[Plasma Chamber Compound Concentration]}$$

$$\% \text{ Bound} = 100 - \% \text{ Free}$$

3.8.5. Determination of cell viability

Cell viability was determined using Vybrant MTT assay protocol. Wi-26 VA4, the human embryonic lung lines, were grown and cultured in MEM with 10% FBS at 37 °C and 5% CO₂. The cells were trypsinized and a uniform cell suspension at a concentration of 10⁵ cells/mL (measured by hemocytometer) was prepared in MEM/FBS media. 100 µL of the above cell suspension (10⁴ cells/well) was inoculated in each well of 96 well plate and allowed to grow in MEM with 10% FBS at 37 °C and 5% CO₂ for 24 hours, where the cells achieved around 10% confluency. From 10 mg/mL compound stock, a solution of 20 µg/mL was prepared in MEM with 10% FBS and was diluted 10-fold serially for six other lower concentrations with MEM/FBS media containing 0.2% DMSO, and after 24 hours, when the cell achieved about 10% confluency, the original media was replaced with 100 µL of the compounds in triplicates for 7 different concentration and was incubated for 72 hours at 37 °C and 5% CO₂. After 72 hours, the compounds in MEM/FBS was removed and 100 µL of fresh MEM/FBS and 10 µL of MTT reagent was added and incubated for 4 hours at 37 °C, Compound solution and MTT reagent solution was replaced by 100 µL of 20% SDS in 0.01 M HCl reagent dissolve the formazan crystals and incubated for 30 minutes followed by 30 minutes of orbital shaking at 250 rpm to dissolve the formazan crystals. The absorbance was measured at 570 nm, and a plot of concentration vs % cell viability was drawn to find the IC₅₀ of the compounds.

$$\% \text{ Cell Viability} = \frac{\text{Absorbance of sample}}{\text{Absorbance of untreated control}} * 100\%$$

**Chapter 4: Conclusion, Future Direction, and Global
Perspective**

4.1 Conclusion

This research project focused on enhancing the pharmacokinetic profiles of the previously reported indole-based antimycobacterial agents where this project explored a novel class of acetamide-based antimycobacterial agents. A ligand-based drug design approach was utilized, and medicinal chemistry principles were applied to optimize acetamide antimycobacterial activity and drug disposition. The acetamides were synthesized via a two-step reaction scheme and isolated in moderate to good yields. The acetamides achieved enhanced aqueous solubility while retaining the efficacy and safety profiles suggesting that the acetamides are a promising class for further preclinical drug development.

The top lead, compound **192**, exhibited an MIC value of 0.5 $\mu\text{g/mL}$ against *M. abscessus* and 0.25 $\mu\text{g/mL}$ against *M. tb*. Since the pharmacophore was retained from previous generations of MmpL3 inhibitors, we believe that these compounds also bind to and inhibit the MmpL3 transporter in mycobacteria. The SAR revealed through this study showed that only the bulky and rigid cycloaliphatic groups such as adamantane and isopinocampheane exhibited excellent activity, while other more flexible cycloaliphatic groups of the previous series such as cyclooctane, cycloheptane, and transmethylcyclohexane were found to be least effective for the acetamides series. The bulky lipophilic groups such as chloro/bromo or bulky electron withdrawing groups such as trifluoromethoxy substituted on the phenyl ring promoted optimal activity, while electron donating groups such as methyl were less effective. Lastly, meta-substitution on the phenyl ring was the most favorable position.

Our primary intention was to enhance the aqueous solubility of this series, because this physicochemical property has a direct influence on the effectiveness of *in vivo*

absorption. The aqueous solubility was enhanced up to 30-fold, achieving nearly 30 $\mu\text{g/mL}$. Coupled with the high antimycobacterial activity this data has validated the hypothesis of this research project.

The permeability profiles of the compounds were moderate, and the HPPBs were generally high. The compounds of the acetamides series were found to be very safe at all concentrations up to 20 $\mu\text{g/mL}$, and the compounds achieved selectivity indices in the range of >10 to >80 . This preliminary data clearly suggests that acetamides are strong candidates to be developed further as antimycobacterial agents.

In conclusion, TB is a global burden and there is an increasing interest in NTM infections due to increasing prevalence and lack of appropriate treatment regimens. Therefore, novel anti-TB and anti-NTM agents are urgently needed. The previously reported indole-based MmpL3 inhibitors exhibited excellent antimycobacterial activity but lacked optimal ADME profiles. The attempt to enhance these profiles yielded acetamides series with equivalent MIC and enhanced pharmacokinetic profiles.

Of 39 compounds synthesized and tested for their antimycobacterial activity and ADME-Tox profiles, 35 of the acetamides were deprioritized for the further drug development. The 28 compounds that possessed an MIC value > 2 were deprioritized as these potencies would not lead to a very effective compounds. Table 24 depicts the 11 lead compounds with the data on MIC against both mycobacterial strains, solubility, permeability, HPPB, and cytotoxicity values. The optimal values considered for these decisions were: a) MIC value $\leq 1 \mu\text{g/mL}$ b) aqueous solubility $> 10 \mu\text{g/mL}$, c) permeability $> 0.5 \times 10^{-6} \text{ cm/s}$, and c) Selectivity indices > 10 . The compounds **176** and **179** possessed low MIC value, poor aqueous solubility and poor permeability profiles, disfavoring their further development. The compounds **187** possessed poor

permeability profile and low MIC value. Compounds **188** possessed MIC value > 1 µg/mL, and compound **190** had poor aqueous solubility. Compound **191** and **196** had poor permeability profiles, deprioritizing their further development. Therefore, compounds **192**, **194**, **198** and **200** are the best leads, with high antimycobacterial activity and significantly improved aqueous solubility and represent the promising acetamide class poised for further development as potential antimycobacterial agents. If we had to further prioritize, lead compounds **192** and **200** were considered the most optimal because of their best efficacy and comparable ADME-Tox profiles.

Table 24. Summary of acetamides MIC and ADME-Tox data

| No. | <i>M. abscessus</i> MIC (µg/ml) | <i>M. tb.</i> MIC (µg/ml) | Aqueous Sol. (µg/ml) | PAMPA (X 10 ⁻⁶ cm/s) | HPPB (% Bound) | SI (<i>M. absc.</i>) | SI (<i>M. tb.</i>) |
|-----|---------------------------------------|---------------------------------|----------------------------|---------------------------------------|----------------------|---------------------------|-------------------------|
| 176 | 2 | 8 | 1.37 ± 0.02 | 0.28 ± 0.04 | 99.6 ± 0.14 | >10 | >2.50 |
| 179 | 2 | 16 | 6.79 ± 0.59 | 0.47 ± 0.05 | 99.8 ± 0.01 | >10 | >1.25 |
| 187 | 4 | 2 | 23.9 ± 0.92 | 0.34 ± 0.19 | 94.3 ± 0.5 | >5 | >10 |
| 188 | 2 | 4 | 20.3 ± 0.40 | 3.12 ± 0.03 | 96.7 ± 0.01 | >10 | >5 |
| 190 | 1 | 4 | 4.53 ± 0.21 | 3.19 ± 0.03 | 95.2 ± 0.05 | >20 | >5 |
| 191 | 1 | 0.25 | 14.30 ± 0.43 | 0.38 ± 0.03 | 95.50 ± 0.10 | >20 | >80 |
| 192 | 0.5 | 0.25 | 16.30 ± 0.37 | 1.33 ± 0.01 | 94.10 ± 0.02 | >40 | >80 |
| 194 | 1 | 0.5 | 18.60 ± 0.37 | 1.01 ± 0.01 | 95.50 ± 0.1 | >20 | >40 |

| No. | <i>M. abscessus</i> MIC (µg/ml) | <i>M. tb.</i> MIC (µg/ml) | Aqueous Sol. (µg/ml) | PAMPA (X 10 ⁻⁶ cm/s) | HPPB (% Bound) | SI (M. abs.) | SI (M. tb) |
|-----|---------------------------------|---------------------------|----------------------|---------------------------------|----------------|--------------|------------|
| 196 | 1 | 1 | 30.30 ± 1.06 | 0.32 ± 0.005 | 99.80 ± 0.01 | >20 | >20 |
| 198 | 1 | 1 | 22.20 ± 1.55 | 1.02 ± 0.02 | 93.20 ± 0.1 | >20 | >20 |
| 200 | 0.5 | 0.25 | 20.40 ± 2.41 | 3.61 ± 0.04 | 94.90 ± 0.3 | >40 | >80 |

4.2 Future Directions

From a broad perspective, our primary goal is to address the current shortcomings, especially long duration of the treatment and lack of effective treatment regimens to the resistant *M. tb* strains and lack of specific treatment for NTM infections, in the treatments for tuberculosis and NTM infections by providing additional antimicrobial options. This thesis explores approaches to mitigate TB and NTM infections from medicinal chemistry perspective that have not been discussed in the literature especially pertaining to MmpL3 inhibition.

4.2.1 Development of the current acetamide series

We are in the early stages of drug discovery and development. The preliminary data clearly suggests the potential of this series to be developed. There are few studies that should be conducted urgently to provide a better understanding. First, the mechanism of action should be determined to confirm MmpL3 inhibition. This will elucidate if the compounds are inhibiting MmpL3 protein or another target. This can be performed

through genetic profiling of generated mycobacterial spontaneous acetamide-resistant mutants or through biochemical MmpL3 inhibition. Second, the compounds should be tested against a panel of NTM pathogens to determine the spectrum of activity. Third, lead acetamides should be evaluated against drug-resistant strains of *M. tb*. Fourth, the metabolic stability should be ascertained, as metabolic lability is a major factor in drug discovery and many compounds have faced attrition due to poor metabolic profiles. The *in vivo* PK profiling is warranted for **192** and **200** to determine if improved aqueous solubility translates to improved oral absorption. *In vivo* PK profiling involves determination of maximum drug concentration (C_{max}), time required to reach maximum drug concentration (T_{max}), plasma clearance, elimination half-life ($t_{1/2}$) and volume of distribution. Subsequently, pending the *in vivo* PK data for **192** and **200**, efficacy studies in *M. tb*- and *M. abscessus*-infected mouse models are also important initial determinants for acetamide translational potential. The *in vivo* efficacy studies involve infecting the animals with *M. tb* or *M. abscessus* and administration of the test compound orally to see the reduction in colony forming units (CFUs) of *Mycobacteria* compared to the untreated control group.

4.2.2 Extension and optimization of the current series

Although several interesting compounds were developed in the acetamide series, further optimization of this series to enhance the ADME profiles while retaining the essential pharmacophore is warranted. The variations in the substitutions in the phenyl core enhanced the activity drastically, therefore it is a rational strategy to synthesize more compounds with contemporary bulky, electron withdrawing and lipophilic functional moieties (Figure 25). The 3-trifluoroxatonyl and trifluoromethylcyclopropyl group imparts sufficient bulk, lipophilicity, and electron

withdrawing property. The N-trifluoropiperazine also provides sufficient bulk and electron withdrawing properties plus some polarity (Figure 25). The meta-substitutions in the aniline core was identified as the optimal position among the three different positions, ortho, meta and para substitutions. The di-meta substitutions in the phenyl ring with the most successful mono-substituents in aniline core with functional groups such as chloro, bromo, and trifluoromethoxy may also result in the increased antimycobacterial activity.

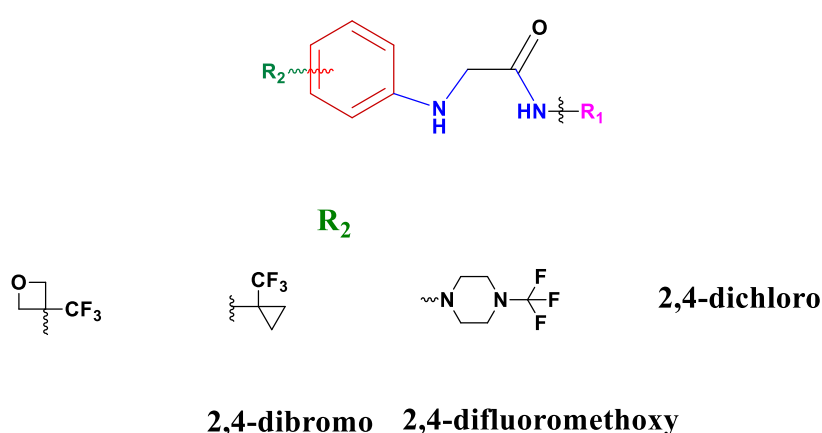


Figure 25. Contemporary and classical functional groups at R₂.

4.2.3 Modification of the acetamide core

Bioisosteric replacements are a routinely employed in practice to develop a new series to optimize one or more parameters. This is because bioisosteric replacements may provide novel compounds with enhanced efficacy and PK/PD profiles. The acetamide is an example of bioisosteric substitutions of indoles. In order to further expand the potential chemotypes and potentially enhance the ADME profiles further, the following scaffolds shown in Figure 26 are proposed.

Scaffold 1 is an acetamide and this thesis project discussed this bioisosteric modification. Scaffolds 2 and 3 represent an oxalyl series and sulfonamide series, respectively, which has a higher proportion of heteroatoms and may further increase the aqueous solubility. While modification to the phenyl of bulky cycloaliphatic core has been commonly pursued to influence activity, bioisosteric modification to the central amide core has not been well-studied. The scaffolds 4, 5, 6, and 7 are non-classical bioisosteres of amides. The pharmacophore requirements for MmpL3 inhibitors in this core are flexible, requiring mainly H-bond acceptors. The oxadiazole functional moiety of 6 and 7 are bioisosteres of amides, and they have strong H-bond accepting properties required for MmpL3 binding. The oxetan functionality attached with amine in scaffold 5 also serve as an amide bioisostere, and it possesses both H-bond donor and acceptor, supporting potential for development as novel antimycobacterial agents.

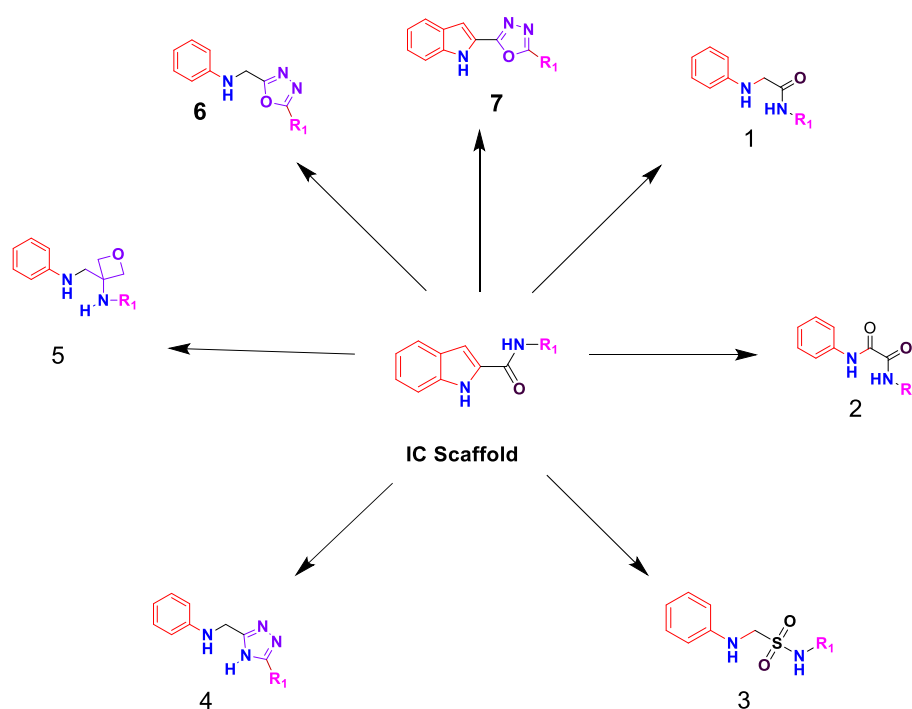


Figure 26. Classical and non-classical bioisosteric replacement of indole-based MmpL3 inhibitors.

4.3 Global Perspectives of the research project

TB is the leading cause of death caused by a single infectious disease. In 2017, 10 million people died from TB (WHO TB report, 2018). Failure to treat TB is due to the development of resistant strains, both MDR and XDR in *M. tb*. The increasing number of patients suffering from HIV-AIDS has made the treatment of TB even more challenging. Therefore, a novel antitubercular agent capable of treating drug-resistant TB is urgently needed.

NTM infections are opportunistic infections that increase in prevalence every year. Current limitations in treating NTM infections are lack of a proper treatment and evidence of efficacy, necessitating the search for effective options.

WHO affiliated countries have signed an ‘End-TB Strategy’ by 2020 in 2014 in Geneva, Switzerland. The amount of investment per annum towards the mitigation and treatment of TB is approximately USD 10.4 billion (WHO TB report, 2018). This suggests a significant vested interest in the management and elimination of TB, however, there has been a paucity of progress in the past four decades.

Towards these efforts of identifying novel antitubercular and anti-NTM agents, acetamide-based compounds **192** and **200** are our best leads owing to their high efficacy and improved ADME. This supports their translational potential to be further developed as a novel antimycobacterial agents that may improve international healthcare, by providing additional effective options to treat devastating mycobacterial infections.

References and Bibliography

Abbaci, Muriel, Muriel Barberi-Heyob, Walter Blondel, François Guillemin, and Jacques Didelon. 2008. "Advantages and limitations of commonly used methods to assay the molecular permeability of gap junctional intercellular communication." *Biotechniques* 45 (1):33-62.

Ahmad, Suhail. 2010. "Pathogenesis, immunology, and diagnosis of latent *Mycobacterium tuberculosis* infection." *Clinical and Developmental Immunology* 2011.

Al Dulayymi, Juma'a R., Mark S. Baird, Evan Roberts, and David E. Minnikin. 2006. "The Synthesis Of Single Enantiomers Of Meromycolic Acids From Mycobacterial Wax Esters". *Tetrahedron* 62 (51): 11867-11880. doi:10.1016/j.tet.2006.09.019.

Alvarez-Figueroa, M Javiera, C David Pessoa-Mahana, M Elisa Palavecino-González, Jaime Mella-Raipán, Cristián Espinosa-Bustos, and Manuel E Lagos-Muñoz. 2011. "Evaluation of the membrane permeability (PAMPA and skin) of benzimidazoles with potential cannabinoid activity and their relation with the Biopharmaceutics Classification System (BCS)." *AAPS PharmSciTech* 12 (2):573-578.

Argyrou, Argyrides, Matthew W Vetting, and John S Blanchard. 2007. "New insight into the mechanism of action of and resistance to isoniazid: interaction of *Mycobacterium tuberculosis* enoyl-ACP reductase with INH-NADP." *Journal of the American Chemical Society* 129 (31):9582-9583.

ATCC Cell culture protocol, 2019

Benet, Leslie Z. 2013. "The role of BCS (biopharmaceutics classification system) and BDDCS (biopharmaceutics drug disposition classification system) in drug development." *Journal of pharmaceutical sciences* 102 (1):34-42.

Bodle, Ethan E, Jennifer A Cunningham, Phyllis Della-Latta, Neil W Schluger, and Lisa Saiman. 2008. "Epidemiology of nontuberculous mycobacteria in patients without HIV infection, New York City." *Emerging infectious diseases* 14 (3):390.

Brittain, HG. 2014. "Thermodynamic vs. kinetic solubility: knowing which is which." *American Pharmaceutical Review* 17 (3):10-16.

Brown, Joshua R, Elton J North, Julian G Hurdle, Christophe Morisseau, Jerrod S Scarborough, Dianqing Sun, Jana Korduláková, Michael S Scherman, Victoria Jones, and Anna Grzegorzewicz. 2011. "The structure–activity relationship of urea derivatives as anti-tuberculosis agents." *Bioorganic & medicinal chemistry* 19 (18):5585-5595.

Chan, Edward D, and Michael D Iseman. 2008. "Multidrug-resistant and extensively drug-resistant tuberculosis: a review." *Current opinion in infectious diseases* 21 (6):587-595.

Chung, Thomas DY, David B Terry, and Layton H Smith. 2015. "In vitro and in vivo assessment of ADME and PK properties during lead selection and lead optimization—guidelines, benchmarks and rules of thumb." In *Assay Guidance Manual* [Internet]. Eli Lilly & Company and the National Center for Advancing Translational Sciences.

Council, National Research. 2013. "A Framework to Guide Selection of Chemical Alternatives 2014." DOI 10:18872.

Curatolo, William. 1998. "Physical chemical properties of oral drug candidates in the discovery and exploratory development settings." *Pharmaceutical Science & Technology Today* 1 (9):387-393.

Cyprotex PAMPA assay, 2019

Dickson, Michael, and Jean Paul Gagnon. 2004. "Key factors in the rising cost of new drug discovery and development." *Nature reviews Drug discovery* 3 (5):417.

Drug Bank, 2019

Dudko, Olga K, Alexander M Berezhkovskii, and George H Weiss. 2004. "Diffusion in the presence of periodically spaced permeable membranes." *The Journal of chemical physics* 121 (22):11283-11288.

Faller, Bernard. 2008. "Artificial membrane assays to assess permeability." *Current drug metabolism* 9 (9):886-892.

Faria, Sonia, Ines Joao, and Luisa Jordao. 2015. "General overview on nontuberculous mycobacteria, biofilms, and human infection." *Journal of pathogens* 2015.

Floto, R Andres, and Charles S Haworth. 2015. "The growing threat of nontuberculous mycobacteria in CF." *Journal of Cystic Fibrosis* 14 (1):1-2.

Forrellad, Marina A, Laura I Klepp, Andrea Gioffré, Julia Sabio y Garcia, Hector R Morbidoni, María de la Paz Santangelo, Angel A Cataldi, and Fabiana Bigi. 2013. "Virulence factors of the *Mycobacterium tuberculosis* complex." *Virulence* 4 (1):3-66.

Fortuna, Ana, Gilberto Alves, and Amílcar Falcão. 2007. "The importance of permeability screening in drug discovery process: PAMPA, Caco-2 and rat everted gut assays." *Pharmacology* 11:2.

Franz, Nicholas D, Juan Manuel Belardinelli, Michael A Kaminski, Louis C Dunn, Vinicius Calado Nogueira de Moura, Michael A Blaha, Dan D Truong, Wei Li, Mary Jackson, and E Jeffrey North. 2017. "Design, synthesis and evaluation of indole-2-carboxamides with pan anti-mycobacterial activity." *Bioorganic & medicinal chemistry* 25 (14):3746-3755.

Grzegorzewicz, Anna E, Ha Pham, Vijay AKB Gundi, Michael S Scherman, Elton J North, Tamara Hess, Victoria Jones, Veronica Gruppo, Sarah EM Born, and Jana Korduláková. 2012. "Inhibition of mycolic acid transport across the *Mycobacterium tuberculosis* plasma membrane." *Nature chemical biology* 8 (4):334.

Guha, Rajarshi, Thomas S Dexheimer, Aimee N Kestranek, Ajit Jadhav, Andrew M Chervenak, Michael G Ford, Anton Simeonov, Gregory P Roth, and Craig J Thomas. 2011. "Exploratory analysis of kinetic solubility measurements of a small molecule library." *Bioorganic & medicinal chemistry* 19 (13):4127-4134.

Huang, Chih-chin, Clare V. Smith, Michael S. Glickman, William R. Jacobs, and James C. Sacchettini. 2001. "Crystal Structures of Mycolic Acid Cyclopropane Synthases From *Mycobacterium tuberculosis*". *Journal of Biological Chemistry* 277 (13): 11559-11569. doi:10.1074/jbc.m111698200.

Hart, ML, DP Do, RA Ansari, and SAA Rizvi. 2013. "Brief overview of various approaches to enhance drug solubility." *J. Dev. Drugs* 2:1000110-1000116.

Hughes, J., Rees, S., Kalindjian, S., & Philpott, K. (2011). Principles of early drug discovery. *British Journal of Pharmacology*, 162(6), 1239-1249. doi: 10.1111/j.1476-5381.2010.01127.x

IUPAC Gold Bank, 2019

Ishida, Seiichi. 2018. "Organs-on-a-chip: current applications and consideration points for in vitro ADME-Tox studies." *Drug metabolism and pharmacokinetics* 33 (1):49-54.

Ishikawa, Minoru, and Yuichi Hashimoto. 2011. "Improvement in aqueous solubility in small molecule drug discovery programs by disruption of molecular planarity and symmetry." *Journal of medicinal chemistry* 54 (6):1539-1554.

Jackson, M. 2014. "The Mycobacterial Cell Envelope--Lipids". *Cold Spring Harbor Perspectives In Medicine* 4 (10): a021105-a021105. doi:10.1101/cshperspect.a021105.

Jankute, Monika, Jonathan AG Cox, James Harrison, and Gurdyal S Besra. 2015. "Assembly of the mycobacterial cell wall." *Annual review of microbiology* 69:405-423.

Jeffrey North, E, Mary Jackson, and Richard E Lee. 2014. "New approaches to target the mycolic acid biosynthesis pathway for the development of tuberculosis therapeutics." *Current pharmaceutical design* 20 (27):4357-4378.

Kansy, Manfred, Frank Senner, and Klaus Gubernator. 1998. "Physicochemical high throughput screening: parallel artificial membrane permeation assay in the description of passive absorption processes." *Journal of medicinal chemistry* 41 (7):1007-1010.

Kariv, Ilona, Hong Cao, and Kevin R Oldenburg. 2001. "Development of a high throughput equilibrium dialysis method." *Journal of pharmaceutical sciences* 90 (5):580-587.

Kerns, Edward H, Li Di, Susan Petusky, Michele Farris, Rob Ley, and Phil Jupp. 2004. "Combined application of parallel artificial membrane permeability assay and Caco-2 permeability assays in drug discovery." *Journal of pharmaceutical sciences* 93 (6):1440-1453.

Khadka, Prakash, Jieun Ro, Hyeongmin Kim, Iksoo Kim, Jeong Tae Kim, Hyunil Kim, Jae Min Cho, Gyiae Yun, and Jaehwi Lee. 2014. "Pharmaceutical particle technologies: An approach to improve drug solubility, dissolution and bioavailability." *Asian journal of pharmaceutical sciences* 9 (6):304-316.

Kompis, Ivan M, Khalid Islam, and Rudolf L Then. 2005. "DNA and RNA synthesis: antifolates." *Chemical reviews* 105 (2):593-620.

Kondreddi, Ravinder Reddy, Jan Jiricek, Srinivasa PS Rao, Suresh B Lakshminarayana, Luis R Camacho, Ranga Rao, Maxime Herve, Pablo Bifani, Ngai Ling Ma, and Kelli Kuhen. 2013. "Design, synthesis, and biological evaluation of indole-2-carboxamides: a promising class of antituberculosis agents." *Journal of medicinal chemistry* 56 (21):8849-8859.

Kumar, Priti, Arvindhan Nagarajan, and Pradeep D Uchil. 2018. "Analysis of cell viability by the MTT assay." *Cold Spring Harbor Protocols* 2018 (6):pdb. prot095505.

Lande, Leah, David C Alexander, Richard J Wallace Jr, Rebecca Kwait, Elena Iakhiaeva, Myra Williams, Andrew DS Cameron, Stephen Olshefsky, Ronit Devon,

and Ravikiran Vasireddy. 2019. "*Mycobacterium avium* in Community and Household Water, Suburban Philadelphia, Pennsylvania, USA, 2010–2012." *Emerging infectious diseases* 25 (3):473.

Lee, Meng-Rui, Wang-Huei Sheng, Chien-Ching Hung, Chong-Jen Yu, Li-Na Lee, and Po-Ren Hsueh. 2015. "*Mycobacterium abscessus* complex infections in humans." *Emerging infectious diseases* 21 (9):1638.

Li, Wei, Casey M Stevens, Amitkumar N Pandya, Zbigniew Darzynkiewicz, Pankaj Bhattarai, Weiwei Tong, Mercedes Gonzales-Juarrero, E Jeffrey North, Helen I Zgurskaya, and Mary C Jackson. 2019. "Direct inhibition of MmpL3 by novel antitubercular compounds." *ACS infectious diseases*.

Li, Wei, Ashutosh Upadhyay, Fabio L Fontes, E Jeffrey North, Yuehong Wang, Debbie C Crans, Anna E Grzegorzewicz, Victoria Jones, Scott G Franzblau, and Richard E Lee. 2014. "Novel insights into the mechanism of inhibition of MmpL3, a target of multiple pharmacophores in *Mycobacterium tuberculosis*." *Antimicrobial agents and chemotherapy*:AAC. 03229-14.

Lin, Chunrong, Chad Russell, Bruce Soll, Dominic Chow, Sapna Bamrah, Richard Brostrom, Wesley Kim, Jerry Scott, and Matthew J Bankowski. 2018. "Increasing Prevalence of Nontuberculous Mycobacteria in Respiratory Specimens from US-Affiliated Pacific Island Jurisdictions." *Emerging infectious diseases* 24 (3):485.

Lin, Jiunn H, and Anthony YH Lu. 1997. "Role of pharmacokinetics and metabolism in drug discovery and development." *Pharmacological reviews* 49 (4):403-449.

Lindström, Mikael S. 2009. "Emerging functions of ribosomal proteins in gene-specific transcription and translation." *Biochemical and biophysical research communications* 379 (2):167-170.

Liu, Xingrong, Matthew Wright, and Cornelis ECA Hop. 2014. "Rational Use of Plasma Protein and Tissue Binding Data in Drug Design: Miniperspective." *Journal of medicinal chemistry* 57 (20):8238-8248.

Lovering, Frank. 2013. "Escape from Flatland 2: complexity and promiscuity." *MedChemComm* 4 (3):515-519.

Lovering, Frank, Jack Bikker, and Christine Humblet. 2009. "Escape from flatland: increasing saturation as an approach to improving clinical success." *Journal of medicinal chemistry* 52 (21):6752-6756.

Lun, Shichun, Haidan Guo, Oluseye K. Onajole, Marco Pieroni, Hendra Gunosewoyo, Gang Chen, Suresh K. Tipparaju, Nicole C. Ammerman, Alan P. Kozikowski, and William R. Bishai. 2013. Indoleamides are active against drug-resistant *Mycobacterium tuberculosis*. *Nature Communications* 4: 2907.

Mandagere, Arun K, Thomas N Thompson, and Kin-Kai Hwang. 2002. "Graphical model for estimating oral bioavailability of drugs in humans and other species from their Caco-2 permeability and in vitro liver enzyme metabolic stability rates." *Journal of medicinal chemistry* 45 (2):304-311.

Marrakchi, Hedia, Gilbert Lanéelle, and Annaïk Quémard. 2000. "InhA, a target of the antituberculous drug isoniazid, is involved in a mycobacterial fatty acid elongation system, FAS-II." *Microbiology* 146 (2):289-296.

Marrakchi, Hedia, Marie-Antoinette Lanéelle, and Mamadou Daffé. 2014. "Mycolic acids: structures, biosynthesis, and beyond." *Chemistry & biology* 21 (1):67-85.

North, E Jeffrey, Michael S Scherman, David F Bruhn, Jerrod S Scarborough, Marcus M Maddox, Victoria Jones, Anna Grzegorzewicz, Lei Yang, Tamara Hess, and Christophe Morisseau. 2013. "Design, synthesis and anti-tuberculosis activity of 1-adamantyl-3-heteroaryl ureas with improved in vitro pharmacokinetic properties." *Bioorganic & medicinal chemistry* 21 (9):2587-2599.

Onajole, Oluseye K, Marco Pieroni, Suresh K Tipparaju, Shichun Lun, Jozef Stec, Gang Chen, Hendra Gunosewoyo, Haidan Guo, Nicole C Ammerman, and William R Bishai. 2013. "Preliminary structure–activity relationships and biological evaluation of novel antitubercular indolecarboxamide derivatives against drug-susceptible and drug-resistant *Mycobacterium tuberculosis* strains." *Journal of medicinal chemistry* 56 (10):4093-4103.

Padmapriyadarsini, C, G Narendran, and Soumya Swaminathan. 2011. "Diagnosis & treatment of tuberculosis in HIV co-infected patients." *The Indian journal of medical research* 134 (6):850.

Pandya, Amit N, Pavan K Prathipati, Pooja Hegde, Wei Li, Kyle F Graham, Subhra Mandal, Kristen M Drescher, Christopher J Destache, Diane Ordway, and Mary Jackson. 2019. "Indole-2-Carboxamides Are Active against *Mycobacterium abscessus* in a Mouse Model of Acute Infection." *Antimicrobial agents and chemotherapy* 63 (3):e02245-18.

Park, In Kwon, and Kenneth N Olivier. 2015. "Nontuberculous mycobacteria in cystic fibrosis and non-cystic fibrosis bronchiectasis." *Seminars in respiratory and critical care medicine*.

Polikanov, Yury S, Nikolay A Aleksashin, Bertrand Beckert, and Daniel N Wilson. 2018. "The mechanisms of action of ribosome-targeting peptide antibiotics." *Frontiers in molecular biosciences* 5:48.

Rao, Srinivasa PS, Suresh B Lakshminarayana, Ravinder R Kondreddi, Maxime Herve, Luis R Camacho, Pablo Bifani, Sarath K Kalapala, Jan Jiricek, Ng L Ma, and Bee H Tan. 2013. "Indolcarboxamide is a preclinical candidate for treating multidrug-resistant tuberculosis." *Science translational medicine* 5 (214):214ra168-214ra168.

Rastogi, Nalin, Valérie Labrousse, and Khye Seng Goh. 1996. *In vitro* activities of fourteen antimicrobial agents against drug susceptible and resistant clinical isolates of *Mycobacterium tuberculosis* and comparative intracellular activities against the virulent H37Rv strain in human macrophages. *Current Microbiology* 33 (3): 167-75.

Reeves, Analise Z, Patricia J Campbell, Razvan Sultana, Seidu Malik, Megan Murray, Bonnie B Plikaytis, Thomas M Shinnick, and James E Posey. 2013. "Aminoglycoside cross-resistance in *Mycobacterium tuberculosis* due to mutations in the 5'untranslated region of whiB7." *Antimicrobial agents and chemotherapy*:AAC. 02191-12.

Riss, Terry L, Richard A Moravec, Andrew L Niles, Sarah Duellman, Hélène A Benink, Tracy J Worzella, and Lisa Minor. 2016. "Cell viability assays."

Rizk, ML, L Zou, RM Savic, and KE Dooley. 2017. "Importance of drug pharmacokinetics at the site of action." *Clinical and translational science* 10 (3):133-142.

Routledge, PhA. 1986. "The plasma protein binding of basic drugs." *British journal of clinical pharmacology* 22 (5):499-506.

Saal, Christoph, and Anna Christine Petereit. 2012. "Optimizing solubility: kinetic versus thermodynamic solubility temptations and risks." *European Journal of Pharmaceutical Sciences* 47 (3):589-595.

Santin, Miguel, Irene Barrabeig, Pierre Malchair, Lucia Gonzalez-Luquero, Miguel A Benitez, Josefina Sabria, Merce Palau-Benavent, Concepcion Cañete, Joan A Lloret-Queraltó, and Maria D Grijota-Camino. 2018. "Pulmonary Infections with Nontuberculous Mycobacteria, Catalonia, Spain, 1994–2014." *Emerging infectious diseases* 24 (6):1091.

Sarathy, Jansy P, Hsin-pin Ho Liang, Danielle Weiner, Jacqueline Gonzales, Laura E Via, and Véronique Dartois. 2017. "An *in vitro* caseum binding assay that predicts drug penetration in tuberculosis lesions." *JoVE (Journal of Visualized Experiments)* (123):e55559.

Saravolatz, Louis D, and James Leggett. 2003. "Gatifloxacin, gemifloxacin, and moxifloxacin: the role of 3 newer fluoroquinolones." *Clinical infectious diseases* 37 (9):1210-1215.

Sarkar, Paramita, Venkateswarlu Yarlagadda, Chandradhish Ghosh, and Jayanta Haldar. 2017. "A review on cell wall synthesis inhibitors with an emphasis on glycopeptide antibiotics." *MedChemComm* 8 (3):516-533.

Savjani, Ketan T, Anuradha K Gajjar, and Jignasa K Savjani. 2012. "Drug solubility: importance and enhancement techniques." *ISRN pharmaceuticals* 2012.

Scherman, Michael S, Elton J North, Victoria Jones, Tamara N Hess, Anna E Grzegorzewicz, Takeo Kasagami, In-Hae Kim, Oleg Merzlikin, Anne J Lenaerts, and Richard E Lee. 2012. "Screening a library of 1600 adamantyl ureas for anti-*Mycobacterium tuberculosis* activity in vitro and for better physical chemical properties for bioavailability." *Bioorganic & medicinal chemistry* 20 (10):3255-3262.

Schmidt, Stephan, Daniel Gonzalez, and Hartmut Derendorf. 2010. "Significance of protein binding in pharmacokinetics and pharmacodynamics." *Journal of pharmaceutical sciences* 99 (3):1107-1122.

Shakya, Neeraj, Gaurav Garg, Babita Agrawal, and Rakesh Kumar. 2012. "Chemotherapeutic interventions against tuberculosis." *Pharmaceuticals* 5 (7):690-718.

Sharma, Sreevalli, Ekaterina Gelman, Chandan Narayan, Deepa Bhattacharjee, Vijayashree Achar, Vaishali Humnabadkar, V Balasubramanian, Vasanthi Ramachandran, Neeraj Dhar, and Neela Dinesh. 2014. "Simple and rapid method to determine antimycobacterial potency of compounds by using autoluminescent *Mycobacterium tuberculosis*." *Antimicrobial agents and chemotherapy* 58 (10):5801-5808.

Shin, Hong-Joon, and Yong-Soo Kwon. 2015. "Treatment of drug susceptible pulmonary tuberculosis." *Tuberculosis and respiratory diseases* 78 (3):161-167.

Smith, Dennis A, Li Di, and Edward H Kerns. 2010. "The effect of plasma protein binding on in vivo efficacy: misconceptions in drug discovery." *Nature reviews Drug discovery* 9 (12):929.

Stec, Jozef, Oluseye K Onajole, Shichun Lun, Haidan Guo, Benjamin Merenbloom, Giulio Vistoli, William R Bishai, and Alan P Kozikowski. 2016. "Indole-2-carboxamide-based MmpL3 inhibitors show exceptional antitubercular activity in an animal model of tuberculosis infection." *Journal of medicinal chemistry* 59 (13):6232-6247.

Sunnetcioglu, Aysel, Mahmut Sunnetcioglu, Irfan Binici, Ali Irfan Baran, Mustafa Kasım Karahocagil, and Muhammed Rıdvan Saydan. 2015. "Comparative analysis of pulmonary and extrapulmonary tuberculosis of 411 cases." *Annals of clinical microbiology and antimicrobials* 14 (1):34.

Szymański, Paweł, Magdalena Markowicz, and Elżbieta Mikiciuk-Olasik. 2012. "Adaptation of high-throughput screening in drug discovery—toxicological screening tests." *International journal of molecular sciences* 13 (1):427-452.

Timmins, Graham S, and Vojo Deretic. 2006. "Mechanisms of action of isoniazid." *Molecular microbiology* 62 (5):1220-1227.

US-FDA report on BCS biowaiver, 2017

USP-NF, 2015

Van der Werf, Marieke J, Csaba Ködmön, Vera Katalinić-Janković, Tiina Kummik, Hanna Soini, Elvira Richter, Dimitrios Papaventsis, Enrico Tortoli, Monique Perrin, and Dick van Soolingen. 2014. "Inventory study of non-tuberculous mycobacteria in the European Union." *BMC infectious diseases* 14 (1):62.

Varma, Manthana V, Iain Gardner, Stefanus J Steyn, Paul Nkansah, Charles J Rotter, Carrie Whitney-Pickett, Hui Zhang, Li Di, Michael Cram, and Katherine S Fenner. 2012. "pH-Dependent solubility and permeability criteria for provisional biopharmaceutics classification (BCS and BDDCS) in early drug discovery." *Molecular pharmaceutics* 9 (5):1199-1212.

Vybrant cell proliferation protocol, 2002

Walsh, Christopher. 2003. "Opinion—anti-infectives: Where will new antibiotics come from?" *Nature Reviews Microbiology* 1 (1):65.

Wan, Hong, and Mikael Rehngrén. 2006. "High-throughput screening of protein binding by equilibrium dialysis combined with liquid chromatography and mass spectrometry." *Journal of Chromatography A* 1102 (1-2):125-134.

Wang, Miao, Chunyan Wang, and Xianlin Han. 2017. "Selection of internal standards for accurate quantification of complex lipid species in biological extracts by electrospray ionization mass spectrometry—What, how and why?" *Mass spectrometry reviews* 36 (6):693-714.

Wang, RA, ZY Ke, Y Liang, T Yang, JH Qin, and L Wang. 2014. "Why is mycobacterium tuberculosis hard to grow? the principle of biorelativity explains." *J Clin Exp Pathol* 4 (3):176.

Watanabe, Motoko, Tsuyoshi Fujita, Malin Ridell, Hidemichi Mitome, David E. Minnikin, Hideo Naoki, and Yutaka Aoyagi. 2002. "Location of Functional Groups In Mycobacterial Meromycolate Chains; The Recognition Of New Structural Principles In Mycolic Acids". *Microbiology* 148 (6): 1881-1902. doi:10.1099/00221287-148-6-1881.

Waters, Nigel J, Rachel Jones, Gareth Williams, and Bindi Sohal. 2008. "Validation of a rapid equilibrium dialysis approach for the measurement of plasma protein binding." *Journal of pharmaceutical sciences* 97 (10):4586-4595.

Wehrli, W. (1983). Rifampin: Mechanisms of Action and Resistance. *Clinical Infectious Diseases*, 5(Supplement_3), S407-S411. doi: 10.1093/clinids/5.supplement_3.s407

WHO TB Report, 2018

Woodcock, Janet, and Raymond Woosley. 2008. "The FDA critical path initiative and its influence on new drug development." *Annu. Rev. Med.* 59:1-12.

Xu, Zhujun, Vladimir A Meshcheryakov, Giovanna Poce, and Shu-Sin Chng. 2017. "MmpL3 is the flippase for mycolic acids in mycobacteria." *Proceedings of the National Academy of Sciences* 114 (30):7993-7998.

Yang, Nicole J, and Marlon J Hinner. 2015. "Getting across the cell membrane: an overview for small molecules, peptides, and proteins." *In Site-Specific Protein Labeling*, 29-53. Springer.

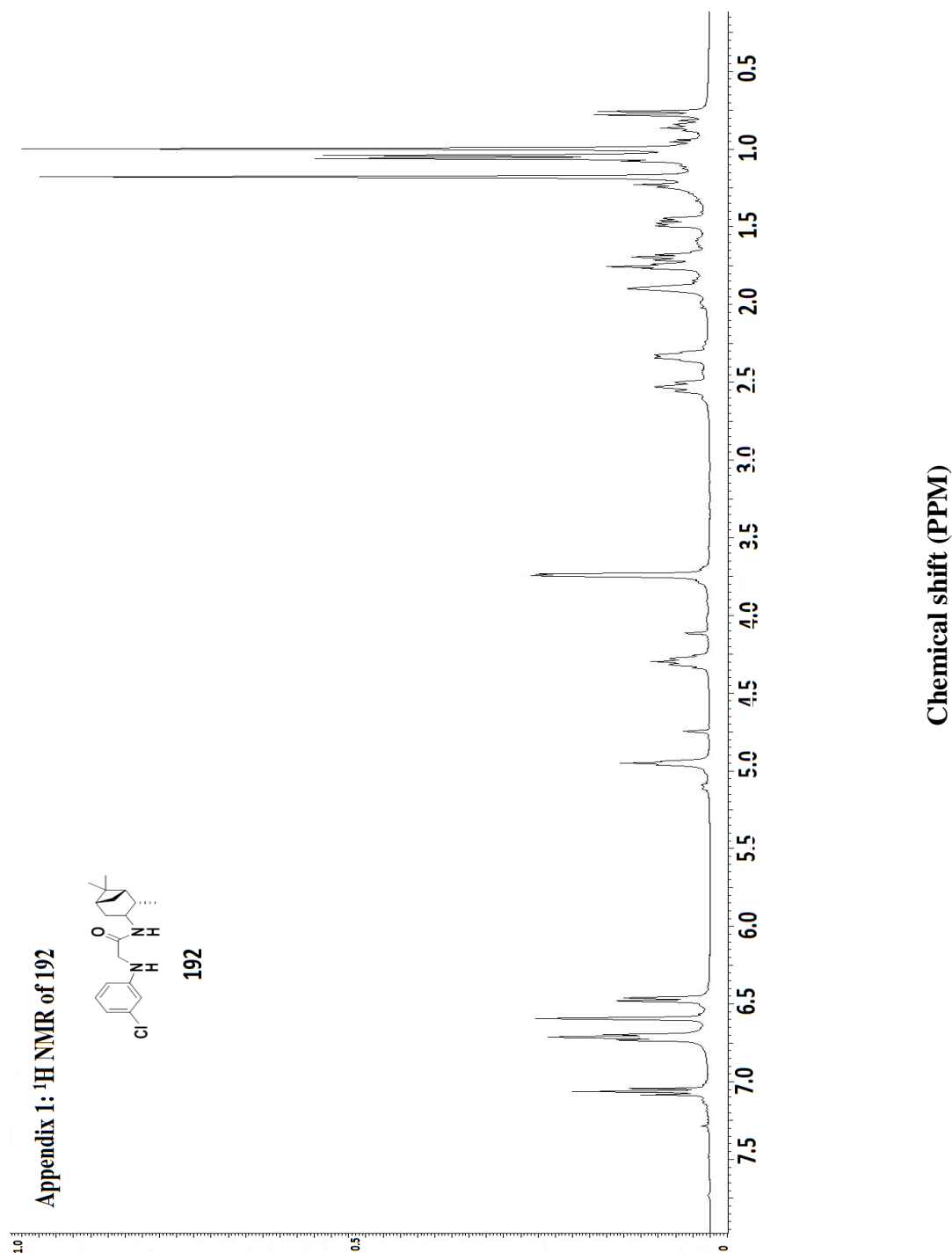
Ye, Zhengqi, Craig Zetterberg, and Hong Gao. 2017. "Automation of plasma protein binding assay using rapid equilibrium dialysis device and Tecan workstation." *Journal of pharmaceutical and biomedical analysis* 140:210-214.

Yu, Hui, Qi Wang, Ying Sun, Ming Shen, He Li, and Yourong Duan. 2015. "A new PAMPA model proposed on the basis of a synthetic phospholipid membrane." *PloS one* 10 (2):e0116502.

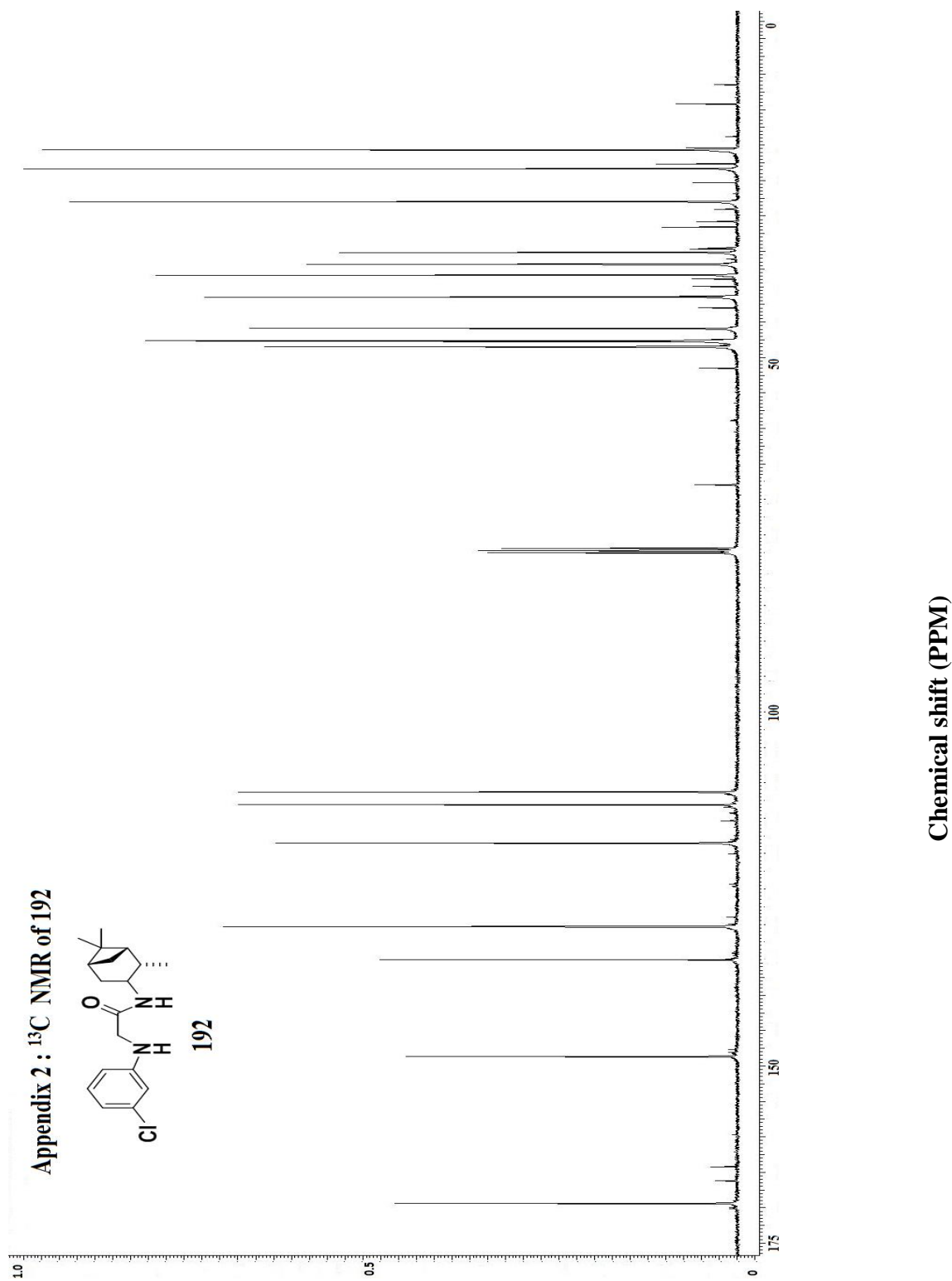
Yuan, Y., and C. E. Barry. 1996. "A Common Mechanism For The Biosynthesis Of Methoxy And Cyclopropyl Mycolic Acids In Mycobacterium Tuberculosis". *Proceedings of The National Academy of Sciences* 93 (23): 12828-12833. doi:10.1073/pnas.93.23.12828.

Zeitlinger, Markus A, Hartmut Derendorf, Johan W Mouton, Otto Cars, William A Craig, David Andes, and Ursula Theuretzbacher. 2011. "Protein binding—do we ever learn?" *Antimicrobial agents and chemotherapy*:AAC. 01433-10.

**Appendix: Characterization data of representative
compounds 192 and 200**

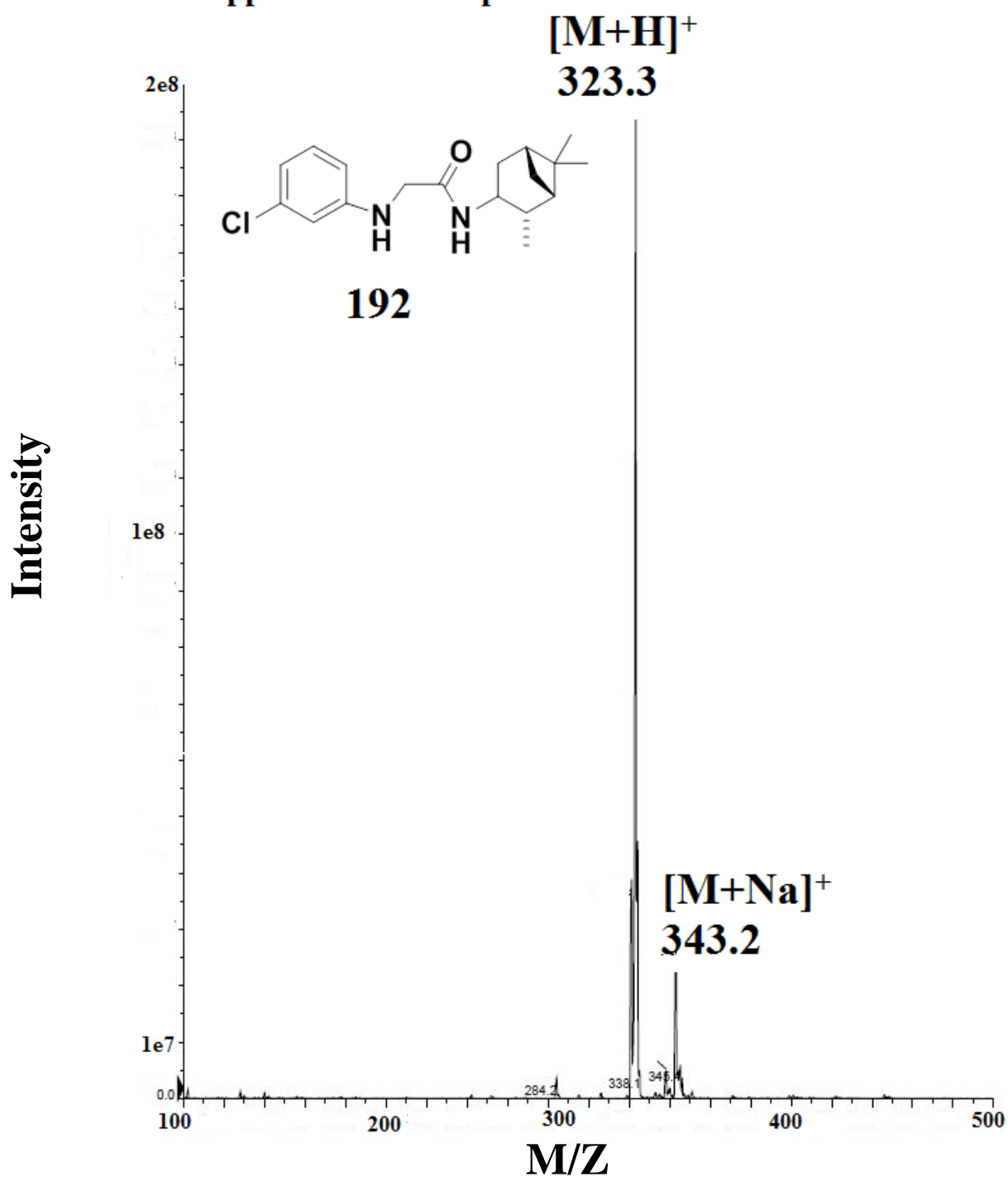


Appendix 1. ¹H NMR of 192; ¹H NMR (CDCl₃) δ = 0.76 (1H, d, J = 8 Hz), 1.0 (3H, s), 1.04 – 1.06 (3H, m), 1.18 (3H, s), 1.44 – 1.49 (1H, m), 1.66 – 1.69 (1H, m), 1.74 – 1.77 (1H, m), 1.89 – 1.90 (1H, m), 2.31 – 2.36 (1H, m), 2.50 – 2.56 (1H, m), 3.74 – 3.78 (1H, m), 4.26 – 4.34 (1H, m), 4.94 – 4.96 (1H, m), 6.46 (1H, d, J = 8 Hz), 6.59 (1H, s), 6.71 (1H, d, J = 8 Hz), 7.06 (1H, t, J = 8 Hz)

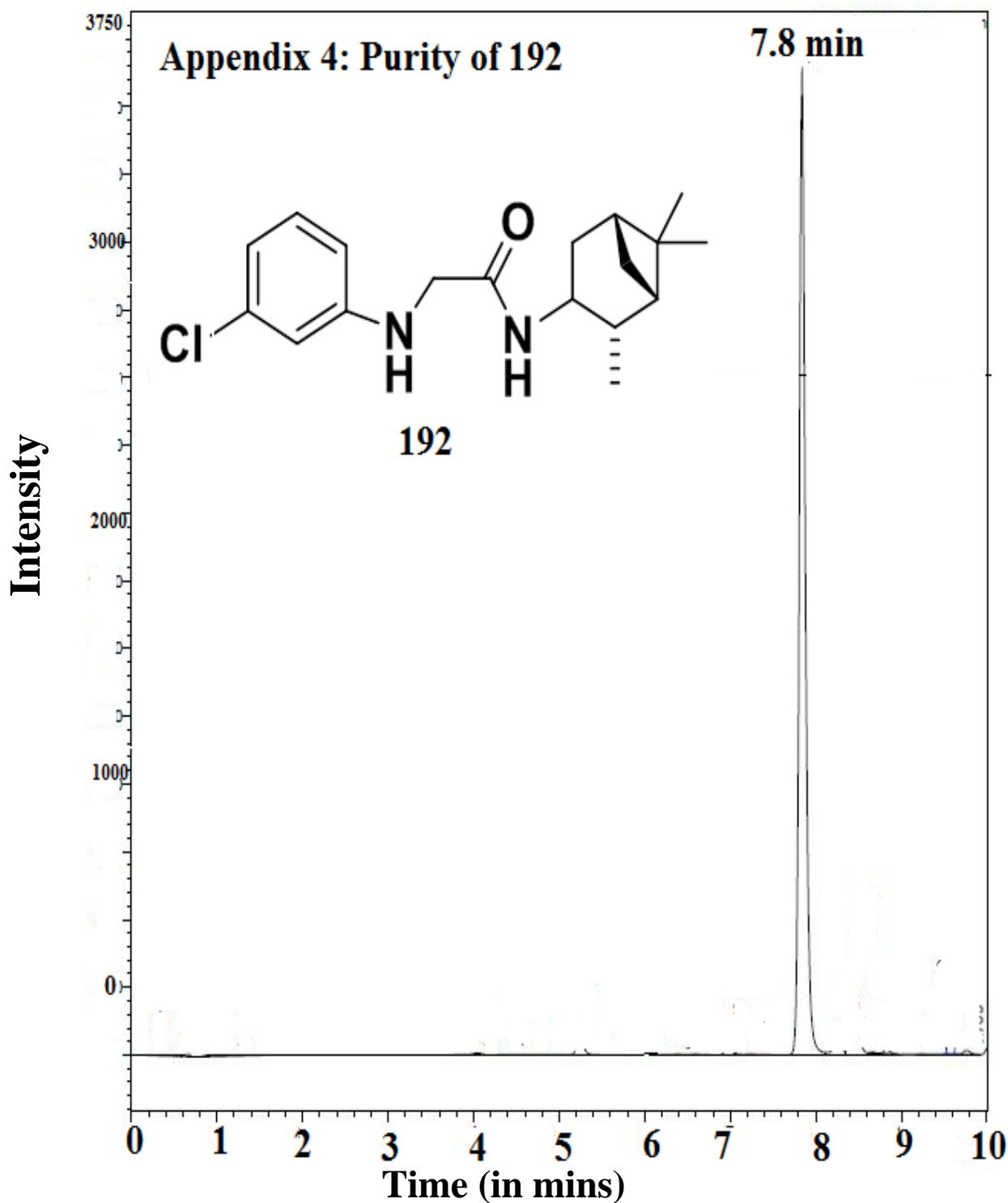


Appendix 2. ^{13}C NMR of 192; ^{13}C NMR (CDCl_3) δ = 20.7, 23.33, 27.97, 35.18, 36.81, 38.36, 41.45, 45.88, 47.61, 48.48, 11.36, 113.31, 118.55, 130.35, 135.02, 148.64, 169.37

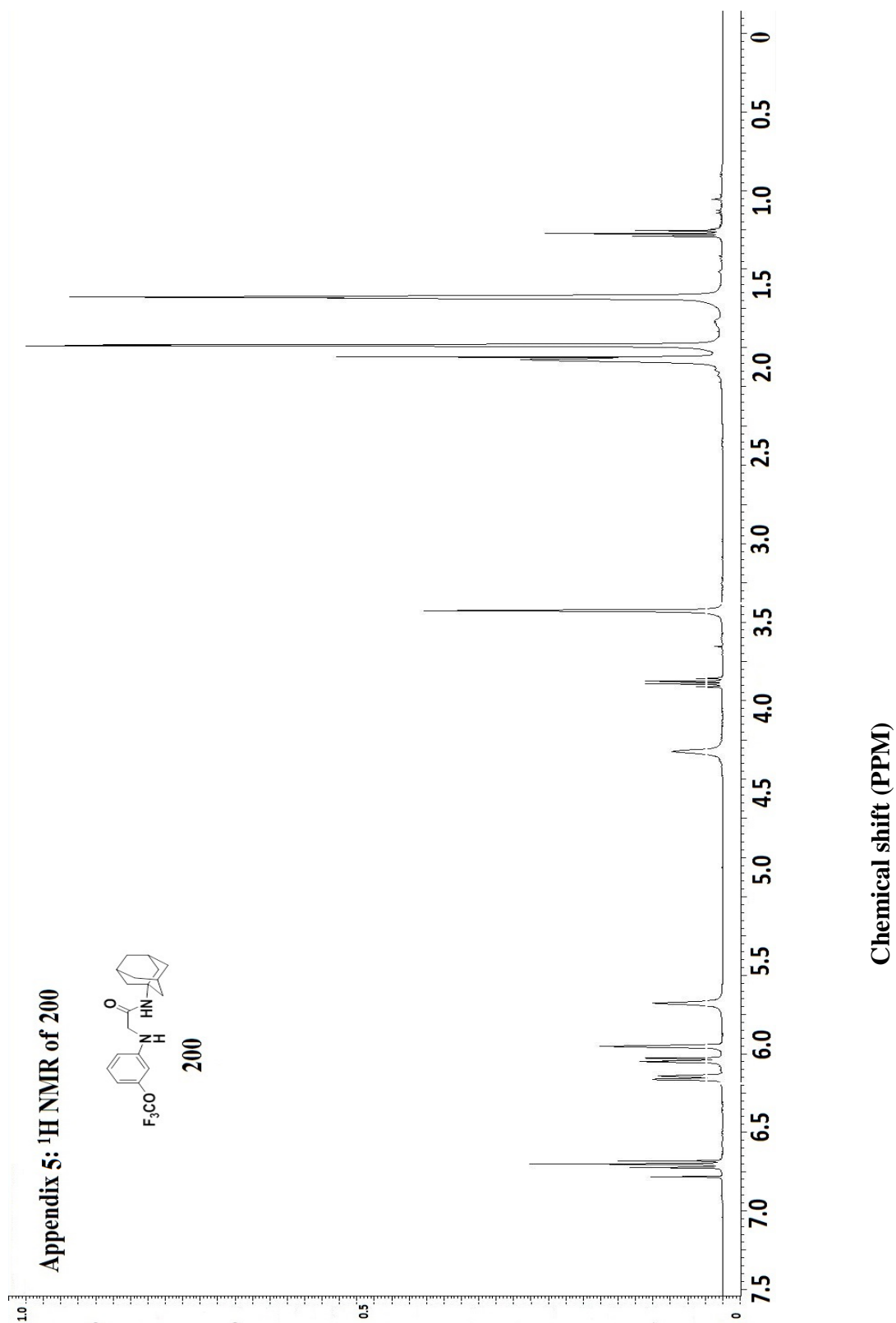
Appendix 3: Mass spec of 192



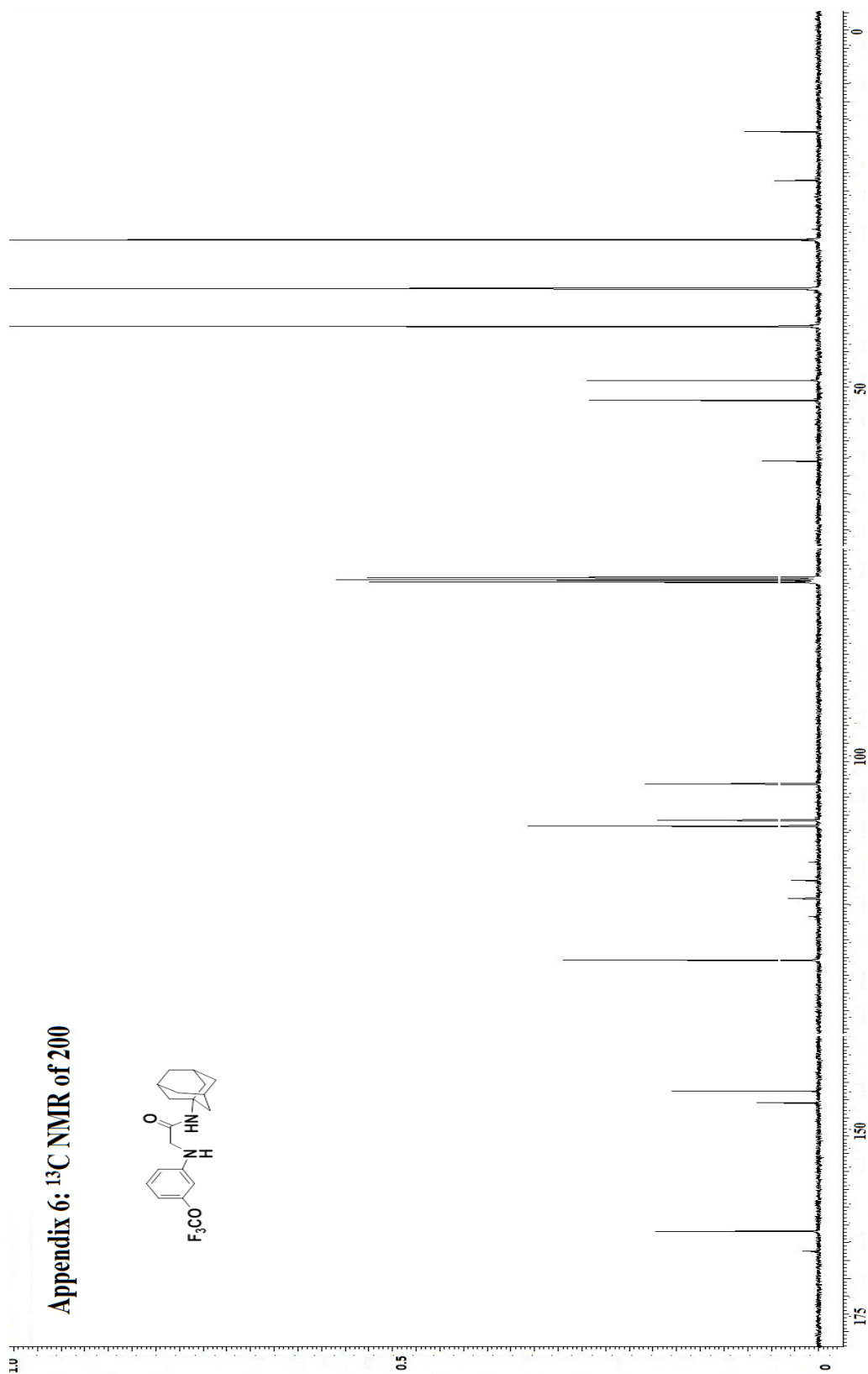
Appendix 3. Mass spec of 192; ESI-MS [M+H]⁺ calculated for C₁₈H₂₅ClN₂O: 321.2, found: 323.3



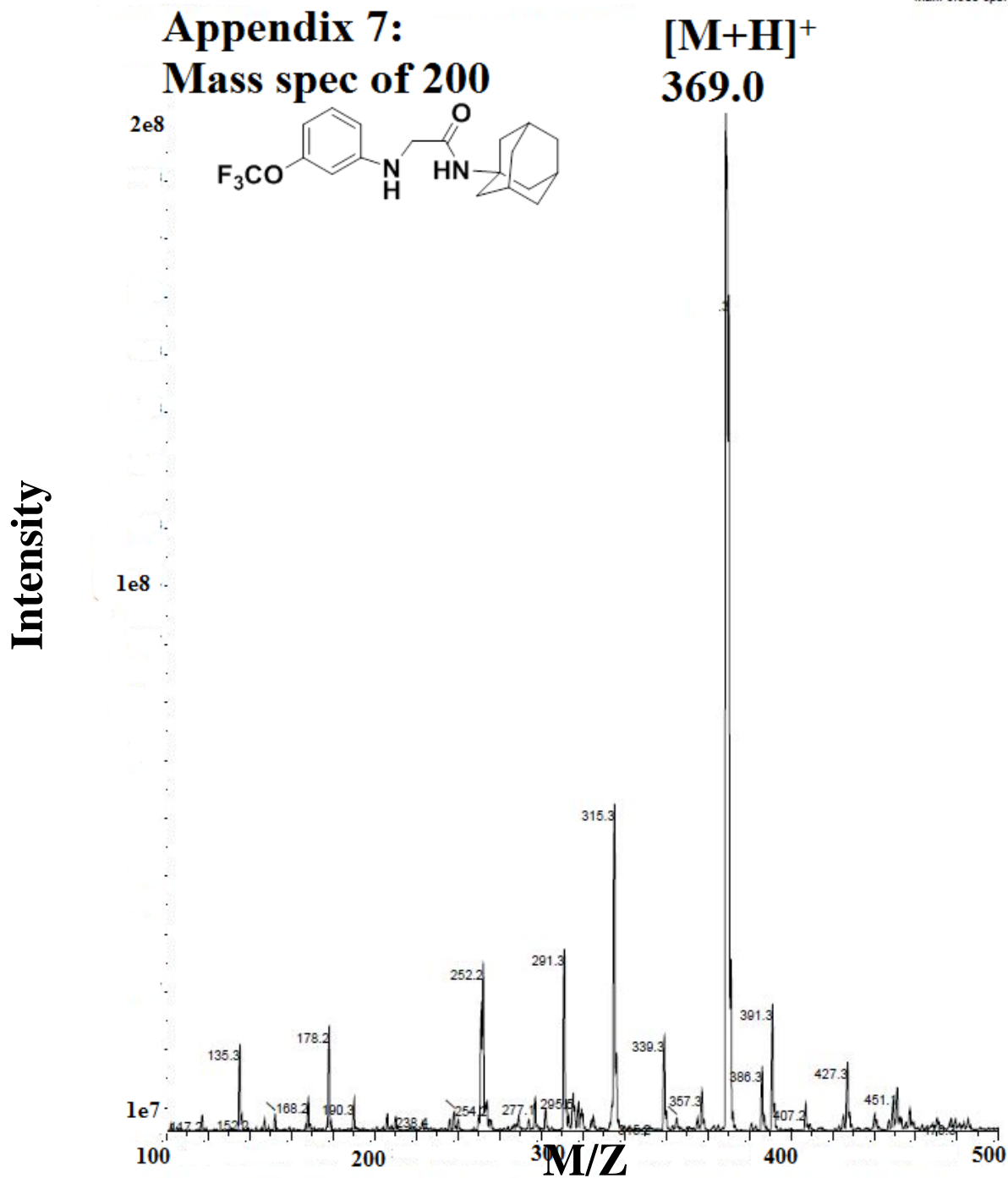
Appendix 4. Purity of 192; HPLC Parameters C18 column (50 X 3 mm; 5 μ m), flow rate of 0.5 mL/min, and a gradient of solvent A (water with 0.1% formic acid) and solvent B (acetonitrile): 0 – 1 min 5% B, 1 – 8 min 5 – 95% B, 8 – 9 min 95% B, 9 – 10 min 95 – 5% B; detection UV absorbance at 254 nm with the HPLC system, RT 7.8 min; >95% pure



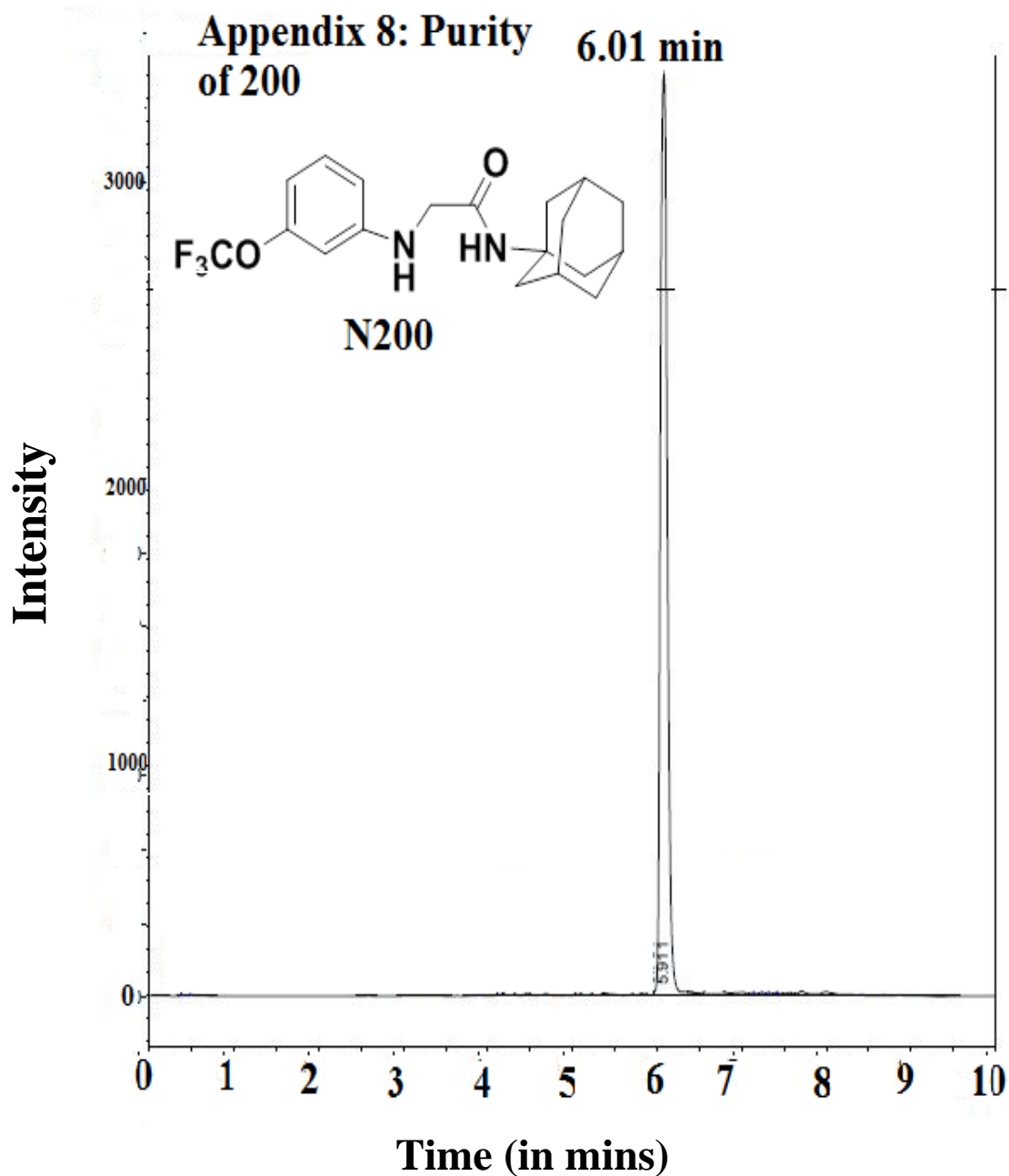
Appendix 5. ^1H NMR of 200; ^1H NMR (CDCl_3) δ = 1.68 (6H, s), 1.99 (6H, s), 2.06 (3H, s), 3.68 (2H, s), 4.57 (1H, s), 6.45 (1H, s), 6.53 (1H, d, J = 8 Hz), 6.64 (1H, d, J = 8 Hz), 7.20 (1H, t, J = 8 Hz)



Appendix 6. ^{13}C NMR of 200; ^{13}C NMR (CDCl₃) δ = 29.37, 36.23, 41.48, 49.10, 51.86, 105.69, 110.74, 111.57, 130.39, 148.75, 150.37, 168.44



Appendix 7. Mass spec of 200; ESI-MS [M+H]⁺ calculated for C₁₉H₂₃F₃N₂O₂: 369.2, found: 369.0



Appendix 8. Purity of 200; HPLC Parameters C18 column (50 X 3 mm; 5 μ m), flow rate of 0.5 mL/min, and a gradient of solvent A (water with 0.1% formic acid) and solvent B (acetonitrile): 0 – 1 min 5% B, 1 – 8 min 5 – 95% B, 8 – 9 min 95% B, 9 – 10 min 95 – 5% B; detection UV absorbance at 254 nm with the HPLC system, RT 6.01 min; >95% pure